Rijkswaterstaat
Ministerie van Infrastructuur en Milieu

Rijkswaterstaat Technisch Document (RTD)

Validation of the Guidelines for Nonlinear Finite Element Analysis of Concrete Structures

Part: Pre-stressed beams

Doc.nr.: RTD 1016-3B:2017
Versie: 1.0
Status: Final
Datum: 15 June 2017

Water. Wegen. Werken. Rijkswaterstaat

Preface

At an international workshop on shear force capacities of concrete structural element, held in Rotterdam, the Netherlands in 2007, predictions of the ultimate limit state of three different girder experiments were presented. This workshop was initiated by the Dutch Ministry of Infrastructure and organized by TNO (Vervuurt & Leeghwater, 2008). The ultimate capacities, predicted by six teams using different nonlinear software packages, showed a large scatter. Also the predicted crack patterns showed a large scatter.

With this in mind, research on the development of a "guideline for nonlinear analysis of concrete girders" was started. The *fib* Model Code 1990 was the background document when Peter Feenstra started with the development of the guideline. Also, Joop den Uijl was involved in validating the guidelines. From 2010 the draft version of the *fib* Model Code 2010 was used as background document. Today, both the MC2010 and the Eurocode2 allow the use of nonlinear analysis to verify the design capacity of concrete objects.

The validation of the guidelines is done by simulating old and new experiments. To verify human and software factors, several people were involved in this project and two commercially available software packages were used. Finally the first version of the guideline was published in May 2012. It is used by the Dutch Ministry of Infrastructure and the Environment when commissioning engineering work for re-examinations of existing concrete structures in the Netherlands to reveal extra remaining structural capacity.

To verify whether the guideline is also valid for a larger group of international end-users and for other software packages, a prediction contest of T-shaped prestressed girders was set up in 2014. The tests were performed by Sebastiaan Ensink in the Stevin Laboratory of the Delft University of Technology. The participants of the contest gathered in a workshop in Parma. The outcome of this contest showed that the guidelines are indeed helpful for reducing model and human factors when predicting the behaviour of concrete structures by means of nonlinear finite element analysis.

As a result of additional validation studies and making use of the experiences of the workshop in Parma a new version of the guidelines has been published in 2016. The present document gives an overview of validations studies for this version of the guideline. Maciej Kraczla has contributed to this document.

This document is one from a series of documents. At the time of writing, the following documents have been drafted:

RTD 1016-1:	Guidelines for Nonlinear Finite Element Analysis of Concrete Structures
RTD 1016-2:	Validation of the Guidelines for Nonlinear Finite Element Analysis of Concrete Structures - Part: Overview of results
RTD 1016-3A:	Validation of the Guidelines for Nonlinear Finite Element Analysis of Concrete Structures - Part: Reinforced beams
RTD 1016-3B:	Validation of the Guidelines for Nonlinear Finite Element Analysis of Concrete Structures - Part: Prestressed beams
RTD 1016-3C:	Validation of the Guidelines for Nonlinear Finite Element Analysis of Concrete Structures - Part: Slabs

Beatrice Belletti, Cecilia Damoni, Max A.N. Hendriks, Ane de Boer
March 2017

Contents

1 Introduction

In the period 2008-2015 the Dutch Ministry of Infrastructure and the Environment has financed a project leading to a set of guidelines for the nonlinear finite element analysis of concrete structures (RWS, 2016). Apart from the guidelines document itself, the project resulted in the present publication: a document that describes the validation of the guidelines.

This introductory chapter begins with describing the background of the project. It continues with presenting the objectives and the outline of the present validation report.

1.1 Background

Modern codes of practice for civil engineering projects offer so-called levels-of-approximations (Muttoni & Ruiz, 2012). Depending on the stage of the project, e.g. preliminary design, executive design or a reassessment study, a modern code distinguishes several levels of design expressions and design methods. The *fib* Model Code for concrete structures 2010 (fib, 2013) is a good example. The idea is: the higher the level-of-approximation, the more sophisticated the analysis, the more realistic the estimation of the safety, the more possibilities of finding "hidden" structural capacities, the higher is the likelihood of avoiding over-conservative designs and reassessments, the more probable is that unnecessary costs can be avoided. The highest level-of-approximation, sometimes denoted as level IV, is a design or a reassessment method based on nonlinear finite element analysis.

Whereas the lower levels-of-approximations are usually well-described using clear-cut expressions, applicability statements and examples, the situation is remarkably different when it comes to using nonlinear finite element analysis for design or reassessment studies. The *fib* Model Code has made an important step by providing safety formats to be used in connection with nonlinear finite element analysis. These safety formats define safety factors for the material properties and the global structural resistance. However the development of specifications on *how to perform* the analyses has not kept pace with the development of safety formats. It is beyond doubt that the results of nonlinear finite element analysis can be substantially influenced by model and human factors.

1.2 Scope and objectives

The development of the guidelines for the nonlinear finite element analysis of concrete structures (RWS, 2016) has the primary goal to advice the analysts and consequently to reduce the model and human factors. The development of the guidelines went hand in hand with the performance of numerical benchmark studies. The guidelines were tuned and, in the end, validated by comparing the results of numerical analyses with experimental results. It is believed that by this process a coherent set of advices was obtained. This document gives an overview of the main case studies that were used during the development of the guidelines.

The case studies include numerical examples with reinforced concrete beams, prestressed beams and slabs. The main objective is to compare the results of the numerical analyses with the experimental results for these cases and, in this way, to validate the set of advices.

Next to the main objective, the case studies reported in this document are used to demonstrate sensitivities of modelling choices, to compare the applications of different safety formats and to show examples of documenting finite element analysis results.

1.3 Outline

After this introductory chapter, Chapter 2 summarizes the used methods. Each subsequent chapter addresses a single case study of a reinforced concrete beam. These chapters use a similar structure of sections, describing respectively: the experimental setup and results, the finite element model adopting the advices of the guidelines, analytical verifications, the nonlinear finite element results using mean or "measured" material properties and the application of safety formats. Additional sections are e.g. used to show sensitivity studies.

2 Methods used for modelling reinforced concrete members

This chapter summarizes the methods that are used in the subsequent chapters.

2.1 Analytical code provisions

The analytical methods used in this report are based on the CEN Eurocode 2 (EC, 2005) and the *fib* Model Code 2010 (fib, 2013).

2.2 Nonlinear finite element modelling approach

There is a great variety of modelling options for modelling the nonlinear behaviour of concrete structures. The guidelines for the nonlinear finite element analysis of concrete structures (RWS, 2016) comprise specific modelling choices. It is important to consider these modelling choices as a coherent set of advices. For the details about these advises the reader is referred to the guidelines document itself. This section includes a summary of the main advices.

Units. The preferred units are the base units of the International System of Units (SI). Possibly, the length unit might be replaced by millimetres.

Constitutive models for concrete. Smeared cracking models are considered. A total strain-based rotating or fixed crack model is preferred. Adequate tensile softening and compressive hardening-softening relations should be considered, based on the specification of tensile and compressive fracture energies and the definition of equivalent lengths to define "crack-band" widths. For the fixed crack models variable shear retention models are recommended. Tension-compression interaction needs to be addressed in structures subjected to multi-axial stress states. These include the reduction of the compressive strength due to lateral cracking and a diminishing Poisson effect upon cracking.

Constitutive models for reinforcement. Elasto-plastic material models with hardening should be used.

Constitutive models for concrete-reinforcement interaction. At the macro-level, simplified models can be used, taking into account tension stiffening effects. Limited attention is devoted to modelling slip and dowel action. These aspects should not be significant in the global behaviour of a structure and are more related to details near the USL load level.

Finite elements for concrete. Elements with quadratic interpolation of the displacement field should be used. Typically, at least 6 elements over the height of a structural element should be used.

Finite elements for reinforcement. Embedded reinforcement elements are preferred; both embedded bars and grids can be used.

Prestressing. Prestressing should be applied taking into account prestress losses.

Existing cracks. Existing cracks in the structure should be taken into account whenever detailed information about the location and crack widths is available.

Loads. The design codes and national guidelines in force should be applied.

Boundary conditions. Unless the objective of the analysis is to study the detailed behaviour of the loading and support points, the supports and loading platens should be modelled such that local stress concentrations are reduced.

Loading. The loading sequence will contain an initial phase where dead weight, permanent loads and, if appropriate, prestressing is applied to the structure. Following the initial phase, the variable loads are increased until a clear failure mode is present or a significant load reduction was achieved.
Note that in the current report, for all cases, we are referring to experimental tests. For this reason, when safety formats are applied to obtain the design resistance, we are considering a load combination of action with a partial safety factor related to self-weight of 1.0.

Equilibrium iterations. Equilibrium between internal and external forces should be achieved iteratively using a Newton-Raphson method with arc-length procedure. Preferably an energy-norm together with a force-norm should be used.

All analyses have been performed with Diana 9.4.4.

2.3 Nonlinear finite element limit state verifications

Serviceability limit states. As requested by current codes (EC2, MC2010) serviceability limit states verifications must be performed as post-analysis checks. For the crack opening calculation, the average strain values are obtained from the analysis, whereas crack spacings are obtained from codes.

Ultimate limit states. Three alternative methods to obtain the design resistance from the non-linear finite element analysis: the Global Resistance Factor method (GRF), the Partial Factor method (PF) and the Estimate of Coefficient of Variation or resistance method (ECOV).

3 Case PB1: Leonhardt, Koch et al. (1973)

The first analysed case is a prestressed beam IP1 from the experiments of Leonhardt. In these experiments a total of ten beams were tested. Beam PB1 (IP1 in experiments) is selected as case study due to its flexural-compressive failure mechanism.

3.1 Experimental setup and results

Geometry

The beam has a total length of 7.0m, a span of 6.5m, a depth of 0.9m and a variable thickness of the web. The geometry, cross-sections, experimental set-up and reinforcement layout are presented in Figure 3-1 and Figure 3-2. The beam is reinforced in the longitudinal direction with bars ϕ8 and ϕ14 and non-symmetric stirrups ϕ16 on the left hand side and ϕ12 on the right hand side spaced 140mm.
The prestressing reinforcement consists of 2 post-tensioned tendons prestressed at both sides made of 12Φ12.2 strands each; the initial stress in each tendon is equal to 635 MPa. The assumed cover of 20 mm is considered.

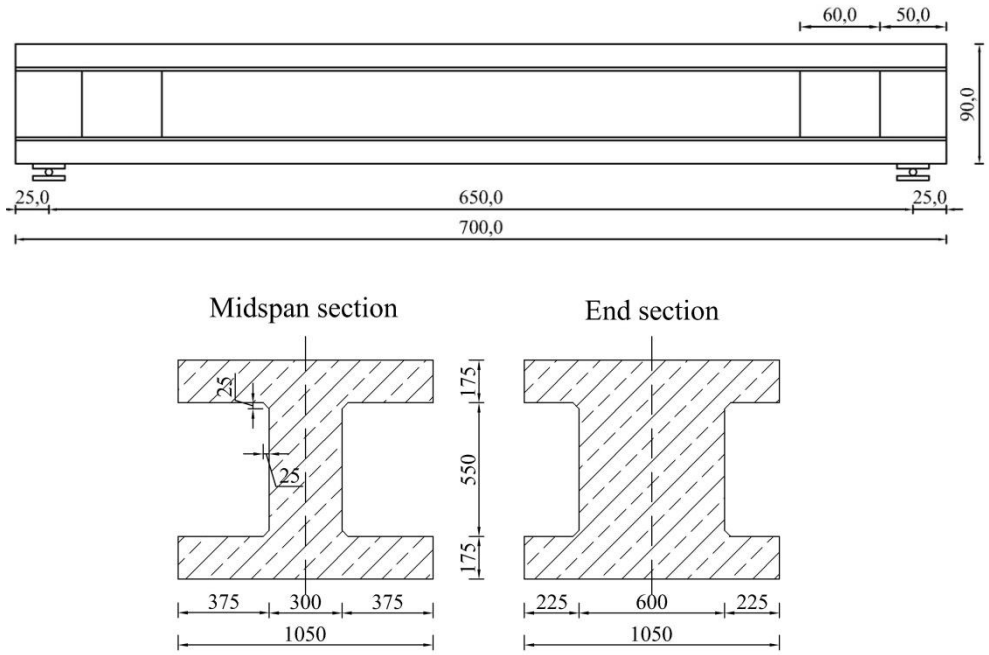

Figure 3-1 Case PB1. Elevation and cross-sectional details (dimensions in cm)(Leonhardt et al. 1973)

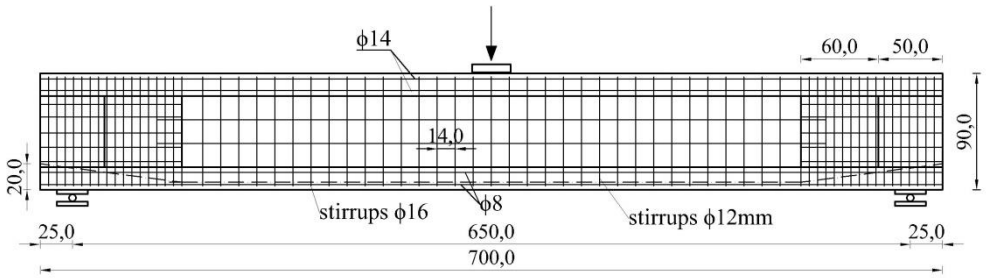

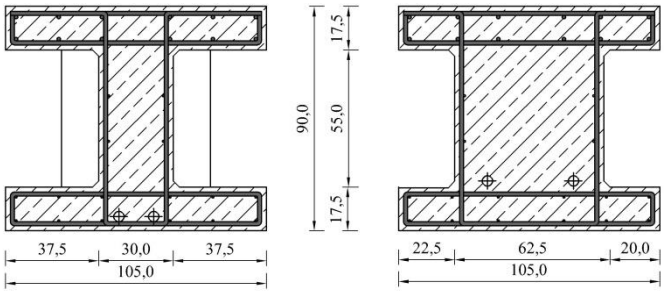

Figure 3-2: Case PB1. Reinforcement (dimensions in cm) (Leonhardt et al. 1973)

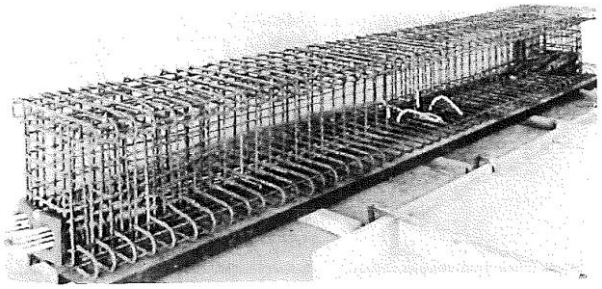

Figure 3-3: Case PB1. Reinforcement cage and prestressing cables (Leonhardt et al. 1973)

Material Properties

Concrete and reinforcement properties as given in references are outlined in Table 3-1.

Table 3-1: Case PB1. Concrete and reinforcement properties

Concrete properties				
f_{cm} (N/mm^2)	$f_{ctm,sp}$ (N/mm^2)	E_c (N/mm^2)	d_{max} (mm)	
25.3	2.4	26675	22	
Reinforcement properties				
Bar	Φ (mm)	A_s (mm^2)	E_s (N/mm^2)	f_{ym} (N/mm^2)	f_{tm} (N/mm^2)
Φ12	12.0	113	203000	500	611
Φ16	16.0	201	195000	400	512
Φ8	8.0	50	197000	460	567
Φ14	14.0	154	207000	397	517
Φ12.2	12×12.2	12×117	207000	1225	1363

Loading and Boundary Conditions

Loading and boundary conditions of the experimental setup are shown in Figure 3-4 and Figure 3-5. The force unit used in the reference is Mp (megaponds) which is approximately equivalent to 9.086 kN. The prestressing was applied at a load level of 995 kN (101.5 Mp) at each cable and after the losses the measured prestressing was equal to 891 kN in each cable. The counteracting point load equal to 196kN (20Mp) was applied simultaneously with prestressing of the tendons. Subsequently, the beam was subjected to 3 point bending until failure.

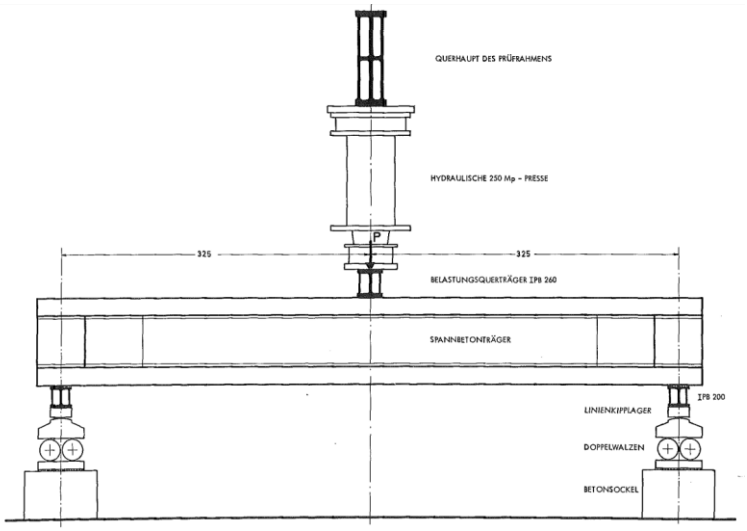

Figure 3-4: Case PB1. Loading and boundary conditions (Leonhardt et al. 1973)

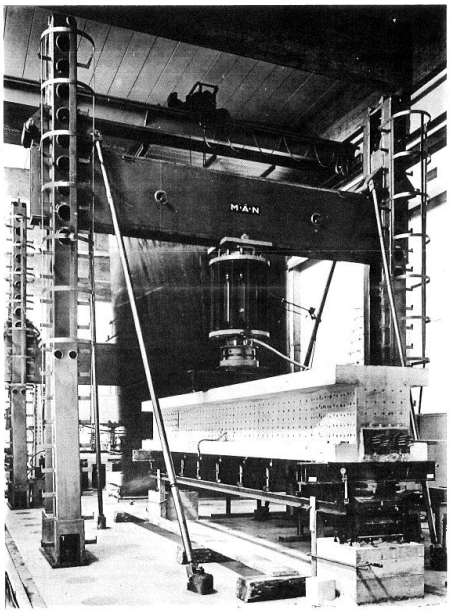

Figure 3-5: Case PB1. Experimental setup (Leonhardt et al. 1973)

Experimental Results

At the load equal to 1897.5 kN (193.5Mp) no further loading was possible and the beam exhibited a flexural-compressive failure mode. In Figure 3-6 the experimental crack pattern is shown at a load equal to 1765 kN (180 Mp). The development of the crack pattern is shown in Figure 3-7. The measured deflections at various points across the span are shown in Table 3-2. The load-deflection curve of the center of the beam (point D0) is shown in Figure 3-8.

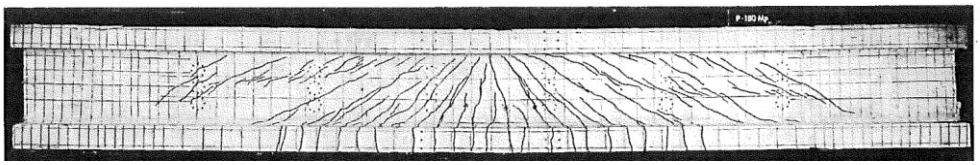

Figure 3-6: Case PB1. Crack pattern at load 1765 kN (Leonhardt et al. 1973)

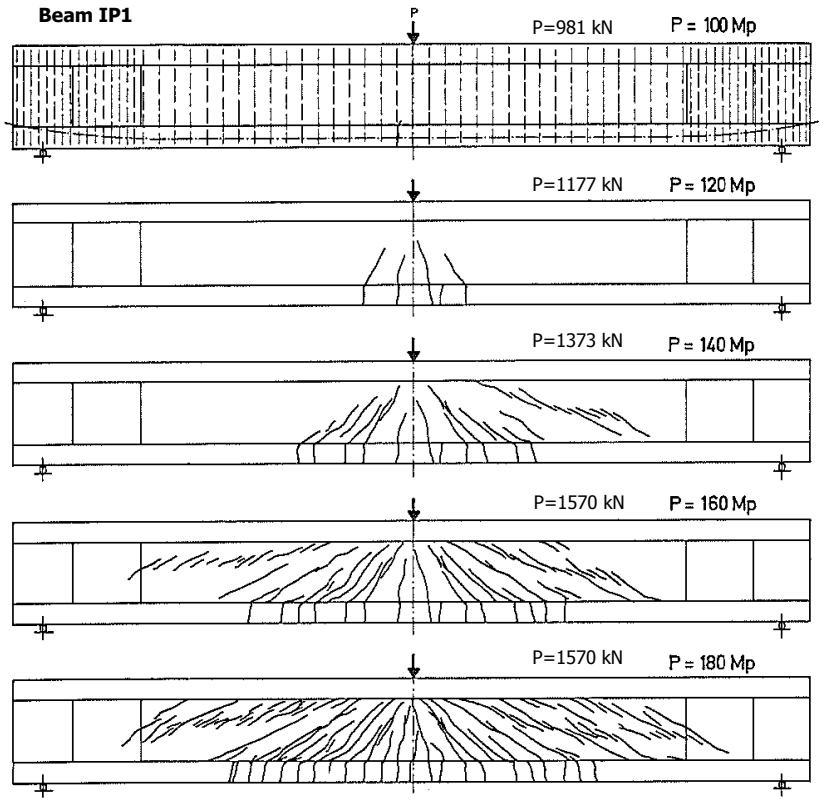

Figure 3-7: Case PB1. Development of the crack pattern during the experiment (Leonhardt et al. 1973)

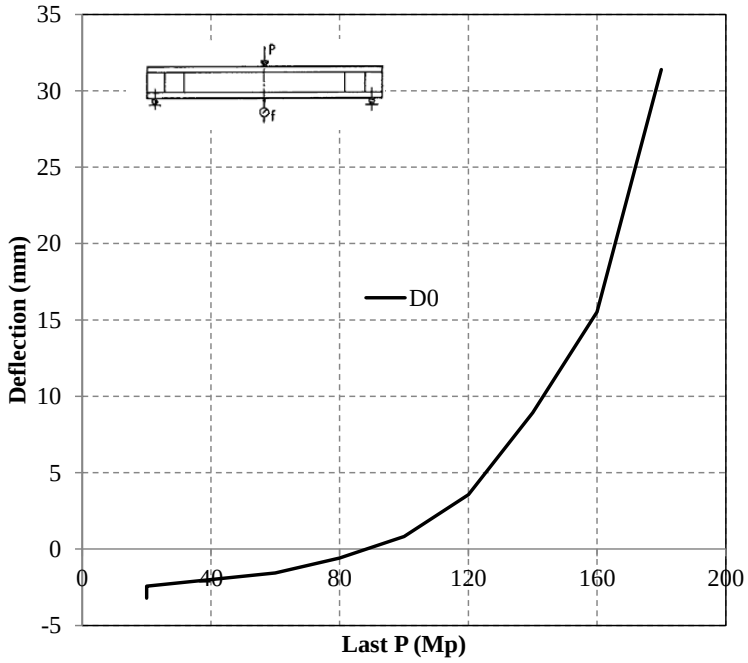

Figure 3-8: Case PB1. Load-deflection of point D0

Table 3-2: Case PB1. Measured deflection at various points across the span (Leonhardt et al. 1973)

LAST P Mp	D3ℓ $\bar{x}$ = 2,437	D2ℓ $\bar{x}$ = 1,625	D1ℓ $\bar{x}$ = 0,812	D0 $\bar{x}$ = 0	D1r $\bar{x}$ = 0,812	D2r $\bar{x}$ = 1,625	D3r $\bar{x}$ = 2,437
20	- 1,60	- 2,50	- 3,00	- 3,22	- 2,96	- 2,52	- 1,59
20	- 1,31	- 2,01	- 1,31	- 2,43	- 2,27	- 2,01	- 1,35
60	- 1,02	- 1,45	- 1,49	- 1,56	- 1,48	- 1,40	- 1,02
80	- 0,68	- 0,82	- 0,61	- 0,59	- 0,66	- 0,75	- 0,63
100	- 0,20	0,09	0,67	0,82	0,62	0,12	- 0,24
120	0,65	1,68	2,95	3,56	2,93	1,67	0,60
140	2,17	4,70	7,52	8,92	7,71	4,76	1,94
160	4,03	8,41	13,28	15,53	13,41	8,42	3,62
180	8,39	17,23	25,79	(31,39)	25,93	17,48	8,16

3.2 Analytical analysis

In Figure 3-9 the load configuration at failure is depicted.

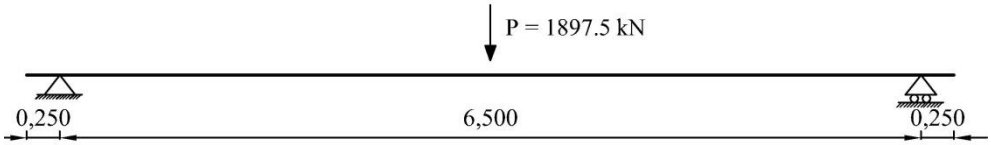

Figure 3-9: Case PB1. Load configuration at failure (force in kN, dimensions in m)

Load case 1:

- self-weight:

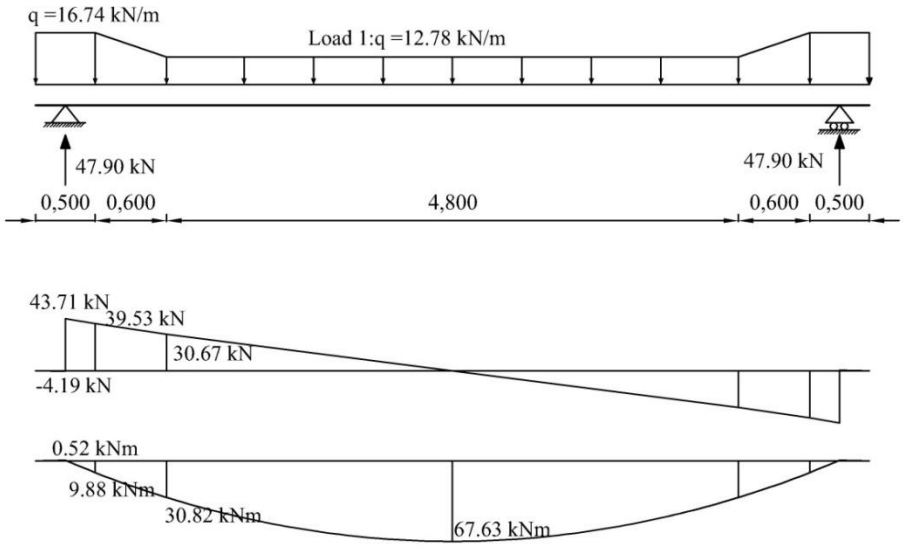

Figure 3-10: Case PB1: Load case 1: self-weight. Internal forces (dimensions in m)

- prestressing

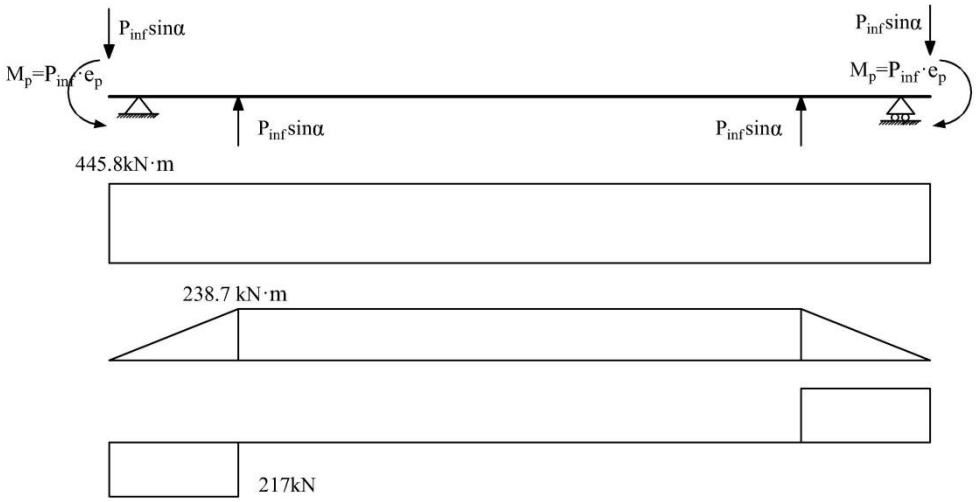

Figure 3-11: Case PB1: Load case 1: prestressing. Internal forces

- Counteracting point load

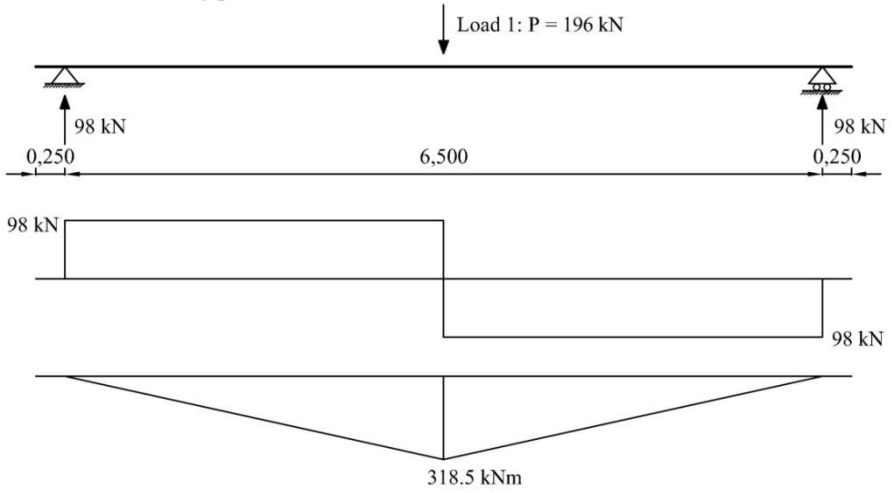

Figure 3-12: Case PB1. Load case 1: Counteracting point load: Internal forces

Load case 2: point load

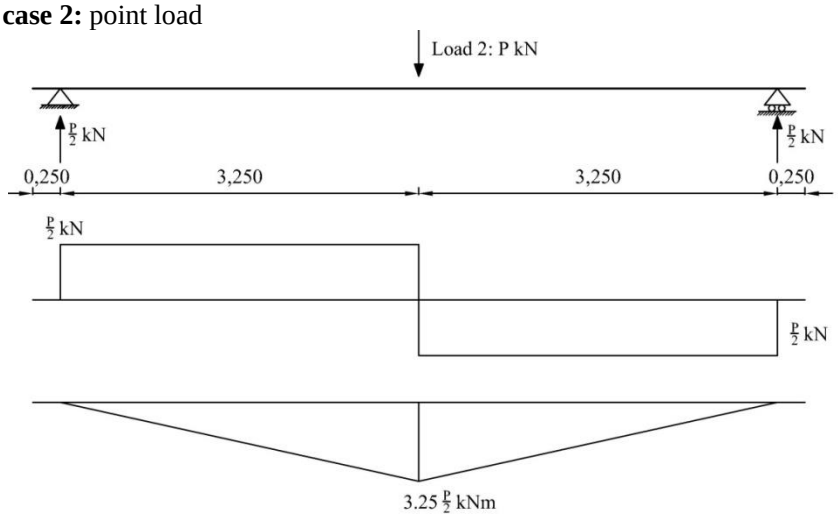

Figure 3-13: Case PB1. Load case 2: internal forces (dimensions in m)

Bending moment resistance:

The height of compression zone is calculated assuming a bilinear stress block and elastic-plastic relationship for reinforcing and prestressing steel. The partial safety factors were taken as: 1.15 for reinforcement and prestressing steel and 1.5 for concrete. The compression zone was determined from the horizontal force equilibrium assuming yielding strains in steel in the top and bottom flanges as well as yielding of one row of steel in the web; see figure below

$$A_{SteelBottomFlange} f_{yd} + A_{SteelWeb} f_{yd} + A_{SteelWeb} \varepsilon_s E_s + A_p \sigma_{p,\inf} + A_p (f_{yd} - \sigma_{p,\inf}) = F_c + A_{SteelTopFlange} f_{yd}$$

The resulting height is $x_{CompZone} = 337mm$

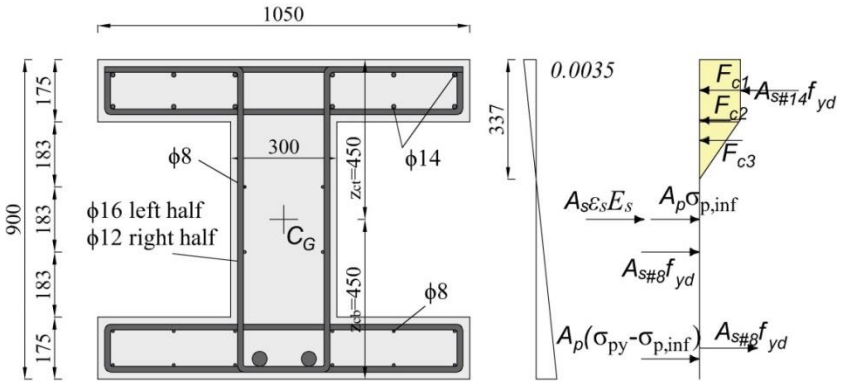

Figure 3-14: Case PB1: Determination of design bending moment resistance

Ultimate moment resistance was calculated around the centroidal axis.

$$F_c(z_{ct} - y) + A_{SteelTopFlange} f_{yd}(z_{ct} - c_{SteelTop}) + A_{SteelBottomFlange} f_{yd}(z_{cb} - c_{SteelBottom}) +$$
$$A_{SteelWeb} f_{yd}(h/2 - 175mm - 183mm) + A_{SteelWeb} \varepsilon_s E_s (175mm + 2 \times 183mm - h/2) +$$
$$+ A_p (f_{yd} - \sigma_{p,\inf})(h/2 - 57mm) = 2389kN \times 0.347m + 577.83kN \times (0.45m - 0.088m) + 2$$
$$17.4kN \times (0.45m - 0.088m) + 0.391kNm + 3.33kNm + 926.1kN \times (0.45 - 57mm) = 1484kNm$$

The maximum load that the beam can carry follows from the summation of all the internal forces from loads, Figure 3-10-Figure 3-13 and equating them to the bending moment resistance.

$$67.63kNm - 445.8kNm - 238.7kNm + 318.5kNm + 3.25m \times P/2 = 1484kNm \rightarrow P_{Rd} = 1097kN$$

Shear force resistance:

Resistance attributed to stirrups:

$$V_{Rd,s} = \frac{A_{sw}}{s} z f_{ywd} \cot(\theta) = \frac{226mm^2}{140mm} \times 754mm \times 393.8MPa \times \cot(29.67^\circ) = 841.4kN$$

Crushing of concrete compressive struts:

$$V_{Rd,c} = \frac{\alpha_{cw} b_w z \nu_1 f_{cd}}{\cot(\theta) + \tan(\theta)} = \frac{1.25 \times 300mm \times 754mm \times 11.54MPa}{\cot(29.67^\circ) + \tan(29.67^\circ)} = 842.06kN$$

Where the effective shear depth *z* was calculated according to (Model Code 2010):

$$z = \frac{z_s^2 A_s + z_p^2 A_p}{z_s A_s + z_p A_p}$$

Shear resistance after extraction of the shear force due to self-weight (considered at distance *d* from the support and equal around 30kN) is $841.4kN - 30kN = 811.4kN$. The maximum load *P* which the beam can withstand without failing in shear is: $P_{Rd} = 2 \times 811.4kN = 1622.8kN$.

From the comparison of the points corresponding to the bending and shear failures, it can be concluded that because $1097kN < 1622.8kN$, the beam fails in flexure.

In Table 3-3 the design value of beam resistance expressed in terms of applied load P_{Rd} obtained with the Eurocode 2 (CEN, 2005) and the Model Code 2010 (fib, 2013) expressions is highlighted.

Table 3-3: Case PB1. Design value of beam resistance expressed in terms of applied load P_{Rd}

P_{Rd} (EC2 – MC2010) (kN)
1097

3.3 Finite element model

Units

Units are N, mm.

Material models and parameters

The concrete model is based on a total strain rotating crack model with

- exponential softening in tension and parabolic behavior in compression,
- variable Poisson's ratio of concrete,
- reduction of compressive strength of concrete due to lateral cracking with a lower limit of 0.6 and
- increase in compressive strength due to lateral confinement according to the model proposed by Selby and Vecchio (Selby and Vecchio 1993).

The mechanical properties are summarized in Table 3-4. In the input file of the analysis, the G_F value has been decreased with a factor $\sqrt{2}$ in order to compensate for an underestimation of the crack band width for cracks with an inclination angle of 45 degrees, $G_{F,reduced} = 0.131/\sqrt{2} = 0.093$. The uniaxial stress-strain curve is shown in Figure 3-15.

The model for the reinforcement bars and stirrups is based on hardening plasticity. Geometrical and mechanical properties of reinforcement are summarized in Table 3-1. The stress-strain curve of the bars Φ8 is plotted in Figure 3-16.

Table 3-4: Case PB1. Constitutive model parameters for concrete

	f_{cm} (N/mm^2)	f_{ctm} (N/mm^2)	E_c (N/mm^2)	v	G_F (Nmm/mm^2)
Mean measured values	25.3	2.16**	26675	var	0.131*

*Not specified in reference; estimated according to Model Code 2010 (fib, 2013)

**Estimated from the mean splitting tensile strength of concrete as $f_{ctm} = 0.9 f_{ctm,sp}$ according to Eurocode 2 formulation (CEN, 2005).
According to Model Code 2010 (fib, 2013) the mean tensile strength of concrete can be estimated from the mean tensile strength of concrete as $f_{ctm} = 1\times f_{ctm,sp}$; hence reasonable values of mean tensile strength of concrete used in calculation range from $0.9 f_{ctm,sp}$ and $1\times f_{ctm,sp}$

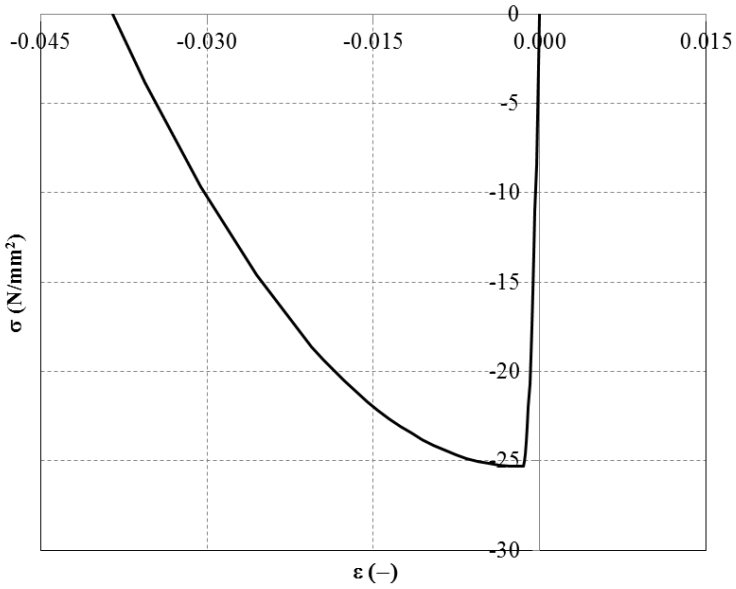

Figure 3-15: Case PB1. Stress-strain curve for concrete

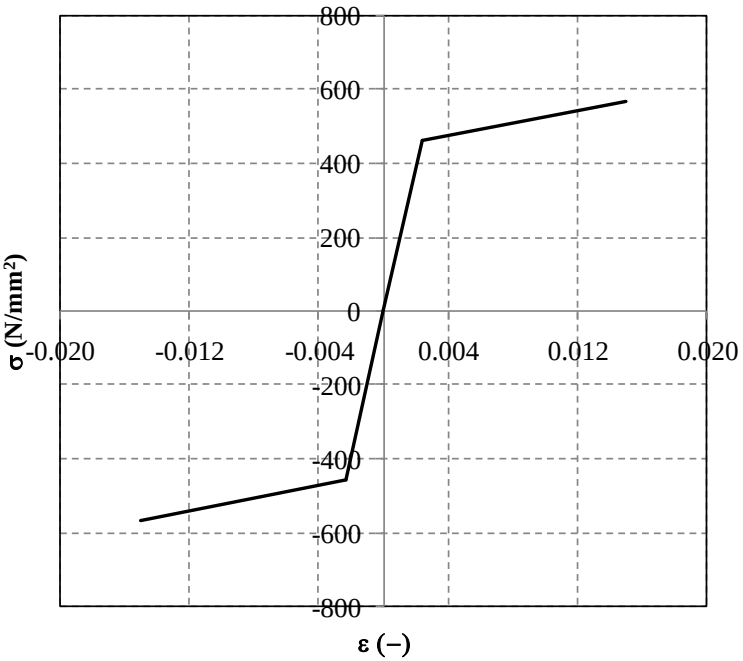

Figure 3-16: Case PB1. Stress-strain curve adopted for bars Φ8

For the steel plates a linear elastic behavior is assumed, see Table 3-5.

Table 3-5: Case PB1. Steel plates properties

E (N/mm²)	ν
200000	0.3

Interface elements were applied between the steel plates and the concrete beam at the supports and at the loading location. The interface stiffness was derived on the basis of concrete properties. The total thickness of interface elements equals 1 mm.

A bilinear behavior in the normal direction (see Figure 3-17) and a linear elastic relation in the shear direction were assumed. The normal stiffness in tension and the stiffness in the shear direction were taken as almost equal to zero. For stableness of the analysis horizontal displacements of one pair of nodes across the interface elements of support plates and loading plate were tied. The mechanical properties of the interface elements are summarized in Table 3-6.

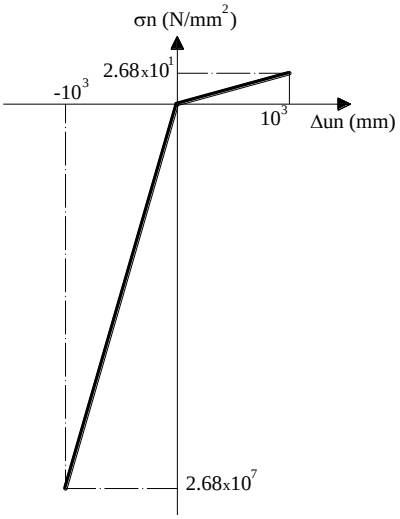

Figure 3-17: Case PB1. Traction-displacement diagram in normal direction for interfaces

Table 3-6: Case PB1. Interface properties

$K_{nn\ in\ tension}$ (N/mm³)	$K_{nn\ in\ compression}$ (N/mm³)	K_t (N/mm³)
2.68E-02	2.68E+04	2.68E-02

Element types and finite element mesh

To discretize concrete beam, 8-node membrane elements (CQ16M) with a full integration scheme (3x3) were used. The average element size is 50×55 mm². The reinforcement bars and stirrups were modelled with embedded truss elements with two Gauss integration points along the axis of the element and the assumption of perfect bond. For the steel plates 8-node membrane elements (CQ16M) were used. The 6-node interfaces elements have three Lobatto integration points.
The dimensions of the beam and the transversal cross section used in the numerical analyses are given in Figure 3-18 and Figure 3-19 respectively.

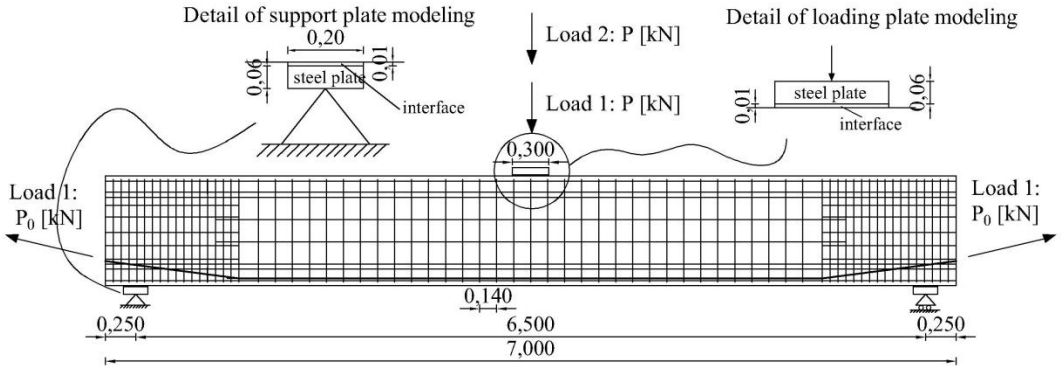

Figure 3-18: Case PB1. Dimensions adopted for the beam (in m)

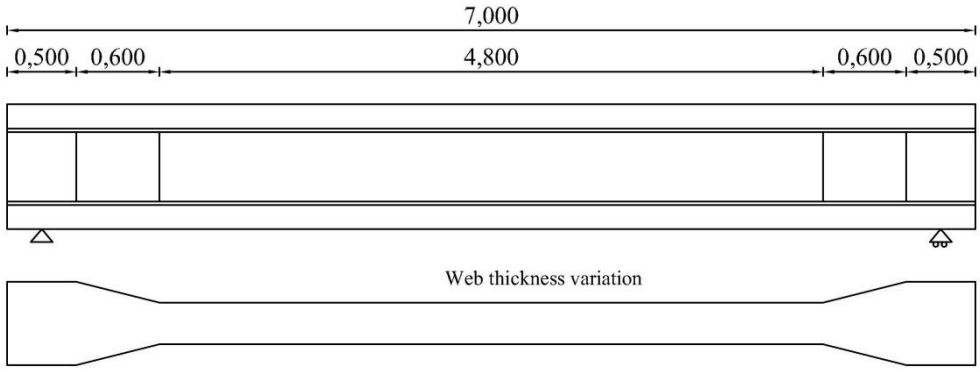

(a)

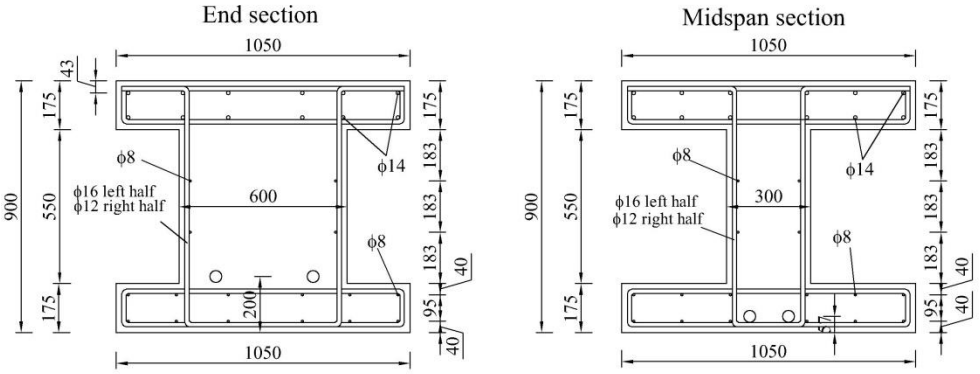

(b)

Figure 3-19: Case PB1. (a) Web thickness variation along length of the beam (dimension in mm) (b) Dimensions adopted for the transversal cross section of the beam (in mm)

The mesh of the beam is presented in Figure 3-20(a). The web thickness variation along the length of the beam was modeled as plotted in Figure 3-20(b). The groups name used to model the web thickness variation, starting from the end to the middle of the beam are: WEB_RING, WEB_VA, WEB_VB, WEB_VC, WEB_VD, WEB_VE, WEB_VF, WEB_VG, WEB_VH, WEB_VI, WEB_VL, WEB_VM and WEB_VN. The different materials are indicated with different colors in Figure 3-20(c).
Different groups of elements were generated to distinguish the concrete elements that can crush during the analyses and the steel elements that can yield during the analysis. In that way these groups of elements can be monitored during the analysis in order to determine the failure mode. For monitoring yielding of steel, groups “REBTOPF14”, “REBWEBF8”, “REBBOTTF8”, “STIRRLEFTF16”, “STIRRRIGHTF12”, “STRANDS” are created and indicated in Figure 3-21(a). Figure 3-21 shows the groups of elements named CRUSHING and SHEAR, used for tracking the inelastic behavior of concrete in compression. The group of elements named CRUSHING has a length equal to 5 times the length of the loading steel plate and a depth equal to the length of the loading steel plate, whereas the group of element named SHEAR has a length equal to the space between the end of the loading plate and the end of the support plate and a depth equal to the distance between upper and lower reinforcement.

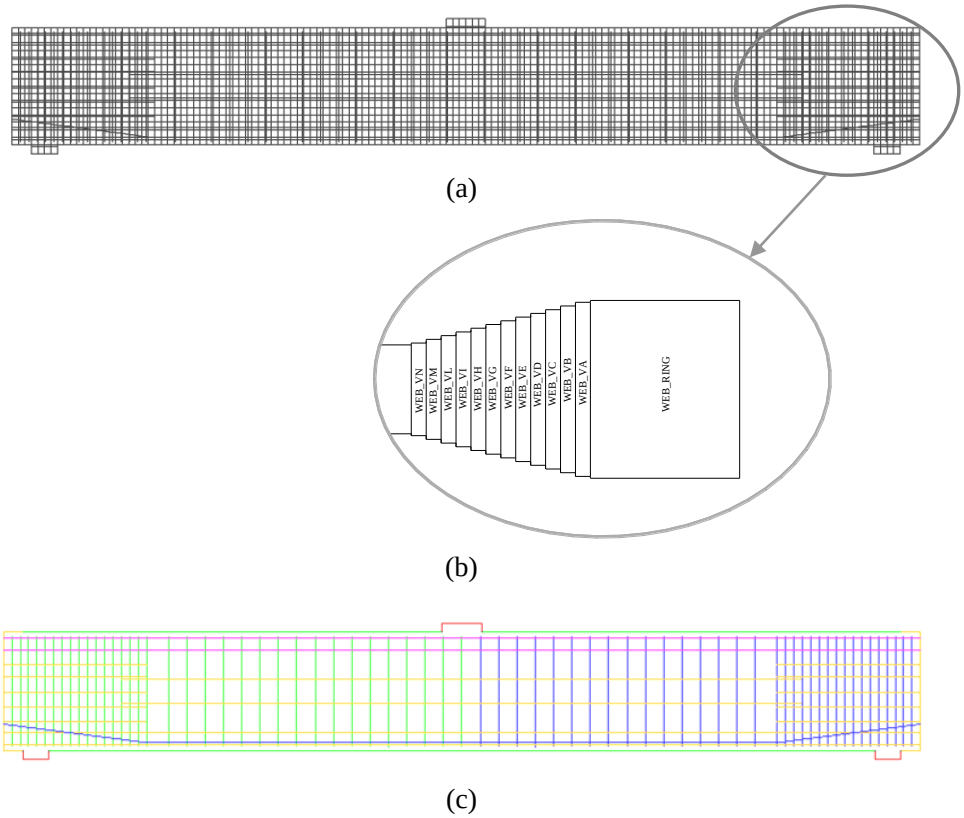

Figure 3-20: Case PB1. (a) Mesh, (b) modeling of web thickness variation, (c) material sets

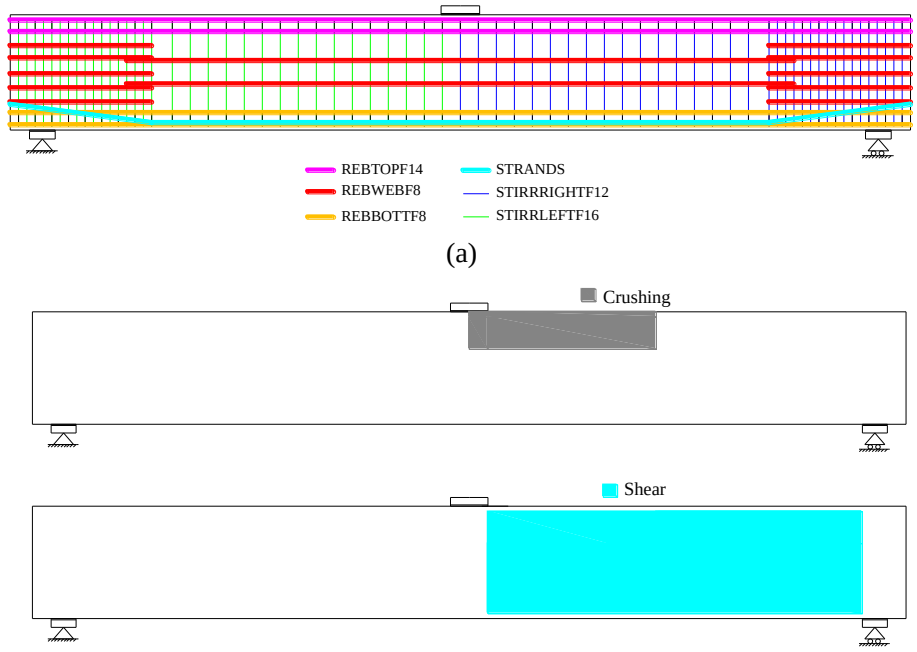

Figure 3-21: Case PB1. Groups of steel elements monitoring (a) yielding of reinforcement, (b) inelastic behavior of concrete

Boundary conditions and loading

Boundary condition are applied to nodes of steel plates; translation along *x* axis and *y* axis at a single node of the left steel plate (support 1) and translation along *y* axis at single nodes of the right steel plates (support 2) are constrained, Figure 3-22.
In Load case 1, dead load q(1), pre-stress [$P_0(1)$] and a concentrated load P [$P_1(1)$] at the middle node of the loading plate equal to 196×10^3 N to counteract the effect of the post- tensioning are applied.
In Load case 2 a concentrated load P [P(2)] applied at the middle node of the loading plate as a unit load of 4×10^3 N is added to load case 1, Figure 3-22.

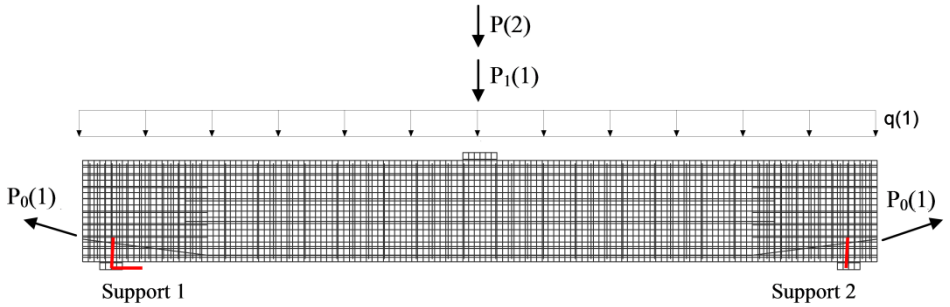

Figure 3-22: Case PB1. Boundary conditions and load cases 2

Load increments and convergence criteria

Load case 1 was applied in a single step. The regular Newton-Raphson method was used.
Load case 2 was applied with automatic adaptive load increments based on energy. The upper limit of the incremental load factor was set to 10. The lower limit of the incremental load factor equaled 5. The maximum number of steps was 170. Arc-length control was applied based on the translation along *y* axis of node 284 ("indirect displacement control"), Figure 3-23. The analysis continues even if the convergence criteria are not satisfied. The convergence tolerances are equal to 1×10^{-3} and 1×10^{-2} for energy and forces respectively. A maximum of 50 iterations is used.

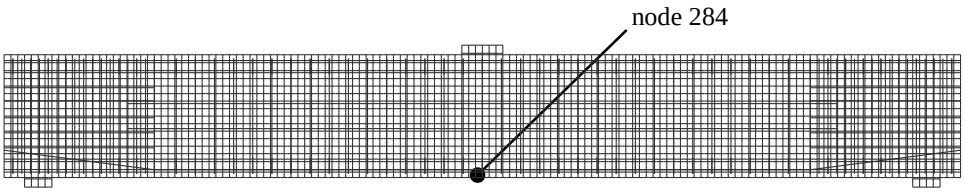

Figure 3-23: Case PB1. `Indirect Displacement control' technique applied referring to node 284

3.4 Nonlinear finite element analysis

Load deflection

The load-deflection curve of the mid-span point is presented in Figure 3-24. In this figure the values of applied load corresponding to the beginning of yielding of bars, yielding of stirrups placed at the right side, yielding of tendons and crushing of concrete are highlighted. The onset of crushing of concrete is defined as the moment at which the first integration point reaches a minimum principal strain value equal to -3.5‰.
For load case 2 the peak load is defined as the highest load step where the energy norm ratio satisfies the fixed tolerance of 1×10^{-3}. The convergence behavior is quite poor after reaching the peak load. After step 137, the analysis continues even if the energy convergence criteria are not satisfied within the maximum number of iterations equal

to 50. The post peak branch of the load- deflection curve is for this reason plotted with a dash-dotted line.

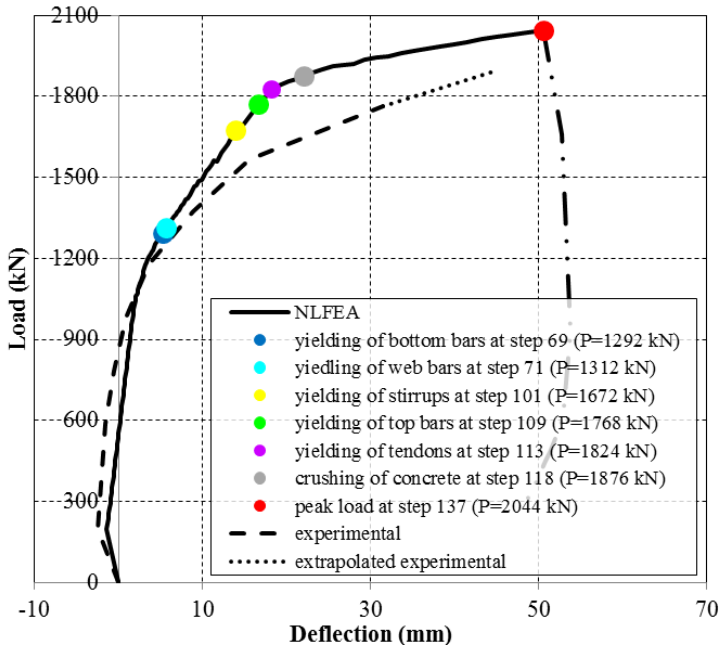

Figure 3-24: Case PB1. Load-deflection curve

Convergence behavior

For most steps convergence is reached on the basis of the energy criterion, Figure 3-25 and Figure 3-26. For load case 2, the energy norm ratio satisfies the fixed tolerance of 1×10^{-3} for all the steps of the analysis until to the peak load, while the force norm ratio is higher than the fixed tolerance for most of the steps. In Figure 3-25 and Figure 3-26, the red circle indicates the peak load position on the graph.

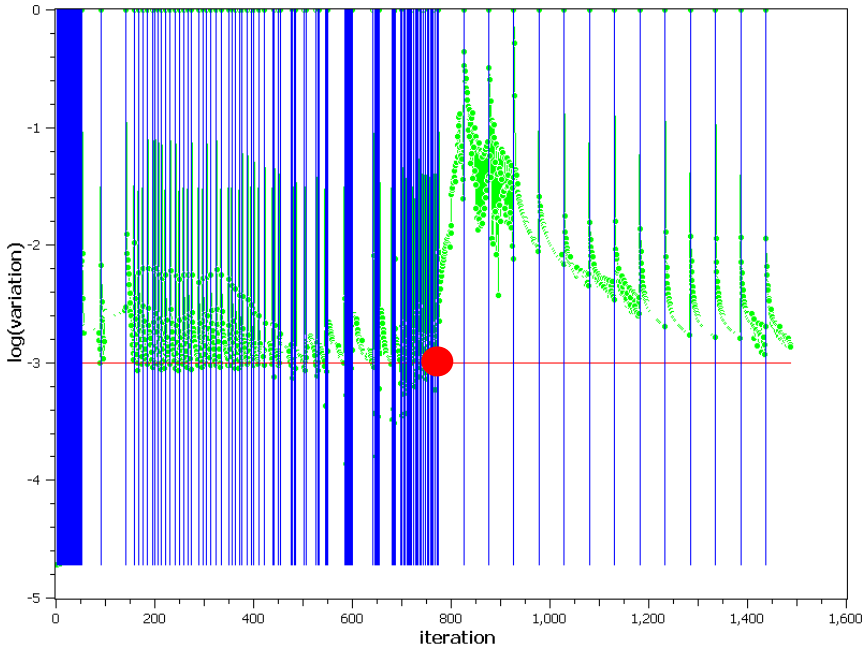

Figure 3-25: Case PB1. Evolution of the energy norm (blue lines indicate steps, red line indicates tolerance, green points indicate iterative results)

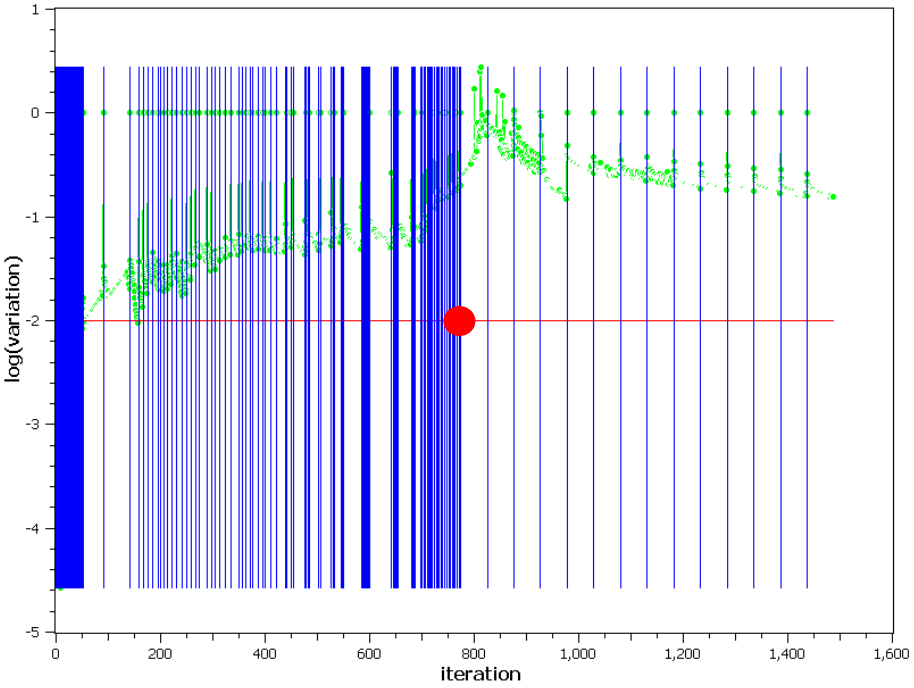

Figure 3-26: Case PB1. Evolution of the force norm (blue lines indicate steps, red line indicates tolerance, green points indicate iterative results)

Strains

Figure 3-27 shows the crack strain values at the peak load at step 137.

The first crack strain value plotted in Figure 3-27, equal to 0.00081, corresponds to the ultimate crack strain value calculated as $\varepsilon_{t,u} = \frac{G_F}{h_{eq} \times f_{ctm}}$ (in this case $h_{eq} = \sqrt{2}h$), while the third crack strain value, equal to 0.0038, is the crack strain value corresponding to 1% of f_{ctm}. An intermediate crack strain value was added in the contour plot.

In Figure 3-28 the minimum principal strain values at the peak load, at step 137, is shown. The first minimum principal strain value presented in Figure 3-28, equal to -0.00032, corresponds to the elastic principal strain value $\varepsilon_{c,el} = \frac{f_{cm}}{3 \times E_c}$; the second minimum principal strain value plotted in Figure 3-28, equal to -0.0016, corresponds to the peak strain value $\varepsilon_{c,p} = -\frac{5}{3}\frac{f_c}{E}$ while the last minimum principal strain value, equal to -0.0385 is the crushing strain value calculated as $\varepsilon_{c,u} = \varepsilon_{c,p} - \frac{3G_C}{2 \times h \times f_{cm}}$. Two intermediate minimum principal strain values have been added between $\varepsilon_{c,p}$ and $\varepsilon_{c,u}$.

From the crack pattern depicted through the contour plot of crack strains at the peak load, it can be observed that the major flexural cracks are open – stress free, hugely exceeding the value of the ultimate crack strain. In addition to that, based on the magnitude of compressive strains at the location of the loading plate (Figure 3-27), concrete undergoes compressive softening. Consequently, from the above considerations, it can be concluded that the beam fails due to flexure with crushing of concrete (flexural-compressive failure mode).

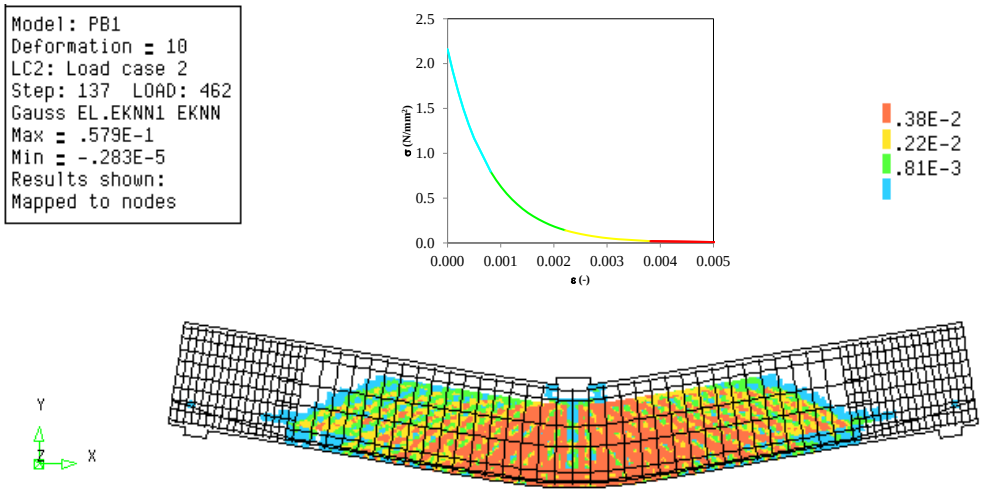

Figure 3-27: Case PB1. Crack strain values at step 137 (peak load)

Crushing is defined as soon as the softening branch in compression is reached. It is at the minimum principal strain of -1.6×10^{-3}.

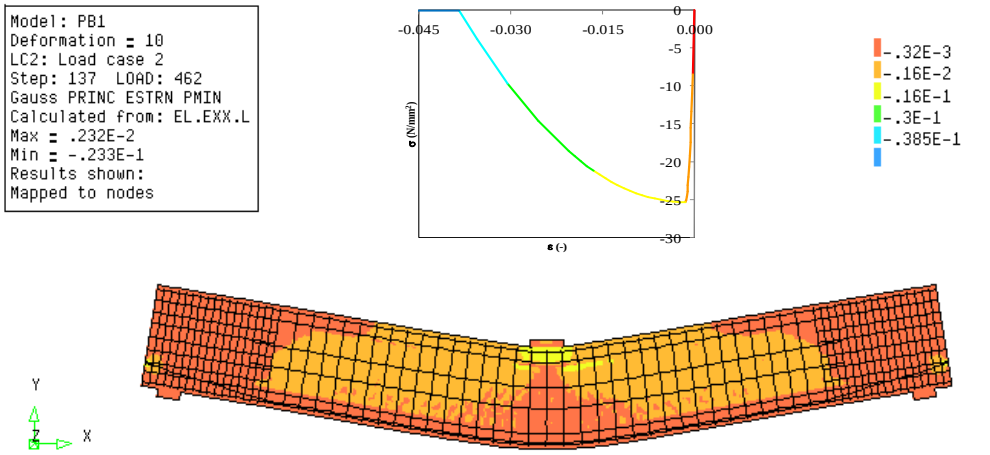

Figure 3-28: Case PB1. Minimum principal strain values at step 137 (peak load)

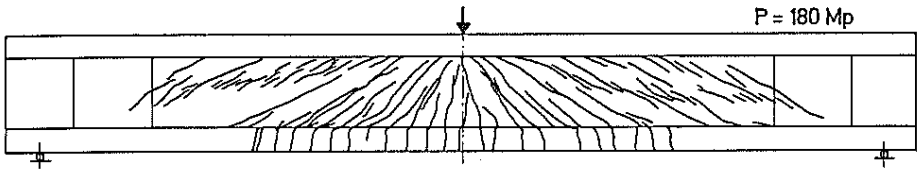

Figure 3-29: Case PB1. Experimental crack pattern at a load $P = 1765kN$

Yielding of the longitudinal rebars Φ8 located in the web and the bottom flange of the beam occurs when strains amount to $460MPa/197GPa = 2.33\times10^{-3}$. The yielding strain in the bars placed in the bottom flange is reached first at the load of 1292 kN (step 69) whereas the web reinforcement starts to yield at later step – 71 and the load equal to 1312 kN. Figure 3-30 shows yielding of the bottom and web bars a few steps after an onset of yielding (step 84).

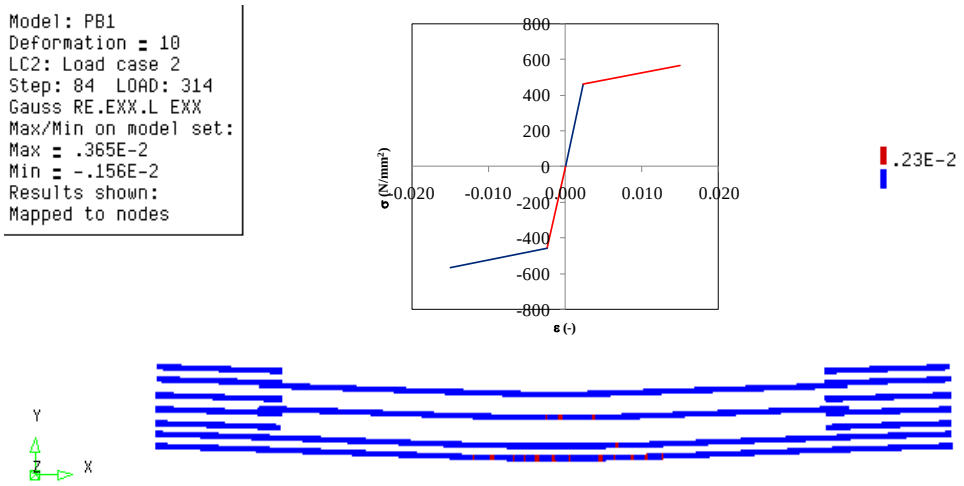

Figure 3-30: Case PB1. Yielding of bottom bars Φ8 at step 84

The yielding strain of stirrups Φ12 is equal to $500MPa/203GPa = 2.46\times10^{-3}$. Stirrups start to yield at the load equal to 1672 kN (step 101). In Figure 3-31, yielding of stirrups a few steps after the first yielding point is shown, at step 115.

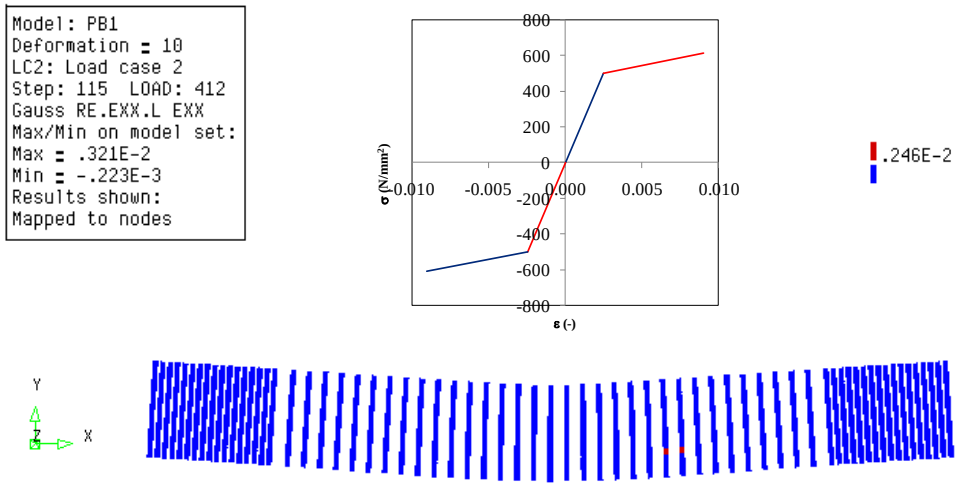

Figure 3-31: Case PB1. Yielding of stirrups Φ12 at step 115

The yielding strain of bars Φ14 placed at the upper flange of the beam is equal to $397MPa/207GPa = 1.9\times10^{-3}$. Bars placed in this region start to yield at a load equal to 1768 kN (step 109). Figure 3-32 shows the yielding of top bars a few steps after the yielding point – at step 117.

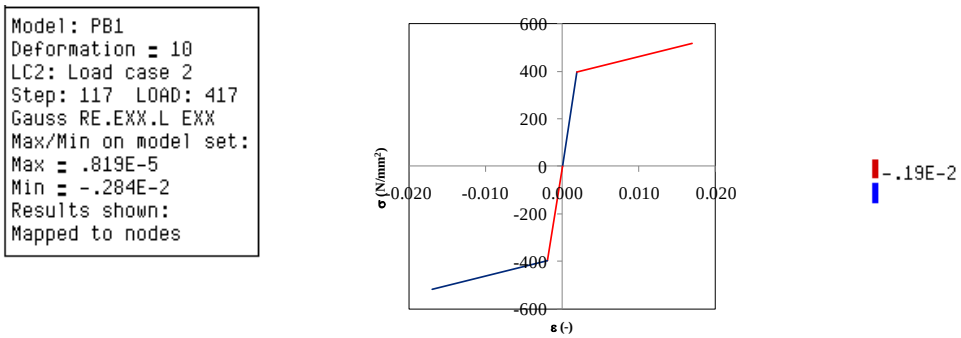

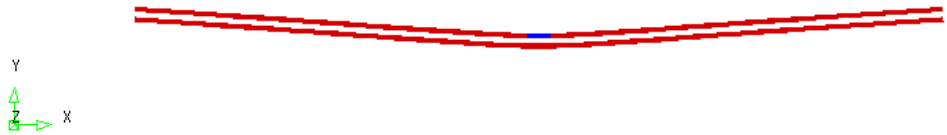

Figure 3-32 Case PB1. Yielding of top bars Φ14 at step 117

The yielding strain of prestressing tendons was assumed to be equal to $1225MPa/207GPa = 5.9\times10^{-3}$. The tendons start to yield at the load equal to 1824 kN (step 113). Figure 3-33 shows yielding of tendons at the yielding point at step 113.

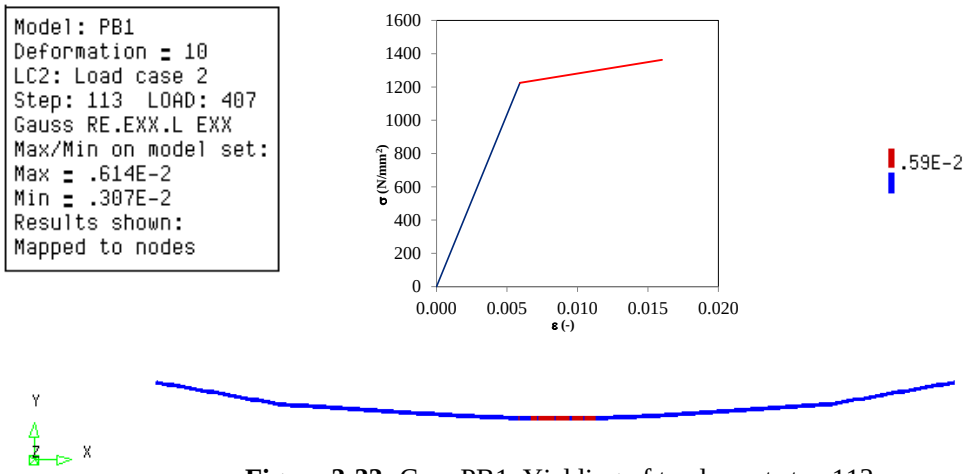

Figure 3-33: Case PB1. Yielding of tendons at step 113

Gauss point statistics

In Table 3-7 the number of cracking points, crushing points and yield points are reported at step 69 (yielding of bottom bars), at step 71 (yielding of web bars), at step 101 (yielding of stirrups placed in the right part), at step 109 (yielding of top bars), at step 113 (yielding of tendons), at step 118 (crushing of concrete) and at step 137 (peak load).

Table 3-7: Case PB1. Number of cracking points, crushing points and yield points

STEP	**69**	**ITERATIONS**		6		
GROUP NAME	**PLAST**	**PRV. PL**	**CRITIC**	**PLAST NEW**	**PRV.PL NEW**	**CRITIC NEW**
REBBOTTF8	1	0	0	1	0	0
TOTAL MODEL	1	0	0	1	0	0
CRACKING LOGGING SUMMARY						
GROUP NAME	**CRACK**	**OPEN**	**CLOSED**	**ACTIVE**	**INACTI**	**ARISES**
FL_INF	415	415	0	252	163	15
CRUSHING	22	22	0	16	6	1
WEB_RING	2	2	0	0	2	0
WEB	328	328	0	234	94	16
SHEAR	433	433	0	319	114	25
TOTAL MODEL	1102	1102	0	749	353	49
STEP	**71**	**ITERATIONS**		7		
GROUP NAME	**PLAST**	**PRV. PL**	**CRITIC**	**PLAST NEW**	**PRV.PL NEW**	**CRITIC NEW**
REBWEBF8	1	0	0	1	0	0
REBBOTTF8	1	0	0	0	0	0
TOTAL MODEL	2	0	0	1	0	0

CRACKING LOGGING SUMMARY						
GROUP NAME	**CRACK**	**OPEN**	**CLOSED**	**ACTIVE**	**INACTI**	**ARISES**
FL_INF	436	436	0	273	163	6
CRUSHING	26	26	0	20	6	2
WEB_RING	2	2	0	0	2	0
WEB	359	359	0	267	92	17
SHEAR	495	495	0	364	131	29
TOTAL MODEL	1211	1211	0	849	362	54

STEP	**101**	**ITERATIONS**		1		
GROUP NAME	**PLAST**	**PRV. PL**	**CRITIC**	**PLAST NEW**	**PRV.PL NEW**	**CRITIC NEW**
FL_SUP	35	0	0	3	0	0
CRUSHING	31	0	0	2	0	0
SHEAR	2	0	0	1	0	0
STIRRRIGHTF12	1	0	0	1	0	0
REBWEBF8	8	0	0	0	0	0
REBBOTTF8	37	1	0	4	0	0
TOTAL MODEL	107	1	0	10	0	0

CRACKING LOGGING SUMMARY						
GROUP NAME	**CRACK**	**OPEN**	**CLOSED**	**ACTIVE**	**INACTI**	**ARISES**
FL_INF	760	760	0	623	137	9
FL_SUP	2	2	0	2	0	0
CRUSHING	198	198	0	167	31	4
WEB_RING	2	2	0	0	2	0
WEB	1049	1049	0	869	180	14
SHEAR	1276	1276	0	1035	241	14
WEB_VL	2	2	0	2	0	1
WEB_VM	3	3	0	3	0	0
WEB_VN	5	5	0	5	0	0
TOTAL MODEL	2916	2916	0	2369	547	36

STEP	**109**	**ITERATIONS**		24		
GROUP NAME	**PLAST**	**PRV. PL**	**CRITIC**	**PLAST NEW**	**PRV.PL NEW**	**CRITIC NEW**
FL_SUP	28	13	0	0	13	0
CRUSHING	23	13	0	0	13	0
SHEAR	3	1	0	1	0	0
STIRRRIGHTF12	1	0	0	0	0	0
REBTOPF14	1	0	0	1	0	0
REBWEBF8	2	9	0	0	9	0
REBBOTTF8	39	22	0	1	19	0
TOTAL MODEL	89	58	0	3	54	0

CRACKING LOGGING SUMMARY						
GROUP NAME	**CRACK**	**OPEN**	**CLOSED**	**ACTIVE**	**INACTI**	**ARISES**
FL_INF	851	851	0	489	362	13
FL_SUP	3	3	0	1	2	0
CRUSHING	275	275	0	185	90	12
WEB_RING	2	2	0	0	2	0
WEB	1176	1176	0	649	527	33
SHEAR	1495	1495	0	796	699	33
WEB_VH	1	1	0	1	0	0
WEB_VI	2	2	0	2	0	0
WEB_VL	4	4	0	4	0	1
WEB_VM	4	4	0	4	0	0
WEB_VN	7	7	0	7	0	0
TOTAL MODEL	3332	3332	0	1821	1511	79

STEP	**113**	**ITERATIONS**		24		
GROUP NAME	**PLAST**	**PRV. PL**	**CRITIC**	**PLAST NEW**	**PRV.PL NEW**	**CRITIC NEW**
FL_SUP	34	11	0	1	11	34

CRUSHING	25	15	0	1	15	25
SHEAR	6	1	0	2	0	6
STIRRRIGHTF12	3	0	0	0	0	3
REBTOPF14	4	0	0	0	0	4
REBWEBF8	5	7	0	0	6	5
REBBOTTF8	51	13	0	0	7	51
STRANDS	12	0	0	12	0	12
TOTAL MODEL	130	47	0	15	39	130
CRACKING LOGGING SUMMARY						
GROUP NAME	**CRACK**	**OPEN**	**CLOSED**	**ACTIVE**	**INACTI**	**ARISES**
FL_INF	883	883	0	600	283	11
FL_SUP	5	5	0	3	2	0
CRUSHING	294	294	0	218	76	11
WEB_RING	2	2	0	0	2	0
WEB	1243	1243	0	769	474	40
SHEAR	1550	1550	0	977	573	27
WEB_VG	1	1	0	1	0	1
WEB_VH	2	2	0	2	0	0
WEB_VI	3	3	0	3	0	0
WEB_VL	4	4	0	4	0	0
WEB_VM	4	4	0	4	0	0
WEB_VN	8	8	0	7	1	0
TOTAL MODEL	3482	3482	0	2202	1280	75
STEP	**118**	**ITERATIONS**		2		
GROUP NAME	**PLAST**	**PRV. PL**	**CRITIC**	**PLAST NEW**	**PRV.PL NEW**	**CRITIC NEW**
FL_SUP	52	0	0	2	0	0
CRUSHING	52	0	0	2	0	0
SHEAR	16	1	0	3	0	0
STIRRRIGHTF12	5	0	0	0	0	0
REBTOPF14	10	0	0	0	0	0
REBWEBF8	21	0	0	0	0	0
REBBOTTF8	101	3	0	9	0	0
STRANDS	44	0	0	3	0	0
TOTAL MODEL	283	4	0	18	0	0
CRACKING LOGGING SUMMARY						
GROUP NAME	**CRACK**	**OPEN**	**CLOSED**	**ACTIVE**	**INACTI**	**ARISES**
FL_INF	925	925	0	719	206	7
FL_SUP	6	6	0	5	1	0
CRUSHING	309	309	0	257	52	5
WEB_RING	2	2	0	0	2	0
WEB	1326	1326	0	964	362	17
SHEAR	1622	1622	0	1225	397	19
WEB_VG	1	1	0	1	0	0
WEB_VH	2	2	0	2	0	0
WEB_VI	4	4	0	4	0	0
WEB_VL	4	4	0	4	0	0
WEB_VM	7	7	0	6	1	0
WEB_VN	9	9	0	7	2	0
TOTAL MODEL	3677	3677	0	2749	928	42
STEP	**137**	**ITERATIONS**		2		
GROUP NAME	**PLAST**	**PRV. PL**	**CRITIC**	**PLAST NEW**	**PRV.PL NEW**	**CRITIC NEW**
FL_SUP	61	10	0	2	1	0
CRUSHING	103	27	0	9	1	0
WEB	28	6	0	2	0	0
SHEAR	80	17	0	9	1	0
STIRRLEFTF16	17	2	0	5	1	0
STIRRRIGHTF12	92	0	0	10	0	0
REBTOPF14	17	0	0	1	0	0

REBWEBF8	82	0	0	5	0	0
REBBOTTF8	155	5	0	0	0	0
STRANDS	77	0	0	3	0	0
TOTAL MODEL	633	57	0	38	3	0
CRACKING LOGGING SUMMARY						
GROUP NAME	**CRACK**	**OPEN**	**CLOSED**	**ACTIVE**	**INACTI**	**ARISES**
FL_INF	1069	1069	0	839	230	3
FL_SUP	12	12	0	9	3	0
CRUSHING	341	341	0	276	65	4
WEB_RING	2	2	0	0	2	0
WEB	1547	1547	0	1174	373	9
SHEAR	1843	1843	0	1493	350	11
WEB_VE	2	2	0	2	0	1
WEB_VF	2	2	0	2	0	0
WEB_VG	4	4	0	4	0	0
WEB_VH	6	6	0	6	0	1
WEB_VI	7	7	0	7	0	1
WEB_VL	10	10	0	7	3	0
WEB_VM	12	12	0	7	5	0
WEB_VN	12	12	0	7	5	0
TOTAL MODEL	4258	4258	0	3323	935	22

3.5 Application of safety format

As proposed by the Model Code 2010 (fib, 2013) (section 7.11.3) safety formats for nonlinear analyses include three numerical methods denoted as GRF (Global Resistance Factor method), PF (Partial Factor method) and ECOV (Method of Estimation of a Coefficient Of Variation of resistance).
In Table 3-8 to Table 3-13, the properties of concrete and steel applied in the nonlinear analyses are summarized.

Table 3-8: Case PB1. Constitutive model parameters for concrete

	f_c (N/mm^2)	f_{ct} (N/mm^2)	E_c (N/mm^2)	ν	G_F (Nmm/mm^2)	G_C (Nmm/mm^2)
Mean measured	25.31	2.16	26675	var	0.131	32.65
Characteristic	17.31	1.51	25349	var	0.122	30.49
Mean GRF	14.72	1.80	24143	var	0.118	29.61
Design	11.54	1.01	22057	var	0.113	28.35

Table 3-9: Case PB1. Constitutive model parameters for reinforcing bars Φ12

	Φ (mm)	A_s (mm^2)	f_y (N/mm^2)	f_t (N/mm^2)	E_s (N/mm^2)	ε_{sy} (-)
Mean measured	12.0	113	500	611	203000	0.0025
Characteristic	12.0	113	452.87	553.41	203000	0.0022
Mean GRF	12.0	113	498.16	608.75	203000	0.0024
Design	12.0	113	393.80	481.23	203000	0.0019

Table 3-10: Case PB1. Constitutive model parameters for reinforcing bars Φ16

	Φ (mm)	A_s (mm^2)	f_y (N/mm^2)	f_t (N/mm^2)	E_s (N/mm^2)	ε_{sy} (-)

Mean measured	16.0	201	400	512	195000	0.0020
Characteristic	16.0	201	362.30	463.74	195000	0.0018
Mean GRF	16.0	201	398.53	510.11	195000	0.0020
Design	16.0	201	315.04	403.25	195000	0.0016

Table 3-11: Case PB1. Constitutive model parameters for reinforcing bars Φ8

	Φ (mm)	A_s (mm^2)	f_y (N/mm^2)	f_t (N/mm^2)	E_s (N/mm^2)	ε_{sy} (-)
Mean measured	8.0	50	460	567	197000	0.0023
Characteristic	8.0	50	416.64	513.56	197000	0.0021
Mean GRF	8.0	50	458.31	564.91	197000	0.0023
Design	8.0	50	362.30	446.57	197000	0.0018

Table 3-12: Case PB1. Constitutive model parameters for reinforcing bars Φ14

	Φ (mm)	A_s (mm^2)	f_y (N/mm^2)	f_t (N/mm^2)	E_s (N/mm^2)	ε_{sy} (-)
Mean measured	14.0	154	397	517	207000	0.0019
Characteristic	14.0	154	359.58	468.27	207000	0.0017
Mean GRF	14.0	154	395.54	515.10	207000	0.0019
Design	14.0	154	312.68	407.19	207000	0.0015

Table 3-13: Case PB1. Constitutive model parameters for strands

	Φ (mm)	A_s (mm^2)	f_y (N/mm^2)	f_t (N/mm^2)	E_s (N/mm^2)	ε_{sy} (-)
Mean measured	12×12.2	1404	1225	1363	207000	0.0059
Characteristic	12×12.2	1404	1109.53	1234.53	207000	0.0059
Mean GRF	12×12.2	1404	1220.49	1357.98	207000	0.0065
Design	12×12.2	1404	964.81	1073.50	207000	0.0046

In Figure 3-34 the load-deflection curves obtained with mean measured, characteristic, mean GRF and design values of material strengths are shown.

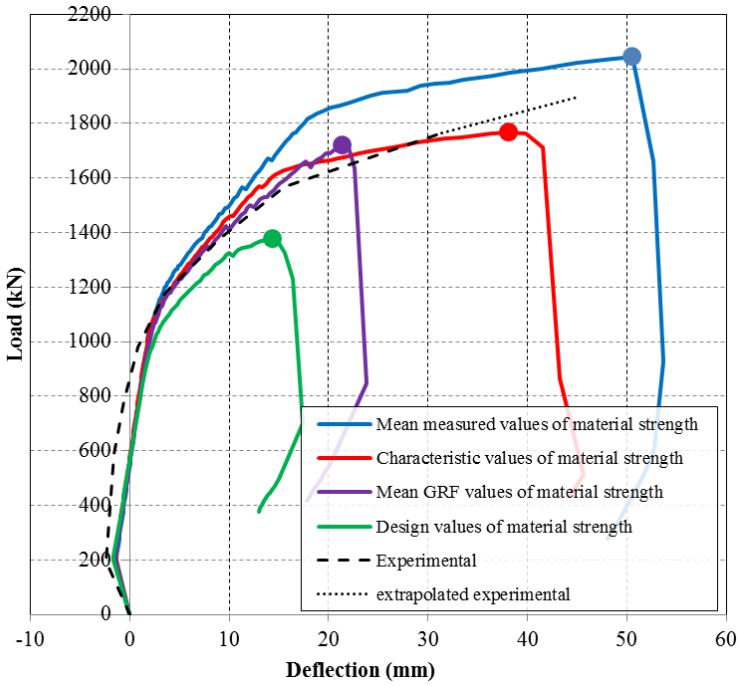

Figure 3-34: Case PB1. Load-deflection curves obtained with mean measured, characteristic, mean GRF and design values of material strength

The ultimate resistance of specimen PB1 was searched for with a use of analytical and numerical approaches. In Figure 3-35, the design values of beam resistance obtained with the designing codes and numerical analyses are compared. The presented results are expressed in terms of a percentage of the ultimate value of applied load from experiments. The analysis titled "no safety format" refers to the NLFE analysis carried out using mean measured materials properties therefore without application of safety coefficient.

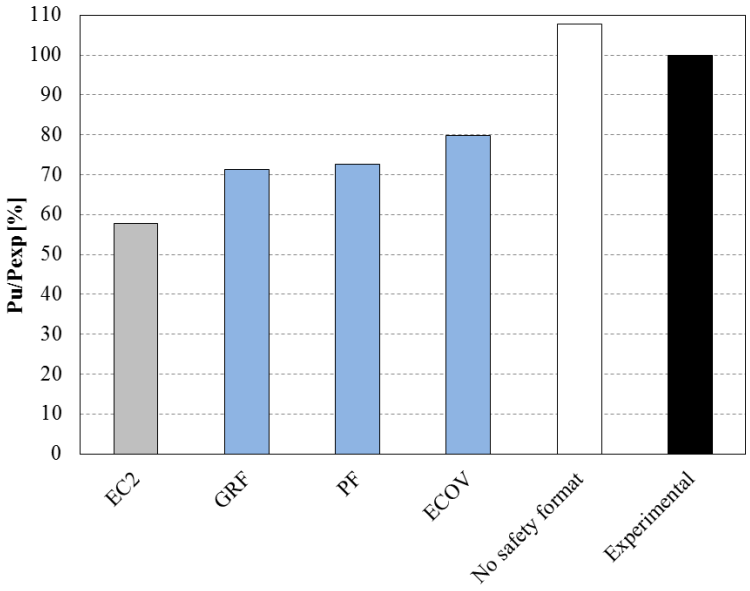

Figure 3-35: Case PB1. Analytical and numerical design values of beam resistance expressed in terms of a percentage of the experimental ultimate value of applied load, $P_{Exp} = 1897.5kN$

In Table 3-14 the design values of beam resistance, expressed in terms of applied load P_{Rd}, obtained from numerical and analytical procedures are outlined.

Table 3-14: Case PB1. Values of beam resistance, expressed in terms of applied load P_{Rd}

P_{Exp} (kN)	EC2,MC2010 (kN)	GRF (kN)	PF (kN)	ECOV (kN)	No Safety Formats (kN)
1897.46	1097	1352.36	1376.20	1513.77	2044.20

3.6 Parametric study on crack models

A parametric study was carried out by varying a number of sensitive parameters of the concrete constitutive model, such as the crack model, and the fracture energy of concrete in tension.

The material parameters implemented in NLFE analyses of the parametric study are listed in Table 3-15. Analyses 1 to 3 refer to the three analyses carried out with mean measured values of material strength and varying material parameters (crack model and tensile fracture energy) of a concrete constitutive model. The numerical models included a parabolic law in compression and an exponential law in tension for concrete as well as an elasto-plastic law with hardening for steel. All models exercised reduction of Poisson's ratio due to cracking.

A limit value of the concrete compressive strength reduction due to lateral cracking was adopted according to Vecchio et al. (Vecchio et al., 1986):

$$\beta_{\sigma,\min} = \frac{f_{c,red}}{f_{cm}} = 0.6$$

The influence of the used value of fracture energy of concrete in tension on the beam response was investigated by adopting the formulation proposed by Model Code 1990 (CEB-FIP, 1993) and the formulation proposed by Model Code 2010 (fib, 2013). The fracture energy of concrete in compression was considered for all analyses equal to $250G_F$ (Nakamura et al. 2001).

In the fixed crack model, a variable shear retention factor dependent on a mean aggregate size d_{aggr}, a crack normal strain ε_n and a crack bandwidth value h was used as follows from:

$$\beta = 1 - \left(\frac{2}{d_{aggr}} \right) \varepsilon_n h$$

In Figure 3-36 the load-deflection curves obtained from the parametric study are plotted. The peak load of each analysis is indicated with a circular marker. The peak load is defined in correspondence of the highest load step for which the energy norm ratio satisfies the fixed tolerance of 1×10^{-3}.The peak load values are reported in Table 3-15.

Table 3-15: Case PB1. Parametric study on crack models

Analysis	Total strain crack model	G_F	G_C	Peak load value (kN)
Analysis 1	rotating	MC2010	250 G_F	2044.20
Analysis 2	rotating	MC1990	250 G_F	2000.20
Analysis 3	fixed (β=variable)	MC2010	250 G_F	1948.20

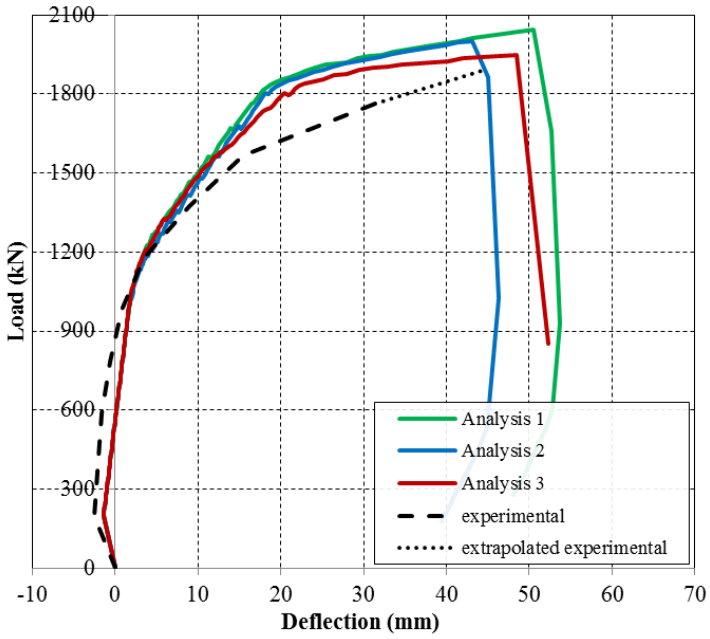

Figure 3-36: Case PB1. Parametric study on crack model

Comparing the models' response from analyses 1 and 2, one can see the influence of the adopted values of fracture energy of concrete in tension $G_{F,MC1990} = 0.078\,N/mm$ ($G_{F,MC2010} = 0.131\,N/mm$) and most importantly, the impact of the corresponding values of compression fracture energy. Due to the fact that the beam fails in bending accompanied with crushing of concrete, the fracture energy of concrete in compression plays a meaningful role on the ductility of the beam – especially on the peak and post-peak deformation. Further, from a comparison of analyses 1 and 3, it can be noted that the crack model (total strain rotating or fixed crack model) has a small influence on the beam response, both in terms of peak load and peak deformation. The experimental crack pattern and failure mode could be better reproduced when the rotating crack model was used.

3.7 Concluding remarks

The selected benchmark prestressed beam PB1 subjected to 3 point bending exhibited in laboratory tests a flexural-compressive failure mechanism at the ultimate applied load *P*=1897.5kN.

In order to simulate the experimental results, a FE model was created and studied in a number of NLFE analyses.The beam was modelled with a total strain rotating crack model, exponential softening in tension and parabolic behavior in compression, variable Poisson's ratio of concrete and reduction of compressive strength of concrete due to lateral cracking with a lower limit of 0.6. The model for the reinforcement bars and stirrups was based on hardening plasticity. The prestressing reinforcement consisted of 2 post-tensioned tendons prestressed with an initial effective stress of 635 MPa.

From NLFEA conducted with mean measured values of material strength, it was possible to obtain a flexural-compressive failure mechanism. The failure occurred at the peak value of the applied load of 2044.2kN and was characterized by crushing of concrete in the web and in the vicinity of loading plate accompanied by yielding of the web and bottom longitudinal reinforcement as well as yielding of stirrups.

Safety formats for nonlinear finite element analyses as proposed by the Model Code 2010 (fib, 2013) were applied to derive the design value of beam resistance expressed in terms of applied load. The design value of beam resistance obtained from safety

formats methods appeared to be higher than the design value of beam resistance obtained with analytical sectional analysis.
In the last part of the chapter, a sensitivity study was carried out. The study investigated the influence of different crack models and varying values of fracture energy of concrete in tension and equivalently in compression. Because the beam failed in bending with crushing of concrete, the response of the models is influenced primarily by input parameters related to compressive behaviour of concrete.
Based on the results it can be concluded that consistent and reliable results can be obtained by applying variable Poisson's ratio, reduction of the compressive strength due to lateral cracking with a low limit of 0.6, total strain rotating crack model and fracture energy of concrete in tension according to Model Code 2010. An energy norm with a tolerance of 10^{-3} is recommended.

References

Leonhardt E.F., Kock R., Rostasy F. S. "Schubversuche an Spannbetontragern", Deutscher Ausschuss fur Stahlbeton, Berlin 1973.

Nakamura H., Higai T., "Compressive Fracture Energy and Fracture Zone Length of Concrete", Benson P. Shing (editor), *J. Str. Eng. ASCE*, 2001, pp. 471-487.

Oliver, J. "A consistent characteristic length for smeared cracking models", International Journal for numerical Methods in Engineering, 1989, 28, 461^474.

Selby R.G., Vecchio F.J. "Three-dimensional Constitutive Relations for Reinforced Concrete", Tech. Rep. 93-02, Univ. Toronto, dept. Civil Eng., Toronto, Canada, 1993.

Vecchio F. J., Collins M. P. (1986), "The modified compression-field theory for reinforced concrete elements subjected to shear", *ACI Journal* **83**, 219-231.

4 Case PB2 (NSEL): Sun and Kuchma (2007)

The objective of the Sun and Kuchma report (Sun and Kuchma 2007) was to develop and improve understanding of the shear behavior and bearing capacity of high strength concrete prestressed girders through detailed analyses of dense experimental test data. To achieve this, HSC prestressed girders were designed according to AASHTO LRFD Bridge Design Specifications, fabricated, instrumented and tested at the Newmark Structural Engineering Laboratory so as to enable a comprehensive evaluation of the mechanism of shear. A total of twenty experiments on ten 1600 mm deep and 15850 mm long bulb-tee girders were planned. Girder 3 was selected as the benchmark for the present case study due to its shear-compressive failure mechanism.

4.1 Experimental setup and results

Geometry

The geometry of the beam and reinforcement details are shown in Figure 4-1 and Figure 4-2, respectively. The beam has a total length of 15.85 m and a total depth of 1.6 m; the T-shape cross section of the beam is shown in Figure 4-1. A concrete deck is casted on top of the girder.

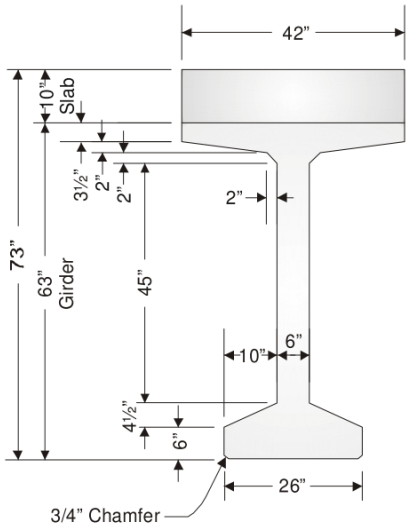

Figure 4-1: Case PB2. Cross section details (dimensions in inch) (Sun and Kuchma 2007)

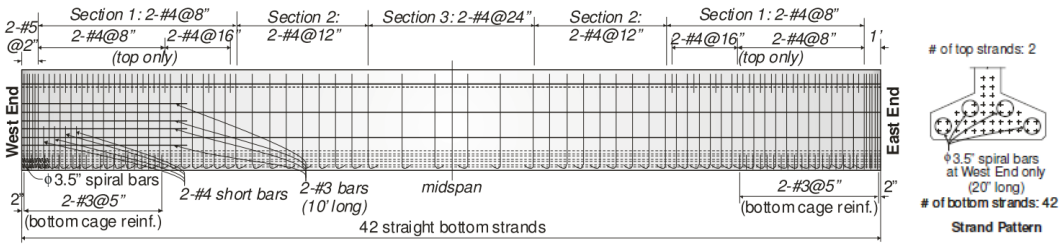

Figure 4-2: Case PB2. Reinforcement and strands details (Sun and Kuchma 2007)

The reinforcement consists of #4 double legged deformed bars with spacing 203 mm In the region with higher shear forces. At both ends of the girder along the length of 500mm, the shear reinforcement was increased to #5 double legged bars with spacing 50 mm apart. The longitudinal reinforcement consisted of two pairs of #3 longitudinal

bars with spacing 458 mm and one layer of #8 longitudinal bar placed in the top flange. The East end was designed to satisfy the LRFD end reinforcement requirements while the West end region contained addition reinforcement. It consisted of additional distributed horizontal reinforcement, vertical reinforcement and confinement reinforcement. The 3048 mm long horizontal bars were distributed along both faces of West web end and consisted of #3 bars at spacing 152.4 mm. Four pairs of #4 vertical bars were provided from the inside face of the support towards the center of the girder to increase horizontal shear strength along the web. The confinement reinforcement #3 was used in the bottom flange for 2540 mm from each end. In the deck, two layers of #6 235 mm spacing were placed.

A total of 44 seven-wire low-relaxation prestressing straight strands with a diameter of 15.2 mm each one were used: 42 strands in the bottom bulb and 2 strands in the top flange. The effective initial stress in prestressing steel σ_{p0}, measured before testing after immediate losses, was equal to 1068 N/mm^2. The actual prestressing loss at the time of testing was determined from displacement measurements of the change in a distance between targets mounted on the bottom bulb of the girder at the level of the centroid of the prestressing steel. The measured prestressing losses ranged from about 15 % to 25 % and these measured values were used in calculations of the nominal capacities of the girders. Four spirals were placed around the strands to reduce strand slip. Lastly, two 229 mm wide steel plates were placed at the support.

Material Properties

Concrete and reinforcement properties from the reference are given in Table 4-1.

Table 4-1: Case PB2. Concrete and reinforcement properties

Concrete properties of girder					
f_{cm} (N/mm^2)	$f_{ctm,sp}$ (N/mm^2)	E_c (N/mm^2)	d_{max} (mm)		
109.63	5.28	52710	13		
Concrete properties of deck					
f_{cm} (N/mm^2)		E_c (N/mm^2)		d_{max} (mm)	
24.82		25076		13	
Bar	Φ (mm)	A_s (mm^2)	E_s (N/mm^2)	f_{ym} (N/mm^2)	f_{tm} (N/mm^2)
#3	9.5	71	200000	413.7	620.5
#4	12.7	129	200000	467.5	731.5
#5	15.9	200	200000	445.4	701.9
#6	19.1	284	200000	413.7	620.5
#8	25.4	510	200000	413.7	620.5
strands,7wire	15.24	140	196500	1675	1862

Loading and Boundary Conditions

The loading and boundary conditions in the experimental setup are shown in Figure 4-3.

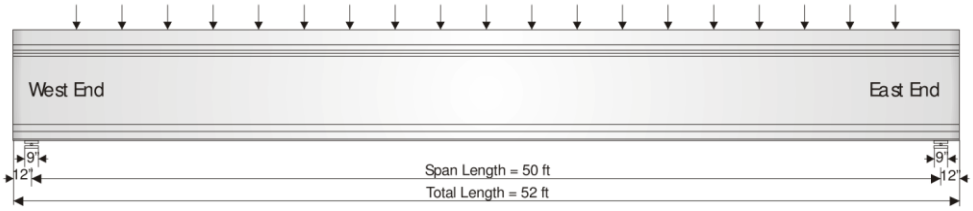

Figure 4-3: Case PB2. Loading, boundary conditions and dimension (in ft) (Sun and Kuchma 2007)

Experimental Results

The beam exhibited a shear-compression failure mechanism with crushing of concrete at the web-bulb interface, Figure 4-4. After the East end failed the test was stopped. The beam was unloaded and the East end was repaired by removing all loose concrete from the failed region, adding reinforcement on either side of the web and casting a 3050 to 4500 mm long repair on either side of the web using self-compacting concrete. Later, the failed region was vertically post-tensioned with post- tensioning bars. The beam was reloaded one week later using the same loading pattern until the West end failed. During the second part of the test, the West end was already damaged from the previous test and it was not repaired before the beginning of the second part of the test. The East end failed at the maximum load equal to 6983.35 kN and the maximum deflection of 76.2 mm whereas the West end failed at the maximum load equal to 7597.92 kN and the maximum deflection of 97.8 mm, Figure 4-5.

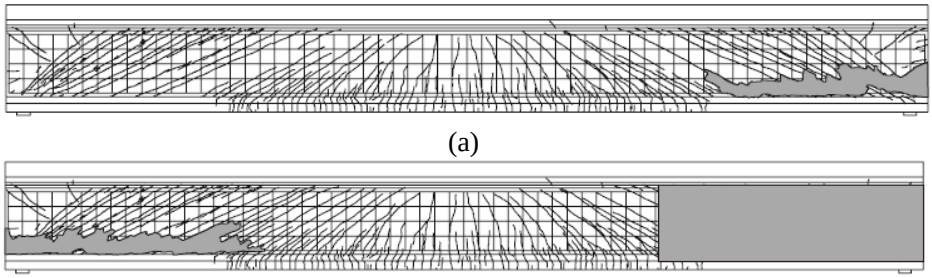

(a)

(b)

Figure 4-4: Case PB2. Failure mechanisms at ultimate load of (a) East end, (b) West end (Sun and Kuchma 2007)

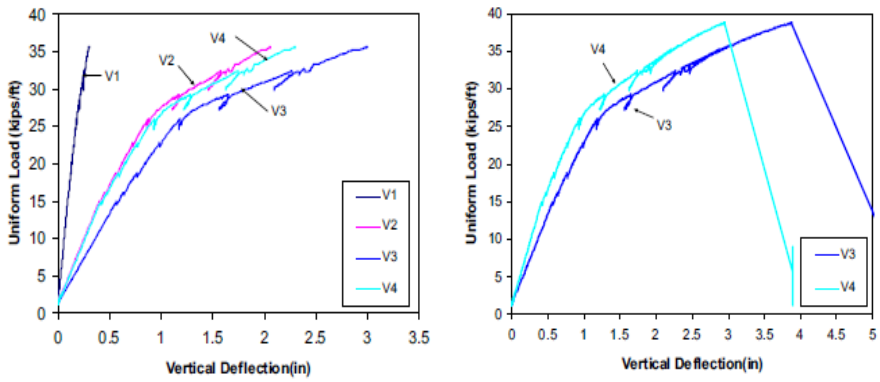

(a) (b)

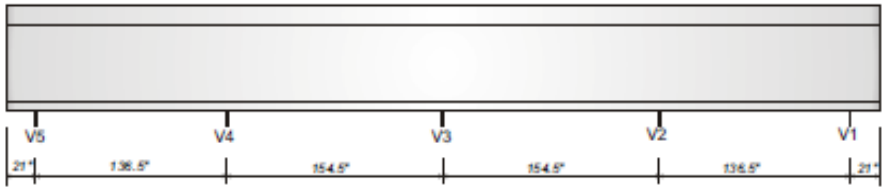

(c)

Figure 4-5: Case PB2. Load-deflection response, (a) East End, (b) West End, (c) Position of LVDTs (in kips/ft/inches)

4.2 Analytical analysis

In Figure 4-6 the load configuration at failure is shown.

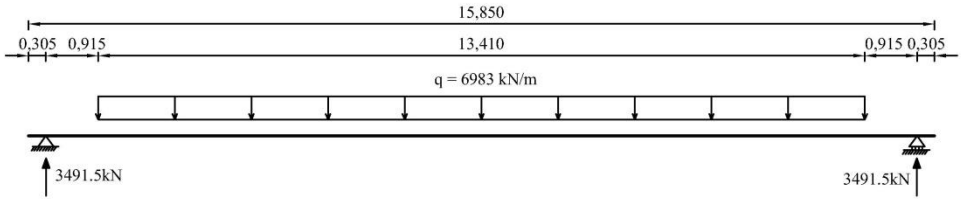

Figure 4-6: Case PB2. Load configuration at failure (dimensions in m)

Load case 1:
the distributed load equivalent to the beam and slab weights is equal to: $q = (A_{beam} + A_{slab}) \times 24kN/m^3 = (0.459m^2 + 0.271m^2) \times 24kN/m^3 = 17.527kN/m$ .The maximum bending moment at the mid-span of the girder then is: $M_{\max} = 508.03kNm$

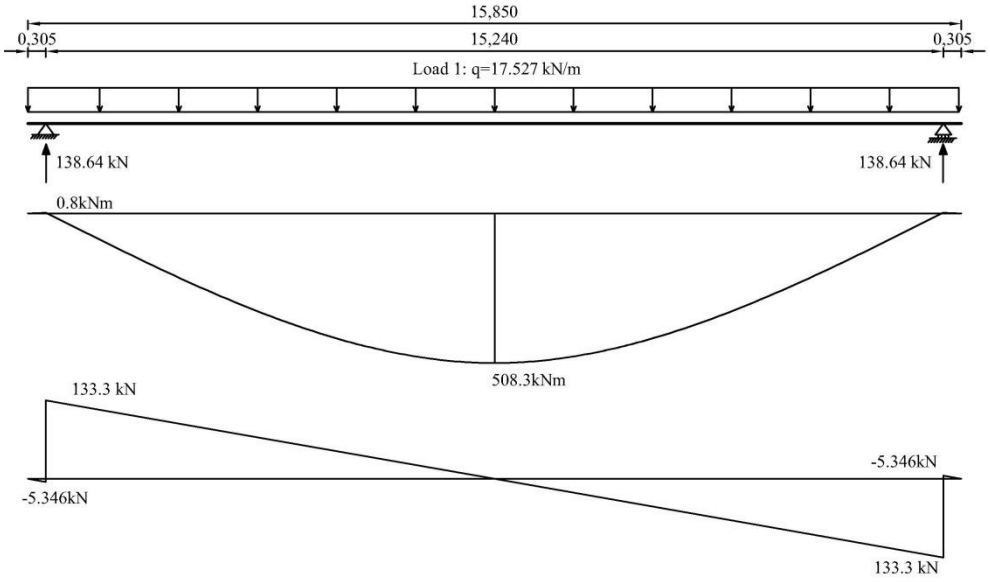

Figure 4-7: Case PB2. Load 1: Internal forces (dimensions in m)

Another external load is prestressing. The beam has 42 strands in the bottom part of the section and 2 strands in the top flange. The resulting moment calculated around the centroidal axis of the beam alone is given below.

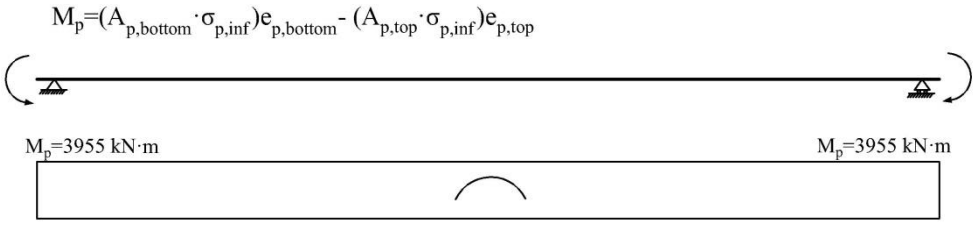

Figure 4-8: Case PB2: Load case 1: Internal forces from prestressing

Load case 2:
Figure 4-9 shows maximum moment at mid-span equal to:

$$M_{\max} = q\frac{13.4m \times 0.915m}{2} + q\frac{(13.41m)^2}{8}$$

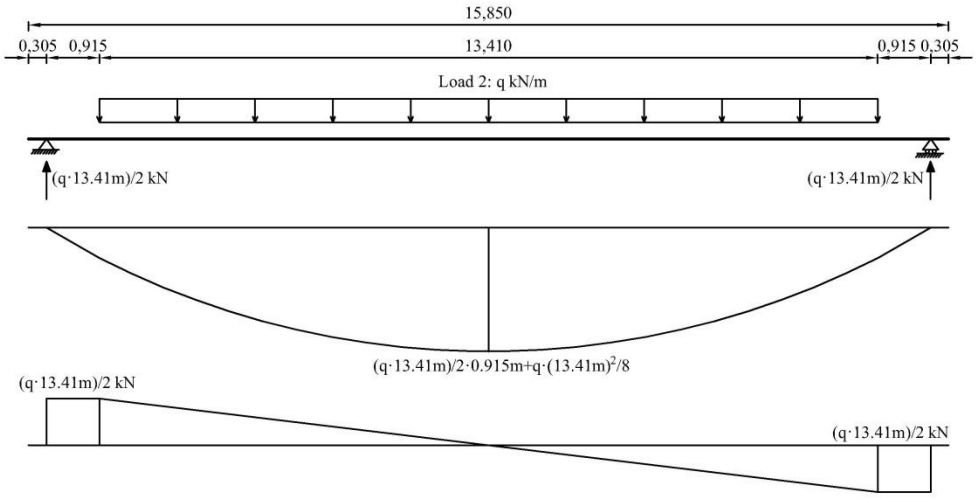

Figure 4-9: Case PB2. Load 2: Internal forces (dimensions in m)

Bending moment resistance:

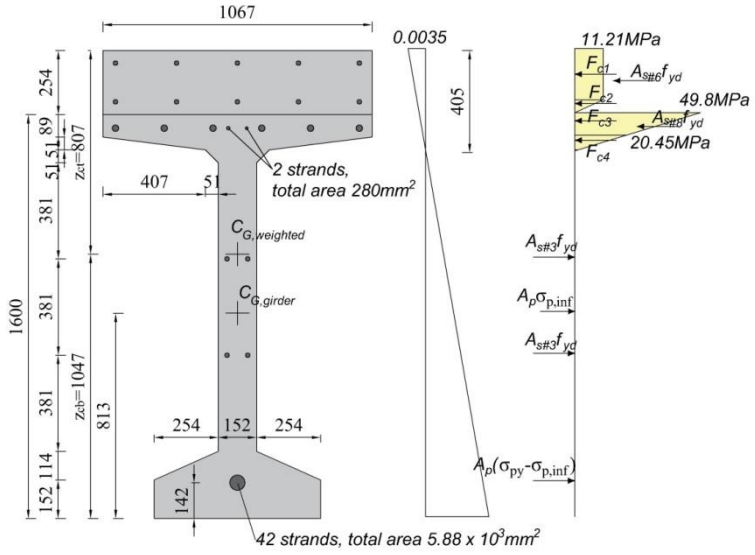

Figure 4-10: Case PB2: Forces acting on section, ULS

The design value of bending moment resistance was calculated assuming a bi-linear stress block for a deck and an elastic-plastic stress-strain relationship for both reinforcement and prestressing steel. The partial safety factors were taken as: 1.15 for reinforcement and prestressing steel and 1.5 for concrete.
The height of compression zone was searched for neglecting strains in the beam alone resulting from the self-weight of the beam and the deck before setting of concrete. It was assumed that bars in the concrete slab, the flange and the web yield which was later verified to be true. Consequently, the horizontal force equilibrium is:

$$F_c + A_{s\#6} f_{yd} + A_{s\#8} f_{yd} = 2A_{s\#3} f_{yd} + A_p \sigma_{p,\inf} + A_p \left(f_{py} - \sigma_{p,\inf} \right)$$

The resulting value of concrete compression zone is: 405mm.
The ultimate bending moment resistance calculated around the centroidal axis:

$$F_c \left(z_{ct} - y \right) + A_{s\#6} f_{yd} \left(z_{ct} - 0.5 h_{deck} \right) + A_{s\#8} f_{yd} \left(z_{ct} - h_{deck} - 54.4mm \right) + A_{s\#3} f_{yd} \times 126mm +$$
$$A_{s\#3} f_{yd} \times 381mm + A_p \sigma_{p,\inf} \left(z_{cb} - C_{G,girder} \right) + A_p \left(f_{py} - \sigma_{p,\inf} \right) \left(z_{cb} - 142mm \right) =$$
$$6702kN \times 0.585m + 629.3kNm + 254.8kNm + 5.83kNm + 17.63kNm + 153.9kNm + 133.6kNm = 7702kNm$$

The maximum value of the distributed load that the beam is able to withstand is:

$$M_{SelfWeight} + M_p + q \frac{13.4m \times 0.915m}{2} + q \frac{(13.41m)^2}{8} = M_{Rd} \rightarrow q = 389.7 kN/m .$$

The resultant of the distributed load is

$$P_{Ed,\max} = q \times 13.41m = 389.7kN/m \times 13.41m = 5226kN$$

Shear force resistance:

Eurocode 2:

$d_p = 1712mm \rightarrow z = 0.9 d_p = 1541mm$ taking into account the concrete slab under the assumption that stirrups are properly anchored in the slab and a truss model can develop.

$$V_{Rd,s} = \frac{A_{sw}}{s} z f_{ywd} \cot\theta = \frac{258mm^2}{203mm} 1541mm \times 365.4MPa \times 2.5 = 1803kN$$

$$V_{Rd,\max} = \frac{f_{cd} b_{web} z \alpha_{cw} \nu_1}{\tan\theta + \cot\theta} = \frac{67.75MPa \times 152.4mm \times 1.211 \times 0.5}{0.4 + 2.5} = 3314kN$$

Where: $\sigma_{cp} = \frac{A_p \sigma_{p,\inf}}{A_{beam}} = \frac{6579kN}{459341mm^2} = 14.322MPa \rightarrow \alpha_{cw} = 1 + \frac{\sigma_{cp}}{f_{cd}} = 1.211$

and $\nu_1 = 0.5$

Model Code 2010

The design value of shear resistance of the beam is also calculated according to the Model Code 2010 (fib, 2013) applying three levels of approximations.

Table 4-2: Case PB2. Parameters used in the calculation of V_{Rd}

	Level I	**Level II**	**Level III**
θ_{min} (°)	25	20	20
θ_{max} (°)	45	45	45
k_ε	0.55	0.65	0.65

Level I Approximation

$$V_{Rd,s}(\theta_{\min}) = \frac{A_s}{s} z f_{ywd} \cot(\theta_{\min}) = \frac{258mm^2}{203mm} 1541mm \times 365.4MPa \times \cot(25°) = 1546kN$$

$$V_{Rd,\max}(\theta_{\min}) = k_c \frac{f_{ck}}{\gamma_c} b_w z \sin\theta_{\min} \cos\theta_{\min} = 0.366 \times \frac{101.63MPa}{1.5} 152.4mm \times 1541mm \times$$
$$\times \sin(25°)\cos(25°) = 2230kN$$

Level II Approximation

For the assumed value of shear resistance $V_{Ed,trial} = 1851kN$, ε_x is negative therefore according to the Model Code 2010, $\varepsilon_x = 0$. This implies that the minimum angle for compressive struts is: $\theta_{\min} = (20\deg + 10000\varepsilon_x) = 20\deg$. From the calculations conducted for this angle, the condition $V_{Rd,\max} > V_{Rd,s}$ was violated. This imposes the need to increase the angle. It is thus assumed that $\theta = 20.28°$. The evaluation for this angle is shown below.

$$\varepsilon_1 = \varepsilon_x + (\varepsilon_x + 0.002)\cot\theta_{\min}^{\ 2} = 0.013$$

$$k_\varepsilon = \frac{1}{1.2 + 55\varepsilon_1} = 0.519$$

$$\eta_{fc} = \left(\frac{30MPa}{f_{ck}}\right)^{\frac{1}{3}} = 0.666 < 1$$

$$k_c = k_\varepsilon \eta_{fc} = 0.346$$

$$V_{Rd,s}(\theta_{\min}) = \frac{A_s}{s} z f_{ywd} \cot(\theta) = \frac{258mm^2}{203mm} 1541mm \times 368.2MPa \times \cot(21.28°) = 1851kN$$

$$V_{Rd,\max}(\theta_{\min}) = k_c \frac{f_{ck}}{\gamma_c} b_w z \sin\theta\cos\theta = 0.346 \times \frac{101.6MPa}{1.5} \times 152mm \times 1541mm \times$$
$$\times \sin(21.28°)\cos(21.28°) = 1856kN$$

Note: the effective shear depth was taken including the depth of the deck. It is

$$z = 0.9d_p = 0.9 \times 1712mm = 1541mm$$

The shear resistance of stirrups is lower than the cut-off limit dictated by crushing of concrete. The shear resistance is 1851kN.

Level III Approximation

For the same reason as explained in the level II approximation calculations, the angle is assumed:

$\theta = 20.28\deg$. It follows then that:

$$V_{Rd,s}(\theta_{\min}) = \frac{A_s}{s} z f_{ywd} \cot(\theta) = \frac{258mm^2}{203mm} 1541mm \times 368.2MPa \times \cot(21.28°) = 1851kN$$

$$V_{Rd,\max}(\theta_{\min}) = k_c \frac{f_{ck}}{\gamma_c} b_w z \sin\theta\cos\theta = 0.346 \times \frac{101.6MPa}{1.5} \times 152mm \times 1541mm \times \sin(21.28°)\cos(21.28°) = 1856kN$$

$$k_v = \frac{0.4}{1 + 1500\varepsilon_x}\left(1 - \frac{V_{Ed,trial}}{V_{Rd,\max}}\right) \approx 0$$

$$V_{Rd,c} = k_v \frac{\sqrt{f_{ck}}}{\gamma_c} b_w z \approx 0$$

$$V_{Rd} = (V_{Rd,s} + V_{Rd,c}) < V_{Rd,\max}(\theta_{\min})$$

$$V_{Rd} = 1851kN$$

The assumed shear resistance is equal to the calculated design shear resistance hence no further iterations are required. Moreover, due to the shear resistance of the value

close to $V_{Rd,\max}$ the contribution of concrete is negligibly small. It means that the shear resistances of levels II and III approximations are the same.

The value of load q was determined in the following way. Shear force caused by the self-weight at a location d from the support is $V_{Ed,SW} = 103kN$. Combining of the actions on the beam and equating them to the shear resistance results in:

$$q\left(\frac{13.41m}{2} - (1.741m - 0.914m)\right) + 103kN = 1851kN \rightarrow q = 295.97kN/m \quad \text{(for LoA II and III)}$$

From the obtained results, it can be seen that the beam fails in shear. The calculated value of the bending moment resistance is higher than shear force resistance attributed to stirrups. The lower value of distributed load $q_{shear,LoAIII} = 295.97\,kN/m$ related to the shear resistance would lead to failure earlier than load $q_{bending} = 389.kN/m$. The resultant corresponding to the shear failure is $P_{Ed,\max,LoAIII} = 3968kN$ for LoA II and III. For LoA I and EC2 it is the resultant of $P_{Ed,\max,LoAI} = 3275kN$ and $P_{Ed,\max,EC2} = 3859kN$ respectively. Note values of distributed load are already reduced by the effect of the self-weight. The values are summarized in Table 4-3.

Table 4-3: Case PB2. Design value of beam resistance expressed in terms of resultant load P_{Rd} (Model Code 2010)

	EC2	**Level I**	**Level II**	**Level III**
P_{Rd} (kN)	3859	3275	3968	3968

4.3 Finite element model

Units

Units are N, mm.

Material models and parameters

The concrete model is based on a total strain rotating crack model with:

- exponential softening in tension and parabolic compression curve,
- variable Poisson's ratio of concrete,
- reduction of compressive strength of concrete due to lateral cracking with a lower limit of 0.6,
- increase in compressive strength due to lateral confinement according to the model proposed by Selby and Vecchio (Selby and Vecchio 1993)

The mechanical properties are summarized in Figure 4-5. On input, the G_F value has been decreased with a factor $\sqrt{2}$ in order to compensate for an underestimation of the crack band width for cracks with an inclination angle of 45 degrees. The uniaxial stress-strain curve is shown in Figure 4-11.

The model for the reinforcement bars and stirrups is based on hardening plasticity. Geometrical and mechanical properties of reinforcement are summarized Table 4-1. The stress-strain curve of the #5 bars is plotted in Figure 4-12.

Table 4-4: Case PB2. Constitutive model parameters for concrete

Girder					
	f_{cm} (N/mm^2)	f_{ctm} (N/mm^2)	E_c (N/mm^2)	ν	G_F (Nmm/mm^2)
Mean measured value	109.63	5.28$^{\#}$	52710	var	0.170*
*Not specified in reference; estimated according to Model Code 2010 (fib, 2013)					
#Estimated according to Model Code 2010 (fib, 2013) as $f_{ctm} = 1 \times f_{ctm,sp}$					
Deck					
	f_{cm} (N/mm^2)	f_{ctm} (N/mm^2)	E_c (N/mm^2)	ν	G_F (Nmm/mm^2)
Mean measured value	24.82	2.65*	25076	var	0.130*
*Not specified in reference; estimated according to Model Code 2010 (fib, 2013)					

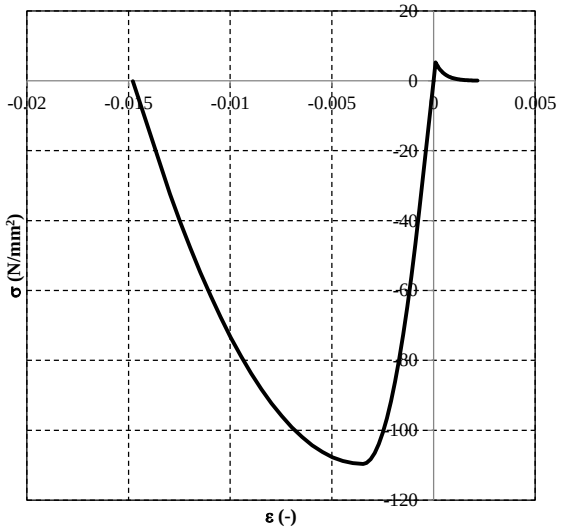

Figure 4-11: Case PB2. Stress-strain curve for concrete girder

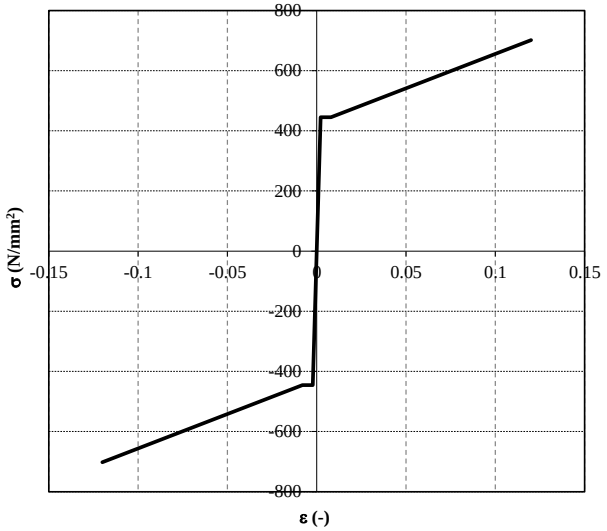

Figure 4-12: Case PB2. Stress-strain curve adopted for #5 bars

For the steel plates a linear elastic behavior is assumed, see Table 4-5.

Table 4-5: Case PB2. Steel plates properties

E (N/mm^2)	ν
200000	0.3

Interface elements were used between the steel support plates and the concrete beam at the supports and loading positions. The interface stiffness was derived on the basis of concrete properties. The total thickness of interface elements equals 1 mm. A bilinear behavior is assumed in the normal direction (see Figure 4-13) and a linear elastic relation is assumed in shear direction. The normal stiffness in tension and the stiffness in shear direction were assumed almost equal to zero.
The mechanical properties of the interface elements are summarized in Table 4-6.

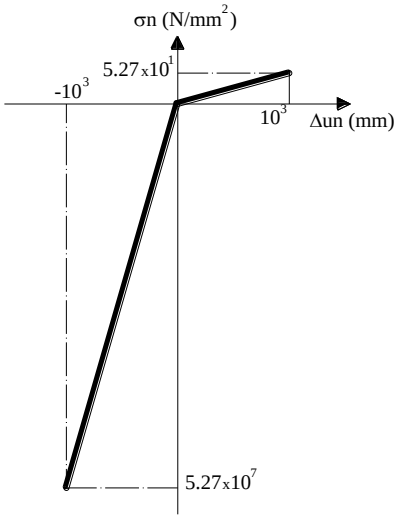

Figure 4-13: Case PB2. Traction-displacement diagram in normal direction for interfaces

Table 4-6: Case PB2. Interface properties

$K_{nn\ in\ tension}$ (N/mm^3)	$K_{nn\ in\ compression}$ (N/mm^3)	K_t (N/mm^3)
5.27E+01	5.27E+04	5.27E+01

Element types and finite element mesh

For meshing concrete, 8-node membrane elements (CQ16M) with a full integration scheme (3×3) were used the beam. The average element size is 50×50 mm^2. The dimensions of the elements were established on the basis of assumed fixed thickness in the flange with variable thickness, see Figure 4-16.
The reinforcement bars and stirrups are modelled with embedded truss elements with two Gauss integration points along the axis of the element. Perfect bond is assumed. The bottoms strands were combined and placed in the centre of gravity. For the steel plates 8-node membrane elements (CQ16M) were used. The 6-node interfaces elements have three Lobatto integration points.
The adopted dimensions of the beam and its transversal cross-section are given in Figure 4-14 and Figure 4-15, respectively.
The mesh of the beam is presented in Figure 4-15(a) whereas the individual materials in the model are indicated with different colors in Figure 4-15(b).

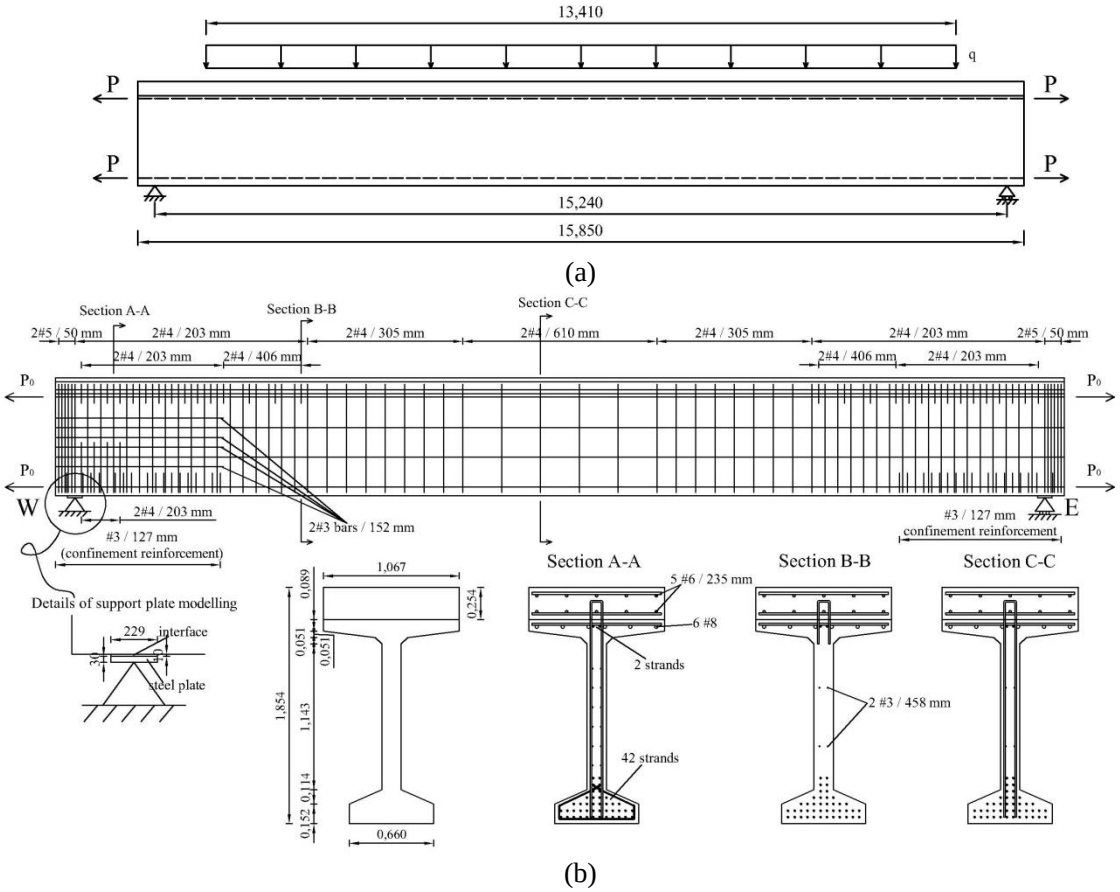

Figure 4-14: Case PB2. (a) Dimensions of the beam (in mm) and loading scheme, (b) Reinforcement, cross section and support plate details (dimensions in mm)

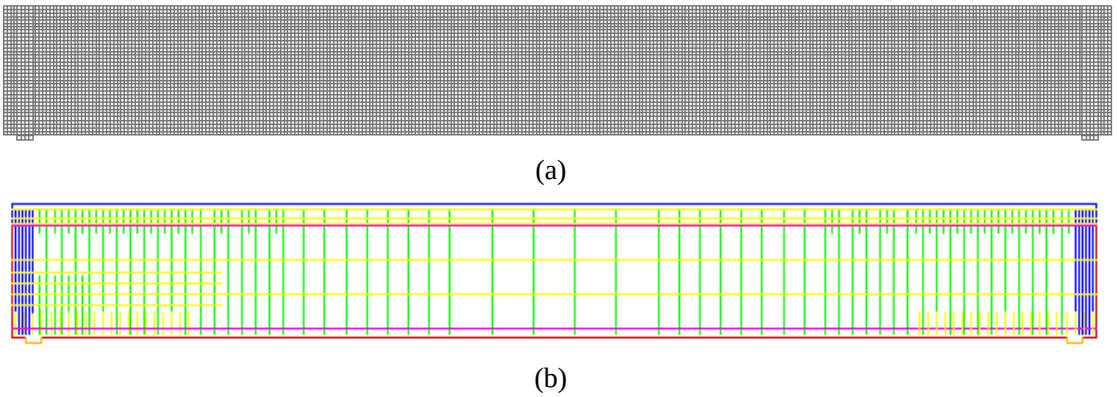

Figure 4-15: Case PB2. (a) Mesh and (b) material sets

Different groups of elements are defined to distinguish the concrete elements and the steel elements. These groups will be used in section 3.4 to monitor the failure mode during the analysis. For monitoring yielding of steel, the groups STIRRUPS, BARS and STRANDS refer to stirrups, bars and strands of the beam respectively, see Figure 4-16(a). Figure 4-16 (b) shows the group of elements named SHEAR which served to track the inelastic behavior of concrete. The groups of elements named FL_INF_C, FL_INF_P, FL_INF_S, WEB FL_SUP_P, FL_SUP_S, FL_SUP_C, DECK given in Figure 4-16(c), were used to model the cross section dimensions.

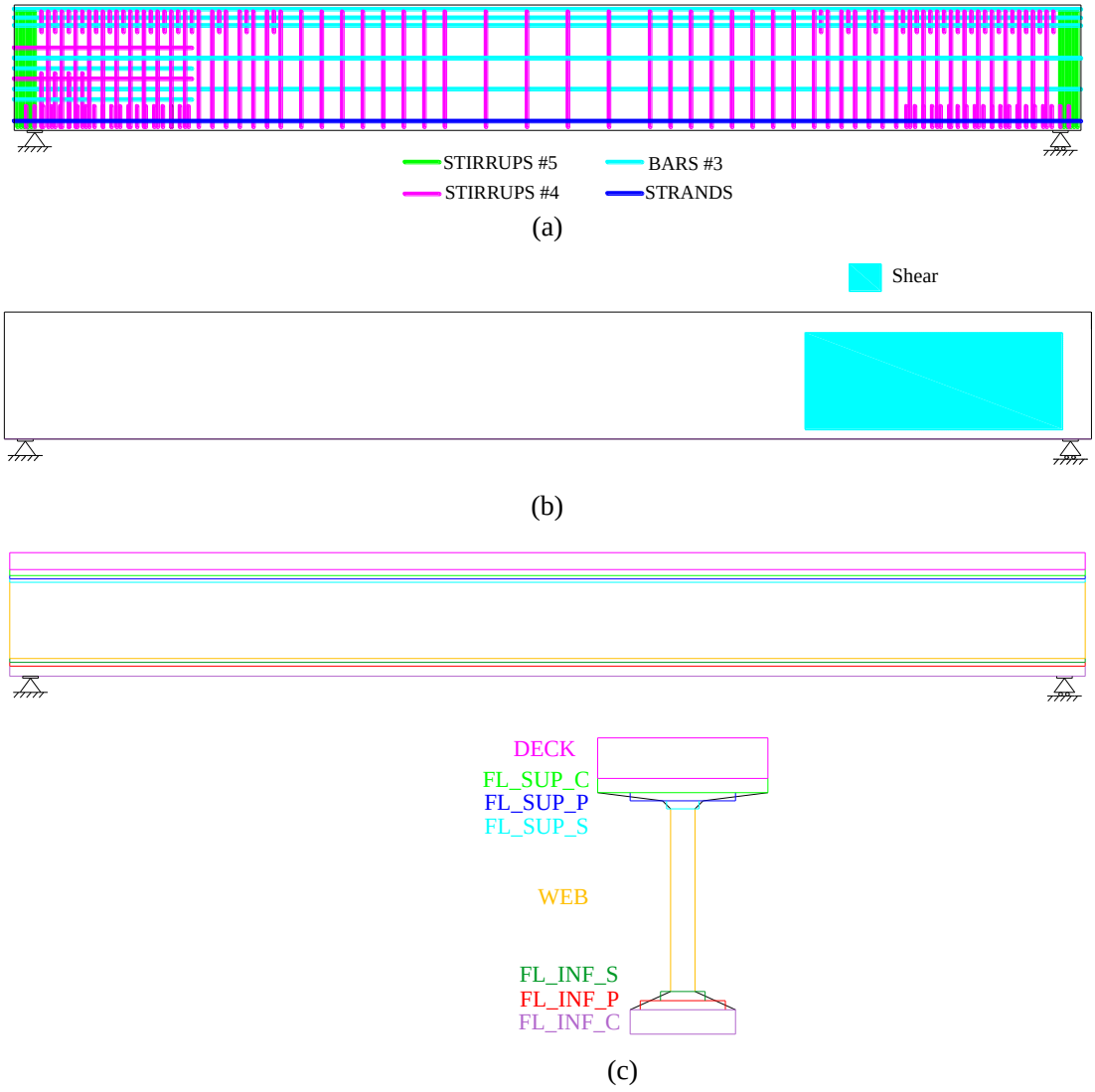

Figure 4-16: Case PB2. Groups of steel elements monitoring (a) yielding of reinforcement, (b) inelastic behavior of concrete, (c) groups of elements used to model the beam cross sectional dimensions

Boundary conditions and loading

The boundary conditions were applied to a single node at each steel plate. In the left steel plate, the constraints of degrees of freedom in both *x* and *y* directions were applied whereas in the second support (right steel plate) only translation in the *y* direction was prevented, Figure 4-17.

In the model two load cases were considered. In the first load case, dead weight *q(1)* and prestressing force $P_0(1)$ were applied. Next, the uniformly distributed load *q(2)* of 1N/mm is applied in the load case 2, Figure 4-17 (a).The initial effective stress in prestressing steel σ_{pcs} ($P_0=\sigma_{pcs}\cdot A_p$), measured during experiments after initial losses to be 1068 N/mm^2, was introduced gradually over a transmission length equal to 610 mm, as indicated by (Sun and Kuchma, 2007).

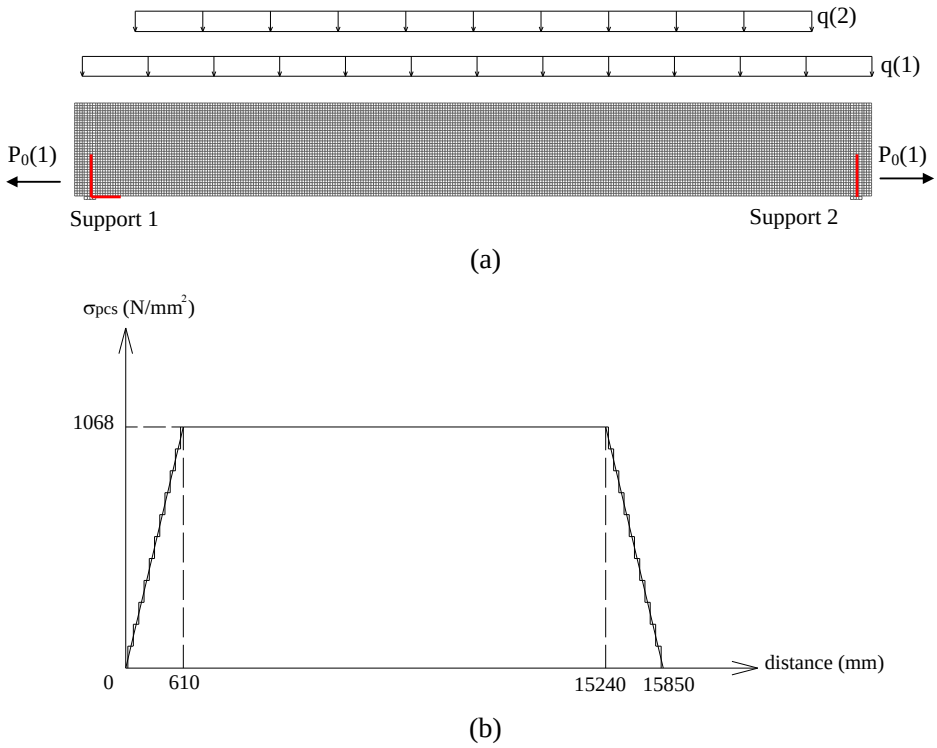

Figure 4-17: Case PB2. (a) Boundary conditions and load cases 1 and 2, (b) initial stress in prestressing steel distribution

Load increments and convergence criteria

Load case 1 was applied in 2 steps. The regular Newton-Raphson method with a maximum of 25 iterations was used. As convergence criteria, the force and energy norms were selected. The analysis was set to continue even if the convergence criteria were not satisfied. The convergence tolerances were 1×10^{-2} for the force norm and 1×10^{-3} for the energy norm. A Line Search algorithm was used to improve the convergence performance.

Load case 2 was applied with automatic adaptive load increments based on energy. The initial load factor equaled 5, the upper limit of the incremental load factor was 10 and the lower limit of the incremental load factor was 2. The maximum number of steps was 100. Arc-length control was applied based on translation along y axis of node 625 ("indirect displacement control"), Figure 4-18. The analysis continued even if the convergence criteria were not satisfied. The convergence tolerance was equal to 1×10^{-3} and 1×10^{-2} for energy and force respectively. The maximum of 50 iterations was used. A line search algorithm was applied to improve the convergence performance.

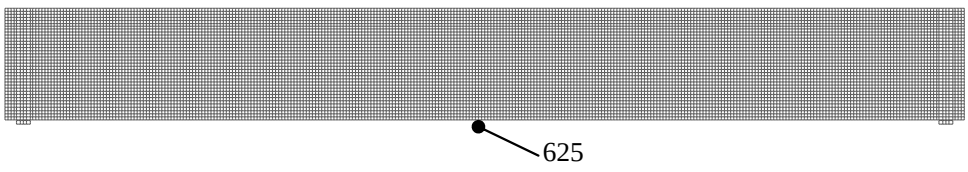

Figure 4-18: Case PB2. `Indirect Displacement control' technique applied referring to node 625

4.4 Nonlinear finite element analysis

Load deflection

The load-deflection curve is presented in Figure 4-19 where the applied load values corresponding to the beginning of yielding of bars #3, yielding of stirrups #4 and crushing of concrete are marked. The onset of crushing of concrete was set to occur when the minimum principal strain of -3.5‰ was reached in an integration point.
For load case 2, the peak load was defined as the highest load step where the energy norm ratio satisfied the fixed tolerance of 1×10^{-3}. The convergence behavior was quite poor after reaching the peak load. After step 72, the analysis continued even if the energy convergence criteria are not satisfied within the maximum number of iterations equal to 50. The post peak branch of the load – deflection curve is for this reason plotted with a dot-dashed line.

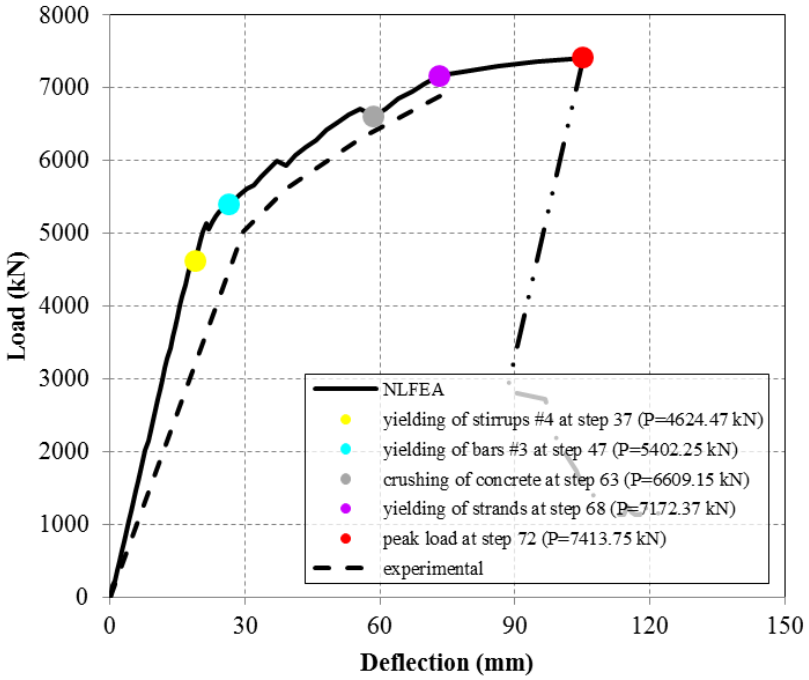

Figure 4-19: Case PB2. Load-deflection curve

Convergence behavior

For most steps, the convergence was reached on the basis of the energy criterion, see. For load case 2, the energy norm ratio satisfied the fixed tolerance of 1×10^{-3} for almost all the steps of the analysis, while the force norm ratio was typically higher than the fixed tolerance. The red circle in Figure 4-20 and Figure 4-21 indicates the peak load position on the above load-displacement curve.

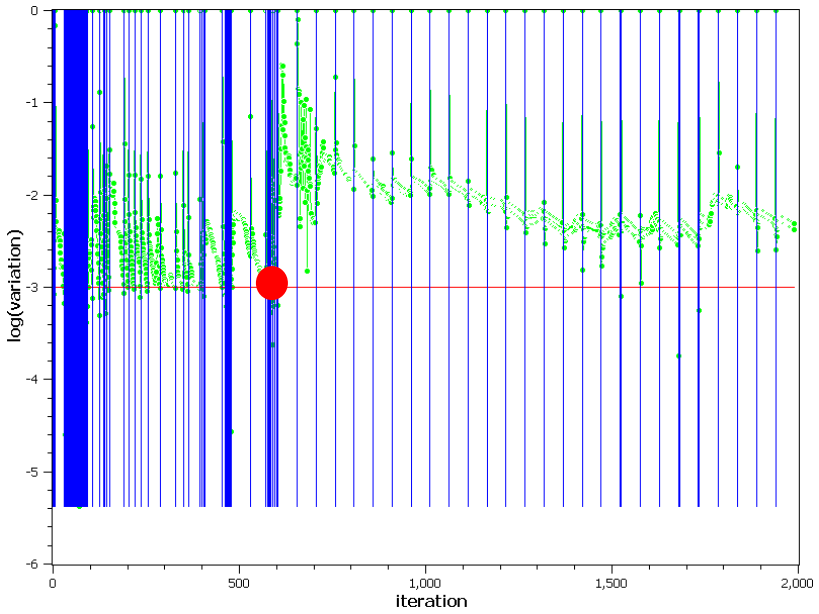

Figure 4-20: Case PB2. Evolution of the energy norm (blue lines indicate steps, red line indicates tolerance, green points indicate iterative results)

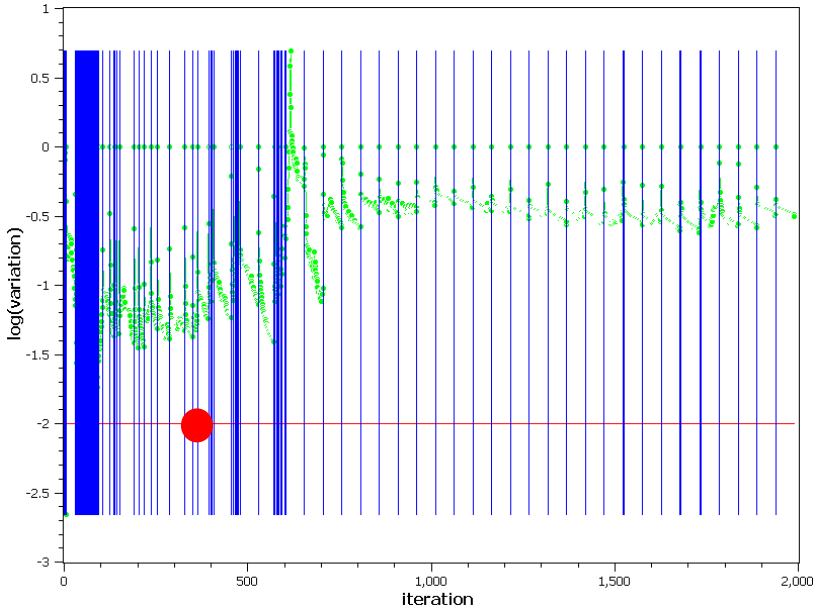

Figure 4-21: Case PB2. Evolution of the force norm (blue lines indicate steps, red line indicates tolerance, green points indicate iterative results)

Strains in concrete

In Figure 4-22 and Figure 4-23, the positive and negative crack strains contours at the peak load 72 are shown. From the depicted contours, which in the case of positive numbers can be regarded as a representation of a crack pattern, and corresponding values, it can be seen that the occurred failure mechanism is due to combined shear and crushing of concrete. Crushing of concrete can be especially well observed in Figure 4-23.

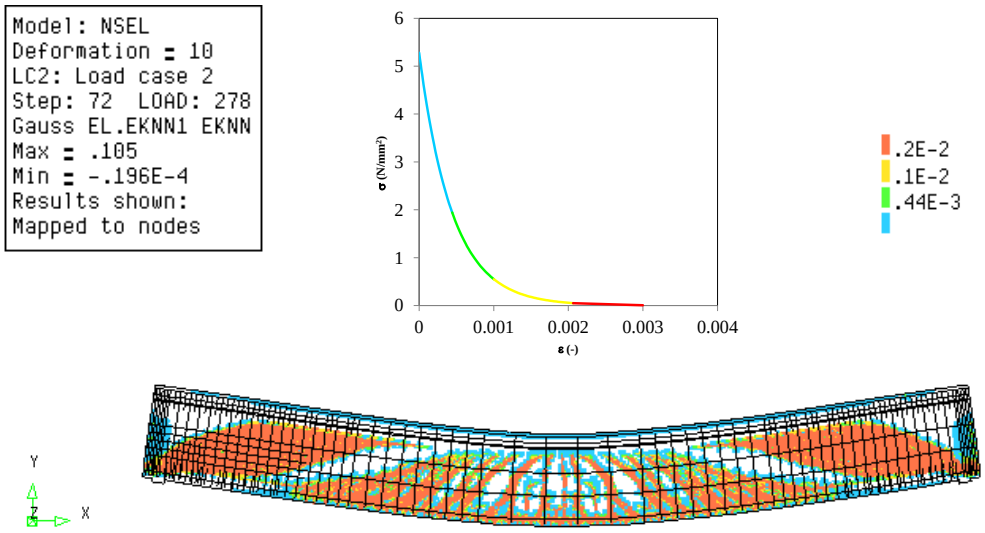

Figure 4-22: Case PB2. Crack strain values at step 72 (peak load)

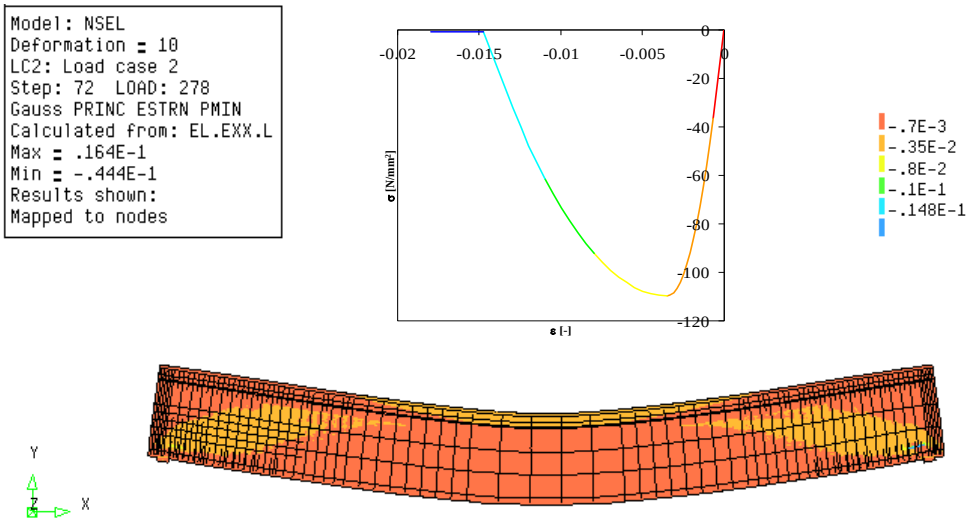

Figure 4-23: Case PB2. Minimum principal strain values at step 72

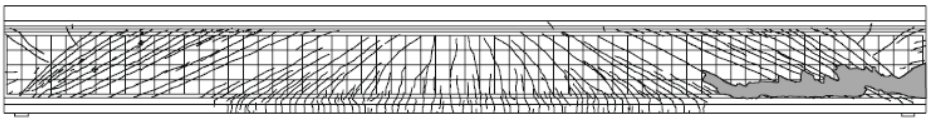

Figure 4-24: Case PB2. Experimental crack pattern at failure (load $P = 6983.35kN$)

Strains in steel

The yielding strain of stirrups #4, which equals to $435MPa/200GPa = 2.33\times10^{-3}$, was reached at the load of 4624.47 kN (step 37). Figure 4-25 shows yielding of stirrups a few steps after the first yielding point (at step 50).

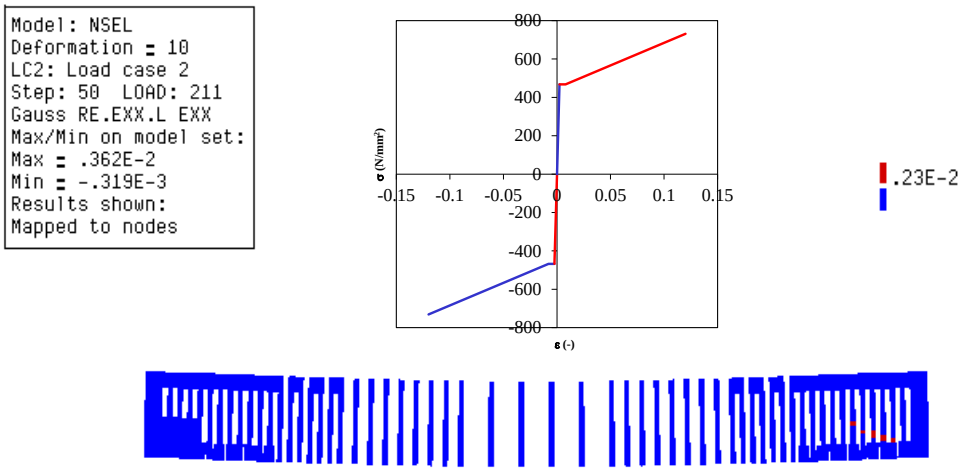

Figure 4-25: Case PB2. Yielding of stirrups #4 at step 50

The yielding strain of bars #3 is equal to $413.7MPa/200GPa = 2.0\times10^{-3}$. The bars began to yield at the load equal to 5402.25 kN (step 47). In Figure 4-26 yielding of longitudinal reinforcement #3 at step 56 is shown.

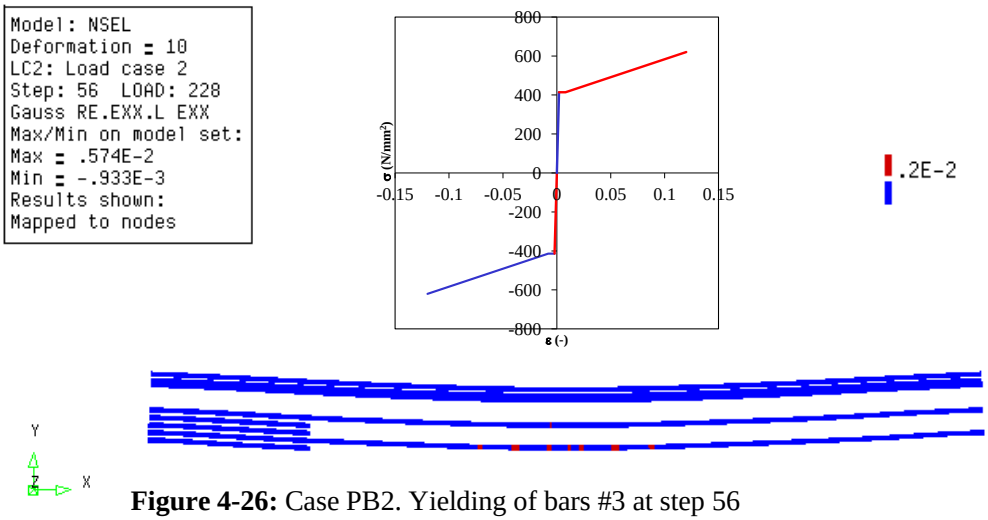

Figure 4-26: Case PB2. Yielding of bars #3 at step 56

The yielding strain of strand equal to $1675MPa/196.5GPa = 8.52\times10^{-3}$ was exceeded at the load value of 7172.37 kN (step 68). Figure 4-27 shows the yielding of strands at step 68:

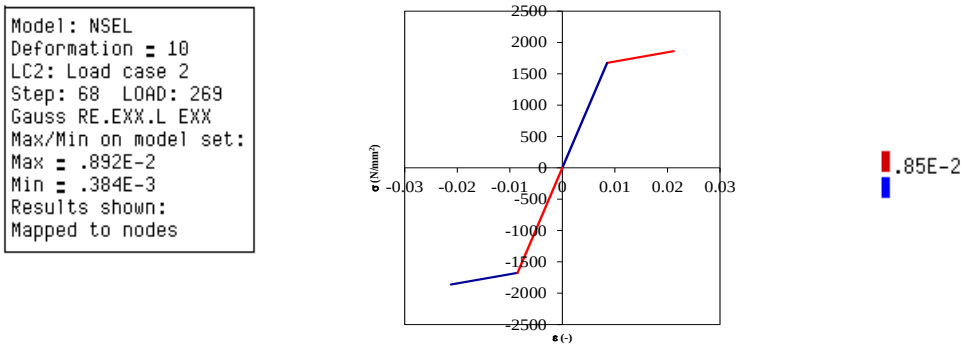

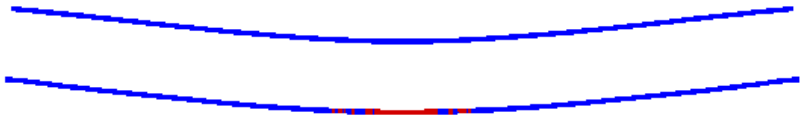

Figure 4-27: Case PB2. Yielding of strands at step 68

Table 4-7: Case PB2. Summary of strains in reinforcement and concrete and corresponding load steps of occurrence

Reinforcement	Yield Strain	Onset of yielding
Stirrups #4	$2.33 \cdot 10^{-3}$	37
Rebars #3	$2.00 \cdot 10^{-3}$	47
Strands	$8.52 \cdot 10^{-3}$	68
Concrete	**Strain**	**Load Step**
Crushing	$-0.35 \cdot 10^{-2}$	63
Peak load	$-0.444 \cdot 10^{-1}$ and 0.105	72

Gauss point statistics

In Table 4-8, numbers of cracking points, crushing points and yield points at step 37 (yielding of stirrups #4), at step 47 (yielding of bars #3), at step 63 (crushing of concrete), at step 68 (yielding of strands) and at step 72 (peak load) are given.

Table 4-8: Case PB2. Number of cracking points, crushing points and yield points

STEP	**37**	**ITERATIONS**		18		
GROUP NAME	**PLAST**	**PRV. PL**	**CRITIC**	**PLAST NEW**	**PRV.PL NEW**	**CRITIC NEW**
STIRRUPS	3	0	0	3	0	0
TOTAL MODEL	3	0	0	3	0	0
CRACKING LOGGING SUMMARY						
GROUP NAME	**CRACK**	**OPEN**	**CLOSED**	**ACTIVE**	**INACTI**	**ARISES**
FL_INF_C	38	38	0	38	0	12
FL_INF_P	64	63	1	50	14	24
FL_INF_S	172	171	1	96	76	14
WEB	9594	9554	40	4834	4760	1554
FL_SUP_P	276	274	2	202	74	198
DECK	2955	2955	0	0	2955	0
SHEAR	4053	4032	21	2779	1274	1113
TOTAL MODEL	13099	13055	44	5220	7879	1802
STEP	**47**	**ITERATIONS**		32		
GROUP NAME	**PLAST**	**PRV. PL**	**CRITIC**	**PLAST NEW**	**PRV.PL NEW**	**CRITIC NEW**
STIRRUPS	2	5	0	2	2	0
BARS	2	0	0	2	0	0
TOTAL MODEL	4	5	0	4	2	0

CRACKING LOGGING SUMMARY						
GROUP NAME	**CRACK**	**OPEN**	**CLOSED**	**ACTIVE**	**INACTI**	**ARISES**
FL_INF_C	2004	1926	78	833	1171	128
FL_INF_P	658	644	14	472	186	63
FL_INF_S	431	407	24	265	166	22
WEB	14520	14298	222	4789	9731	939
FL_SUP_P	529	529	0	172	3.57E+02	21
DECK	2955	2955	0	0	2955	0
SHEAR	5904	5835	69	1975	3929	294
TOTAL MODEL	21097	20759	338	6531	14566	1173
STEP	**63**	**ITERATIONS**		50		
GROUP NAME	**PLAST**	**PRV. PL**	**CRITIC**	**PLAST NEW**	**PRV.PL NEW**	**CRITIC NEW**
WEB	87	65	0	1	65	0
DECK	641	718	0	212	718	0
SHEAR	43	49	0	1	49	0
STIRRUPS	73	282	0	33	274	0
BARS	1	70	0	0	66	0
TOTAL MODEL	802	1135	0	246	1123	0

CRACKING LOGGING SUMMARY						
GROUP NAME	**CRACK**	**OPEN**	**CLOSED**	**ACTIVE**	**INACTI**	**ARISES**
FL_INF_C	5008	4849	159	1726	3282	487
FL_INF_P	1929	1888	41	826	1103	238
FL_INF_S	1562	1506	56	853	709	199
WEB	35369	34314	1055	14982	20387	7413
FL_SUP_P	760	760	0	213	547	28
DECK	3046	3046	0	28	3.02E+03	5
SHEAR	10144	9984	160	3328	6816	1553
TOTAL MODEL	47674	46363	1311	18628	29046	8370
STEP	**68**	**ITERATIONS**		2		
GROUP NAME	**PLAST**	**PRV. PL**	**CRITIC**	**PLAST NEW**	**PRV.PL NEW**	**CRITIC NEW**
WEB	312	1	0	29	1	0
DECK	2167	0	0	162	0	0
SHEAR	170	1	0	15	1	0
STIRRUPS	533	42	0	111	2	0
BARS	62	21	0	7	0	0
STRANDS	49	0	0	49	0	0
TOTAL MODEL	3123	64	0	358	3	0

CRACKING LOGGING SUMMARY						
GROUP NAME	**CRACK**	**OPEN**	**CLOSED**	**ACTIVE**	**INACTI**	**ARISES**
FL_INF_C	5703	5525	178	3729	1974	204
FL_INF_P	2163	2081	82	1688	475	40
FL_INF_S	1788	1706	82	1451	337	35
WEB	39965	37440	2525	22304	17661	420
FL_SUP_P	866	866	0	776	90	20
DECK	3103	3103	0	113	2990	17

SHEAR	11589	11205	384	6286	5303	141
TOTAL MODEL	53588	50721	2867	30061	23527	736
STEP	**72**	**ITERATIONS**		2		
GROUP NAME	**PLAST**	**PRV. PL**	**CRITIC**	**PLAST NEW**	**PRV.PL NEW**	**CRITIC NEW**
FL_INF_C	2	0	0	2	0	0
FL_INF_S	2	0	0	2	0	0
WEB	444	137	0	150	44	0
DECK	2919	0	0	159	0	0
SHEAR	243	87	0	95	15	0
STIRRUPS	765	57	0	78	20	0
BARS	166	11	0	32	0	0
STRANDS	182	0	0	18	0	0
TOTAL MODEL	4480	205	0	441	64	0
CRACKING LOGGING SUMMARY						
GROUP NAME	**CRACK**	**OPEN**	**CLOSED**	**ACTIVE**	**INACTI**	**ARISES**
FL_INF_C	6723	6559	164	4683	2040	355
FL_INF_P	2350	2268	82	1983	367	56
FL_INF_S	2043	1963	80	1682	361	89
WEB	43102	40606	2496	26788	16314	862
FL_SUP_P	1168	1168	0	987	181	60
FL_SUP_S	96	96	0	92	4	43
DECK	3130	3130	0	60	3070	7
SHEAR	12241	11857	384	7118	5123	196
TOTAL MODEL	58612	55790	2822	36275	22337	1472

4.5 Application of safety format

As proposed by the Model Code 2010 (fib, 2013) safety formats for non-linear analyses include three numerical methods denoted as GRF (Global Resistance Factor method), PF (Partial Factor method) and ECOV (Method of Estimation of a Coefficient of Variation of resistance).
In Table 4-9to Table 4-16 the mechanical properties of concrete and steel applied in the non-linear analyses are summarized.

Table 4-9: Case PB2. Constitutive model parameters for concrete girder

	f_c (N/mm^2)	f_{ct} (N/mm^2)	E_c (N/mm^2)	ν	G_F (Nmm/mm^2)	G_C (Nmm/mm^2)
Mean measured	109.63	5.28	52710*	var	0.170	42.5060
Characteristic	101.63	3.70	43107	var	0.168	41.9302
Mean GRF	86.39	5.86	41055	var	0.163	40.7214
Design	67.75	2.46	38170	var	0.156	38.9790

* Note that the used value of mean measured value for Young's modulus is questionable. Strictly applying the guidelines will lead to lower value of mean measured E_c

Table 4-10: Case PB2. Constitutive model parameters for concrete deck

	f_c (N/mm^2)	f_{ct} (N/mm^2)	E_c (N/mm^2)	ν	G_F (Nmm/mm^2)	G_C (Nmm/mm^2)
Mean measured	24.82	2.64	25076*	var	0.130	32.5332
Characteristic	16.82	2.09	25130	var	0.121	30.3327
Mean GRF	14.30	1.88	23934	var	0.118	29.4582
Design	11.21	1.59	22251	var	0.113	28.1978

* Note that the used value of mean measured value for Young's modulus is questionable. Strictly applying guidelines will lead to higher value of mean measured E_c

Table 4-11: Case PB2. Constitutive model parameters for reinforcing bars (#3)

	Φ (mm)	A_s (mm^2)	f_y (N/mm^2)	f_t (N/mm^2)	E_s (N/mm^2)	ε_{sy} (-)
Mean measured	9.5	71	413.70	620.50	200000	0.0021
Characteristic	9.5	71	374.71	562.01	200000	0.0019
Mean GRF	9.5	71	412.18	618.21	200000	0.0021
Design	9.5	71	325.83	488.71	200000	0.0016

Table 4-12: Case PB2. Constitutive model parameters for reinforcing bars (#4)

	Φ (mm)	A_s (mm^2)	f_y (N/mm^2)	f_t (N/mm^2)	E_s (N/mm^2)	ε_{sy} (-)
Mean measured	12.7	129	467.50	731.53	200000	0.0023
Characteristic	12.7	129	423.43	662.58	200000	0.0021
Mean GRF	12.7	129	465.78	728.84	200000	0.0023
Design	12.7	129	368.20	576.15	200000	0.0018

Table 4-13: Case PB2. Constitutive model parameters for reinforcing bars (#5)

	Φ (mm)	A_s (mm^2)	f_y (N/mm^2)	f_t (N/mm^2)	E_s (N/mm^2)	ε_{sy} (-)
Mean measured	15.9	200	445.40	701.89	200000	0.0022
Characteristic	15.9	200	403.42	635.73	200000	0.0020
Mean GRF	15.9	200	443.76	699.30	200000	0.0022
Design	15.9	200	350.80	552.81	200000	0.0018

Table 4-14: Case PB2. Constitutive model parameters for reinforcing bars (#6)

	Φ (mm)	A_s (mm^2)	f_y (N/mm^2)	f_t (N/mm^2)	E_s (N/mm^2)	ε_{sy} (-)
Mean measured	19.1	284	413.70	620.50	200000.00	0.0021
Characteristic	19.1	284	374.71	562.01	200000.00	0.0019
Mean GRF	19.1	284	412.18	618.21	200000.00	0.0021
Design	19.1	284	325.83	488.71	200000.00	0.0016

Table 4-15: Case PB2. Constitutive model parameters for reinforcing bars (#8)

	Φ (mm)	A_s (mm^2)	f_y (N/mm^2)	f_t (N/mm^2)	E_s (N/mm^2)	ε_{sy} (-)
Mean measured	25.4	510	413.70	620.50	200000	0.0021
Characteristic	25.4	510	374.71	562.01	200000	0.0019
Mean GRF	25.4	510	412.18	618.21	200000	0.0021
Design	25.4	510	325.83	488.71	200000	0.0016

Table 4-16: Case PB2. Constitutive model parameters for reinforcing bars (strands)

	Φ (mm)	A_s (mm^2)	f_y (N/mm^2)	f_t (N/mm^2)	E_s (N/mm^2)	ε_{sy} (-)
Mean measured	44×15.24	44×140	1675.00	1862.00	196500	0.0085
Characteristic	44×15.24	44×140	1517.12	1686.49	196500	0.0077
Mean GRF	44×15.24	44×140	1668.83	1855.14	196500	0.0085
Design	44×15.24	44×140	1319.23	1466.52	196500	0.0067

In Figure 4-28, the load-deflection curves obtained with mean measured, characteristic, mean GRF and design values of material strengths are shown.

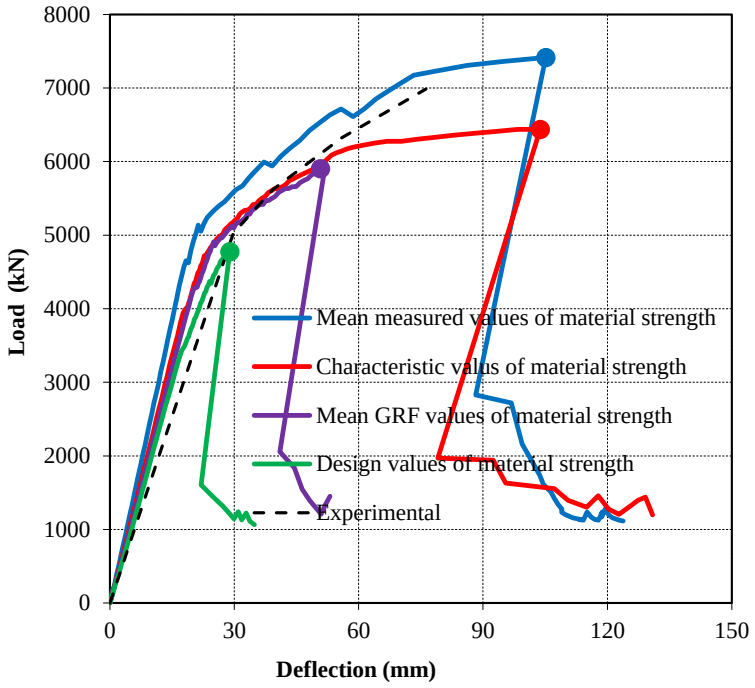

Figure 4-28: Case PB2. Load-deflection curves of analyses with mean measured, characteristic, mean GRF and design mechanical properties

The resistance of the beam along with the governing failure mechanism were check analytically by means of expressions from codes and numerically with the application of NLFEA. In Figure 4-29 the comparison of analytical and numerical design values of beam resistance P_{Rd} expressed in terms of a percentage of the experimental ultimate value of applied load are shown.

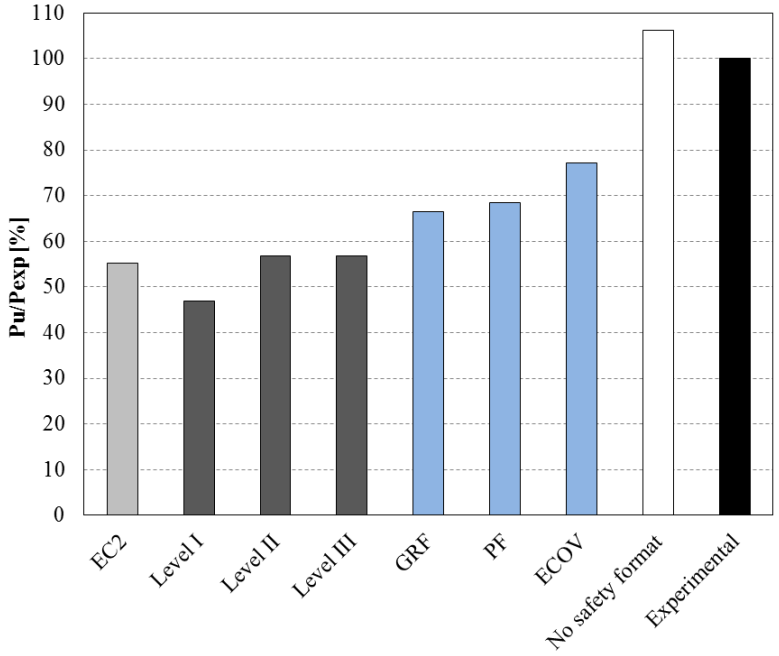

Figure 4-29: Case PB2. Analytical and numerical design values of beam resistance expressed in terms of a percentage of the experimental ultimate value of applied load, P_{Exp}=6983.35kN

The analysis named "no safety format" refers to the NLFE analysis carried out using mean measured values of material strengths without application of safety coefficient.
In Table 4-17, the design values of beam resistance, expressed in terms of applied load P_{Rd}, obtained from numerical and analytical analyses are summarized.

Table 4-17: Case PB2. Values of beam resistance, expressed in terms of applied load P_{Rd} (in kN)

P_{Exp}	EC2	Level I MC2010	Level II MC2010	Level III MC2010	GRF	PF	ECOV	No safety formats
6983.35	3859	3275	3968	3968	4638.68	4773.96	5390.96	7413.75

4.6 Parametric study on crack models

A parametric study was carried out by varying a number of sensitive parameters of the concrete constitutive model, such as the crack model and the fracture energy of concrete in tension.
In Table 4-17 the material parameters implemented in NLFE analyses performed for the parametric study are given. The analyses 1 to 3 refer to the three analyses carried out by varying the aforementioned material parameters. All the analyses were conducted considering mean measured values of material strengths. Parabolic law in compression and exponential law in tension were used for concrete, while an elasto-plastic law with hardening was applied for steel. The analyses were carried out in load-control with arc-length control. A variable Poisson ratio and a limit value of the reduction of the compressive strength of concrete due to lateral cracking according to:

$$\beta_{\sigma,\min} = \frac{f_{c,red}}{f_{cm}} = 0.6$$

were adopted for all analyses. The effects of the applied value of the fracture energy of concrete in tension on the beam response was investigated by means of comparison of

the formulation of Model Code 1990 (CEB-FIB, 1993) and Model Code 2010 (fib, 2013). The fracture energy of concrete in compression was always considered to be $250G_F$ (Nakamura et al. 2001).
In the fixed crack model, a variable shear retention factor, that depends on the mean aggregate size d_{aggr}, the crack normal strain ε_n and the crack bandwidth value h was used:

$$\beta = 1 - \left(\frac{2}{d_{aggr}} \right) \varepsilon_n h$$

Table 4-18: Case PB2. Parametric study on crack models

Analysis	Total strain crack model	G_F	G_C	Peak load value (kN)
Analysis 1	rotating	MC2010	250 G_F	7413.75
Analysis 2	rotating	MC1990	250 G_F	7279.65
Analysis 3	fixed	MC2010	250 G_F	8057.43

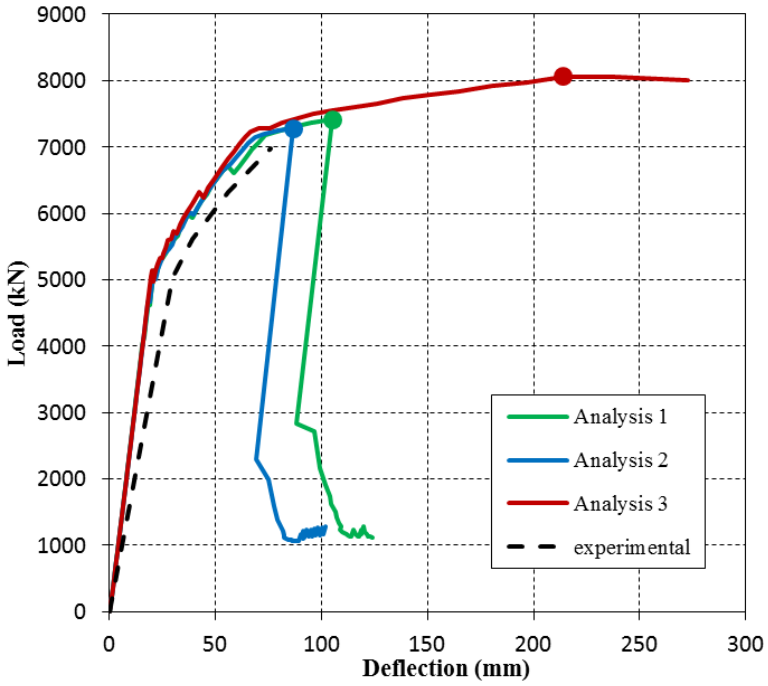

Figure 4-30: Case PB4. Parametric study

In Figure 4-30 the load-deflection curves obtained from the parametric study are plotted and the peak load of each analysis is marked with a circular indicator. The peak load is defined in correspondence of the highest load step where the energy norm ratio satisfies the fixed tolerance of 1×10^{-3}. The peak load values are reported in Table 4-18.

Comparing analysis 1 with analysis 2, the relatively small influence of the adopted value of the fracture energy of concrete in tension ($G_{F,MC1990} = 0.149\,N/mm$; $G_{F,MC2010} = 0.170\,N/mm$) and the relative value of the fracture energy of concrete in compression ($G_{F,MC1990} = 37.33\,N/mm$; $G_{F,MC2010} = 42.51\,N/mm$) can be noted, despite the beam having failed in shear compression. This is due to the fact that by increasing the compressive strength value, the difference between the fracture energy of concrete

in tension calculated according to the Model Code 2010 and the Model Code 1990 decreases-fracture energy of concrete in tension is exponentially dependent on the compressive strength. Therefore, because the compressive strength of PB2 beam is equal to 109.63 MPa, the difference between the fracture energy of concrete in tension calculated according to the Model Code 2010 and the Model Code 1990 is relatively small.

From the comparison of analyses 1 and 3, it can be seen that the adopted crack model (total strain rotating or fixed crack model) has a big influence on the beam response, especially in terms of peak deformation. The peak load and peak deformation are significantly overestimated when a fixed crack model with a shear retention factor dependent on the aggregate size diameter is adopted. Furthermore, the crack pattern and failure mode from experiments can be better reproduced with the analysis containing rotating model.

4.7 Concluding remarks

Prestressed beam PB2 subjected to uniformly distributed load exhibited a shear-compressive failure mechanism at a load equal to $P = 6983.35kN$. The simulation of the experiment was executed with a FEA model studied in multiple analyses. The concrete beam was modelled with a total strain rotating crack model, exponential softening in tension and parabolic behavior in compression, variable Poisson's ratio of concrete and reduction of compressive strength of concrete due to lateral cracking. The model for the reinforcement bars and stirrups was based on hardening plasticity.
As presented in the preceding section, the NLFEA with mean measured values of material strength resulted in a shear-compressive failure mechanism. The failure occurred at the peak load of 7413.75kN and was characterized by crushing of concrete at the level of the web-bulb interface near the support along with yielding of #4 stirrups and longitudinal #3 rebars.
Safety formats for non-linear finite element analyses as proposed by the Model Code 2010 (fib, 2013) were applied to derive the design value of beam resistance. The design values of beam resistance obtained from safety formats methods were higher than the design value of beam resistance obtained with analytical sectional analysis.
Besides the application of safety formats, a sensitivity study investigating the influence of applied fracture energy of concrete and a crack model on the specimen's response was conducted. Because the beam failed in shear due to crushing of concrete, the beam response and failure mode are substantially influenced by the applied crack model, but also by the values of fracture energy of concrete in tension and compression. The shear resistance computed with the fixed crack model was significantly overestimated.
Based on the results of the analyses, it can be concluded that consistent and reliable results can be obtained by applying variable Poisson's ratio, reduction of the compressive strength due to lateral cracking with a low limit of 0.6, total strain rotating crack model and fracture energy of concrete in tension according to Model Code 2010. An energy norm with a tolerance of 10^{-3} is recommended.

5 Case PB3 (MnDOT): Runzell et al. (2007)

This prestressed beam case is beam PB3 from the experiments of Runzell, Shield, French (Runzell et al. 2007), in which two ends of a 26.822 m girder removed from Mn/DOT Bridge No. 73023 were tested. The original bridge girder was likely more than 20 years old when it was removed from service. This means that the girder was designed according to either the 1983 Standard or 1979 Interim specifications.

5.1 Experimental setup and results

Geometry

The original length of the girder was 26.82 m.
The test specimens were brought to the University of Minnesota Structures Laboratory and tested with a MTS 600 kip Universal Testing Machine. The specimens were moved into the testing apparatus using the Structures Laboratory crane, which had a maximum capacity of 15 tons. To avoid exceeding this capacity, the specimen length delivered to the laboratory was limited to 9.29 m with the bridge deck removed.
To investigate the effect of the deck on shear capacity, the specimens were tested with and without a deck, referred to subsequently as Specimens I and II, respectively. Since the deck had been removed prior to transport, a new deck was added to the specimen after it was situated in the testing apparatus. The maximum deck width that the 600kip Universal Testing Machine could accommodate was 12.19 m. The bridge deck was designed to be the same thickness and have the same longitudinal steel layout as the deck from the in-service bridge.
The testing machine was designed to apply a single concentrated load to the specimens. To avoid transferring shear to the support via a direct compressive strut, it was decided to maintain a shear span-to-depth ratio of at least 2.7. The depth of Specimen I was 1.6 m, which made it necessary to apply the load at least 4.3 m away from either support to achieve the proper shear span. With the test setup used the predicted shear capacity from for Specimen I was 276 kips according to the 2002 Standard code, which was close to the maximum capacity that could be attained with the 600 kip testing machine for the desired shear span-to-depth ratio. Thus, it was decided to modify the test specimens to maintain the shear span-to-depth ratio of 2.7 and provide ample buffer between the predicted shear capacity and maximum capacity of the MTS machine.
The specimen modification involved lengthening the beams from 9.29 m to approximately 12.19 m by splicing a cast-in-place beam extension onto the original prestressed girder section. The cast-in-place extension was designed to resist the moment and shear from the maximum possible load applied by the 600 kip machine.
In Figure 5-1, the original girder geometry is illustrated while in Figure 5-2 and Figure 5-3 the modified specimen and the construction phase of the extension are shown. In Figure 5-4 the cross sectional details are depicted.

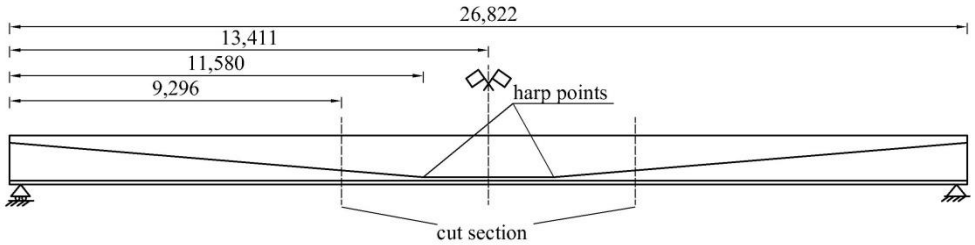

Figure 5-1: Case PB3. Girder of Mn/DOT Bridge No. 73023 (dimensions in mm)

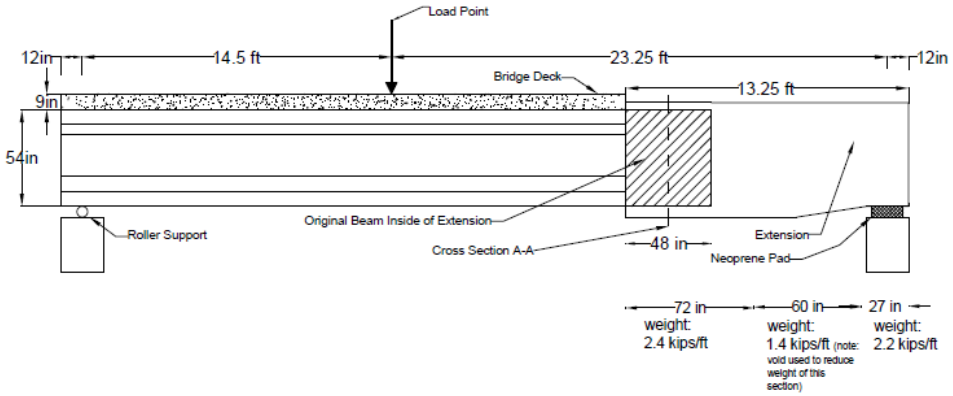

Figure 5-2: Case PB3. Modified specimen (Runzell et al. 2007)

(a) (b)

Figure 5-3: Extension construction (a) before casting, (b) after casting (Runzell et al. 2007)

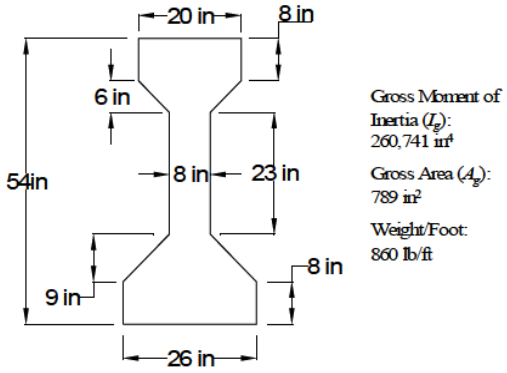

Figure 5-4: Cross-sectional dimensions (in ft and in) of the girder (Runzell et al. 2007)

The beam has 10 draped and 33 straight 13 mm diameter strands, prestressed with stress in prestressing steel after all losses σ_{pcs} equal to 864 N/mm^2.
The plans for Mn/DOT Bridge No. 73023 indicated that during fabrication the prestressing strands were initially stressed to 189 ksi (1303 MPa), which was 70% of their 270 ksi (1862 MPa) ultimate strength. At release, the immediate source of loss in the prestressing strands was due to elastic shortening of the concrete beam. The other sources of loss were long term and occurred over the life of the beams. These losses included creep and shrinkage of concrete, and relaxation of the prestressing strand. To experimentally verify σ_{pcs}, two strands from each of the test specimens were exposed, instrumented with strain gauges, and cut. The recorded change in strain was used to find the measured σ_{pcs} and verify the code predicted losses. Prestressing strands on the

non-test end, for shear, were cut prior to the ultimate shear test to ensure σ_{pcs} was measured from undamaged strands. The test location was approximately 1.27 m from the end, which was well outside the 760 mm transfer region. A jackhammer was used to expose a 381 mm section of the bottom, outer strand on each side of the beam as shown in Figure 5-5(a). The concrete was carefully removed to avoid damaging the strand with the jackhammer. At least three FLK-1-11-5LT strain gauges were attached to the strand and oriented along the axis of the wire as shown in Figure 5-5(b). A wet paper towel along with several rebar ties were then attached to the strand a short distance away from the strain gages, Figure 5-5(c), to protect them from heat during cutting and to prevent the strand from unwinding. The prestressing strand was then flame-cut with an oxy-acetylene torch while strain data were recorded.
The strains were measured before the bridge deck was added to Specimen I. The average change in strain values from all of the gauges was 3,964 με, neglecting the extreme high and low values. Because the change in strain was measured using strain gauges oriented along the axis of the wires, it was necessary to measure the apparent modulus of elasticity of the strand along this axis so the change in strain could be converted to an effective prestressing. To measure the apparent modulus of elasticity, several samples of prestressing strand were removed from the specimens after the ultimate shear tests. These samples were fitted with strain gauges oriented along the axis of the strand and tested to ultimate. The apparent modulus of elasticity of the prestressing strand was 217875 N/mm^2, which was obtained from the stress-strain curves of the prestressing strands. Using the average change in strain of 3.964με and the apparent modulus of elasticity of 217875 N/mm^2 that corresponded with the gauge orientation, the effective prestressing for the two test beams was 864 N/mm^2. The effective prestressing subtracted from the initial prestressing of 1303 N/mm^2 gave losses of about 34%.

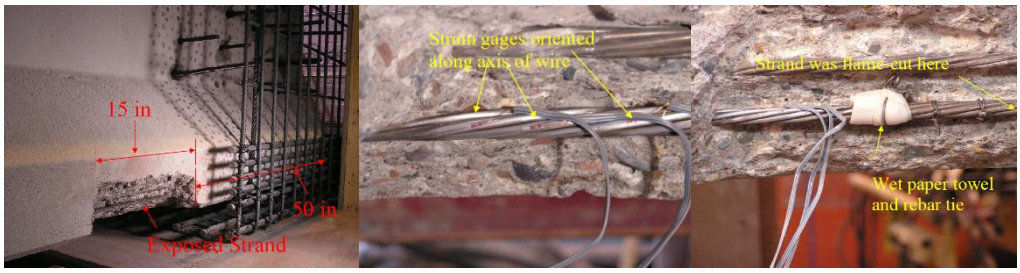

(a) (b) (c)

Figure 5-5: Case PB3. (a) Prestressing Strand Test Location, (b) Strain Gages on Prestressing Strand, (c) Final Prestressing Strand Test Setup, (Runzell et al. 2007)

The stirrups spacing in the specimens is 531 mm over the entire length of the beam, except at the original ends of the 26.82 m girder, which had closer spacing over the support in the prestressing strand anchorage zone. The stirrups are double leg, Grade 420, with diameter 13 mm. In addition to the full depth stirrups there are stirrups spaced at 531 mm for horizontal shear; these are non-continuous stirrups that are terminate at the top web/flange intersection, and were designed to ensure composite action between the girder and bridge deck. In the bridge deck two layers of Grade 60, 13 mm diameter longitudinal reinforcement spaced at 457 mm and 229 mm are added. In Figure 5-6 and Figure 5-7 the reinforcement details are depicted.

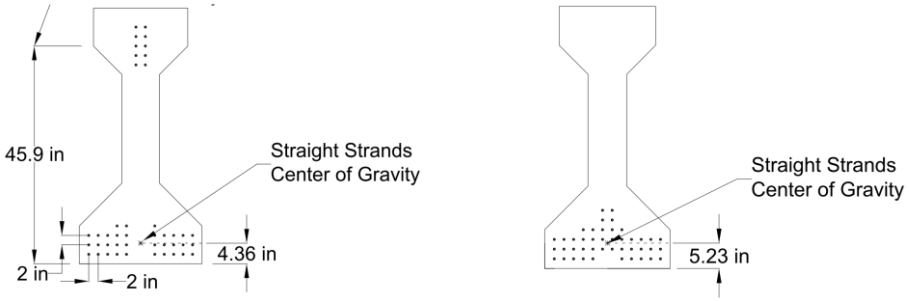

Figure 5-6: Case PB3. Prestressing strand pattern at: (a) girder end; (b) harp point (Runzell et al. 2007)

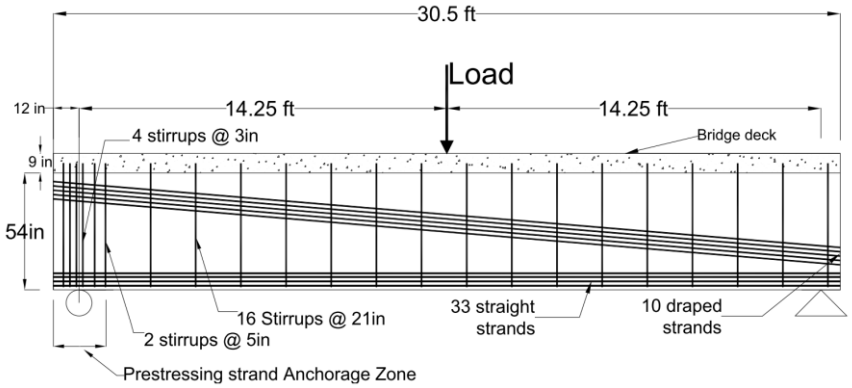

Figure 5-7: Case PB3. Reinforcement layout (Runzell et al. 2007)

Material Properties

Concrete and reinforcement properties given in references are shown in Table 5-1.

Table 5-1: Case PB3. Concrete and reinforcement properties

Concrete properties					
f_{cm} **(N/mm^2)**		E_c **(N/mm^2)**		d_{max} **(mm)**	
69.84		34819		16	
Bar	Φ **(mm)**	A_s **(mm^2)**	E_s **(N/mm^2)**	f_{ym} **(N/mm^2)**	f_{tm} **(N/mm^2)**
Φ13	13.0	132.73	210000	464	570
strands Φ11.2	43x11.2	43x98.77	196500	1675	1862

Loading and Boundary Conditions

The loading and boundary conditions in the experimental setup are shown in Figure 5-8.

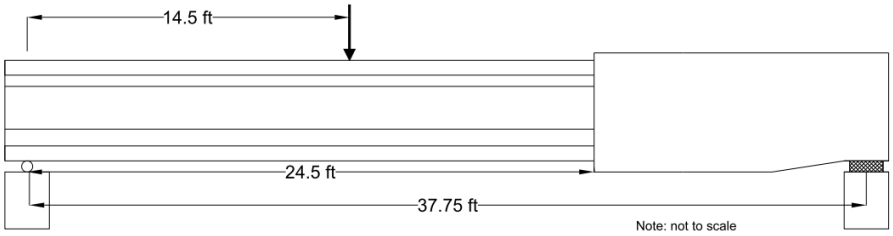

Figure 5-8: Case PB3. Loading, boundary conditions and dimensions (Runzell et al.)

Experimental Results

The beam exhibited a shear-compressive failure mechanism with crushing of concrete at the web/flange interface, see Figure 5-9 and Figure 5-10. The first visible cracks were flexural cracks on the bottom flange directly below the applied load. At a certain level of load an audible popping sound was heard and several large web cracks formed simultaneously. These cracks continued to grow and widen and many flexural cracks formed. When the test terminated there was significant crushing at the web/flange interface that resulted in spalling of the web concrete.

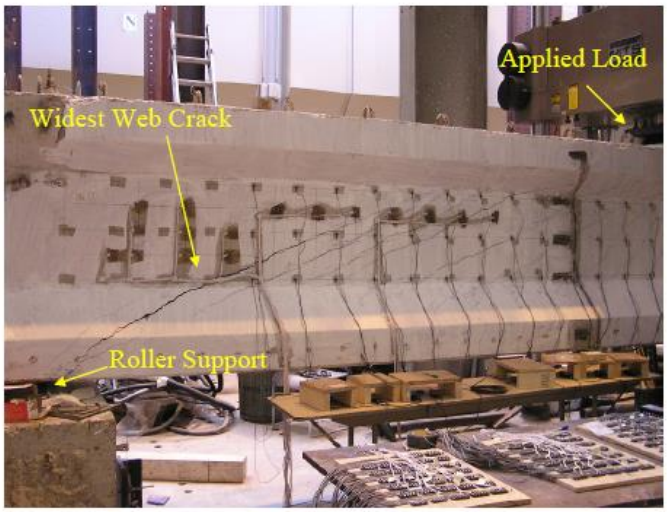

(a)

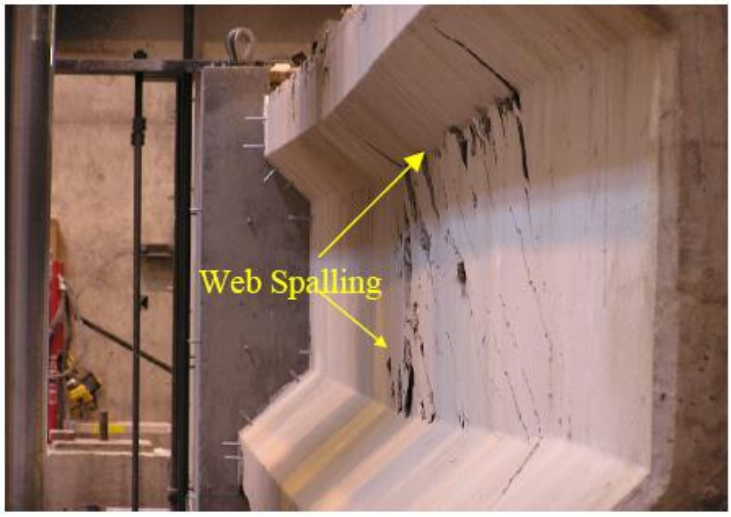

(b)

Figure 5-9: Case PB3. Failure mechanisms at peak load: (a) cracking, (b) web crushing, (Runzell et al. 2007)

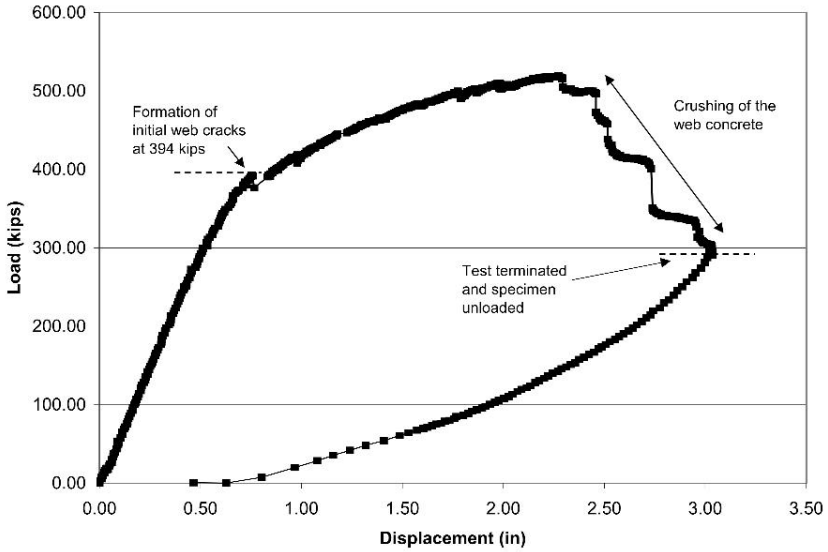

Figure 5-10: Case PB3. Load-deflection curve of Specimen II (Runzell et al. 2007)

5.2 Analytical analysis

In Figure 5-11 the load configuration at failure is reported.

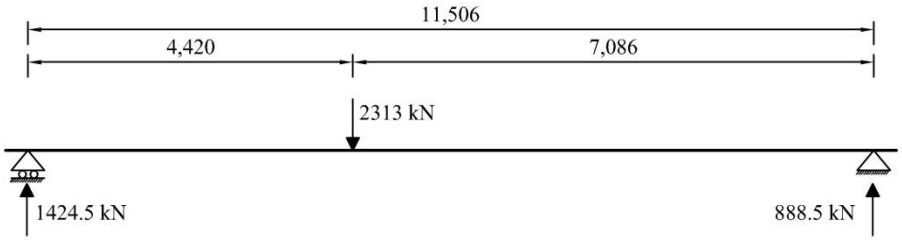

Figure 5-11: Case PB3. Load configuration at failure (dimensions in m)

Load case 1:

Self-weight was taken into account through the equivalent distributed load – $q_{extension} = 35.1 kN/m$ and $q_{extension} = 35.1 kN/m$. In Figure below the bending moment of interest is at the location of application of the point load. It is 257.5kNm.

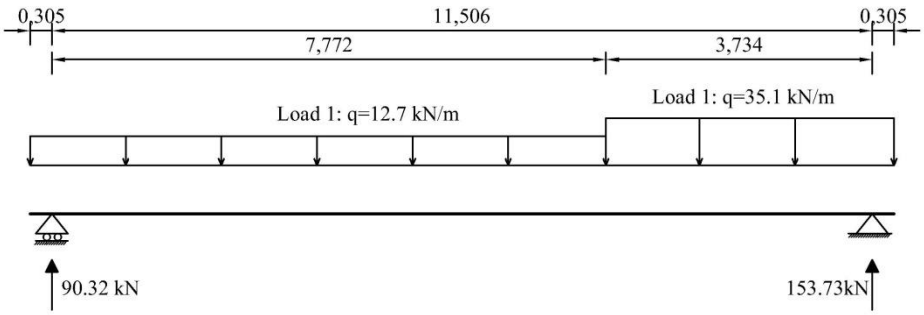

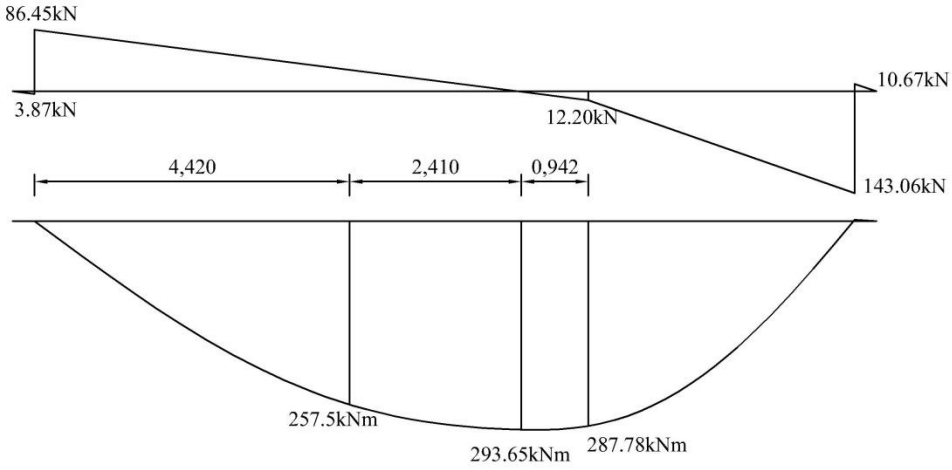

Figure 5-12: Case PB3. Load case 1: self-weight (dimensions in m)

The loading effect of prestressing on the member was included through equivalent bending moment and shear forces at each end. The bending moment is calculated as the effective prestressing force in the fictitious tendon acting on an eccentricity respect to the centroidal axis of the beam. From the source document, the center of gravity of strands at the free end is 0.356m and hence the eccentricity $C_G - C_s = 0.629m - 0.356m = 0.272m$; where C_G is the center of gravity of the concrete section. In a similar fashion, the estimated eccentricity at the enclosed end is $0.629m - 0.16m = 0.469m$. The resulting internal forces are depicted in Figure 5-13.

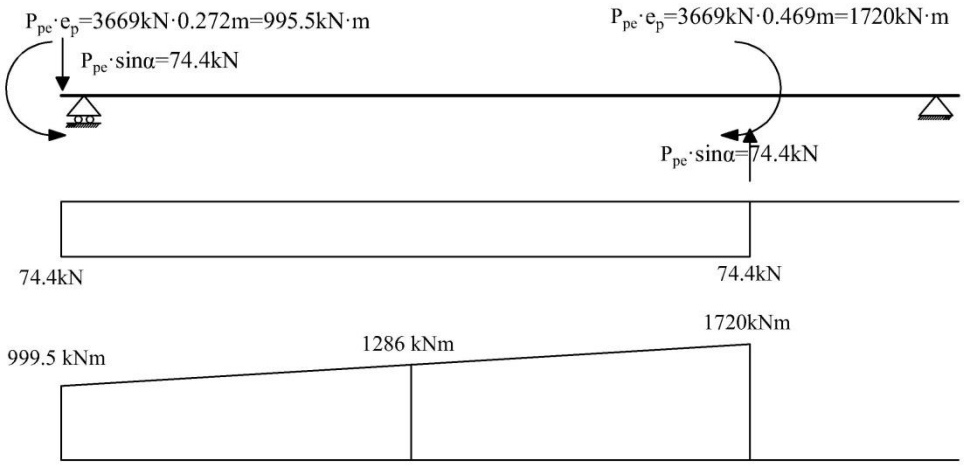

Figure 5-13: Case PB3. Load case 1: prestressing (dimensions in m)

Load case 2:
The moment and shear force envelope as a result of the loading from the testing machine is given below, Figure 5-14. The unknown magnitude of force *P* is searched for.

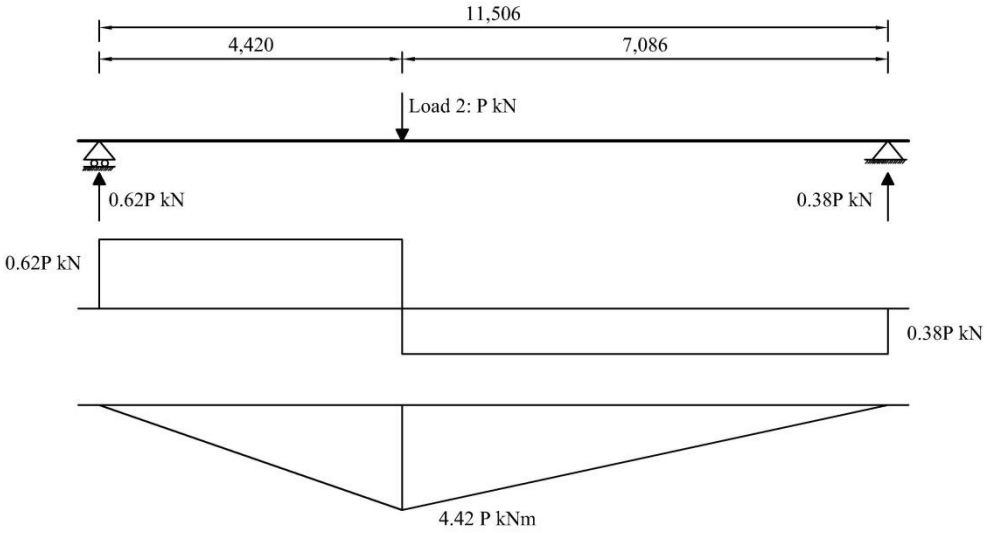

Figure 5-14: Case PB3. Load 2: Internal forces from testing machine (dimensions in m)

Bending moment resistance

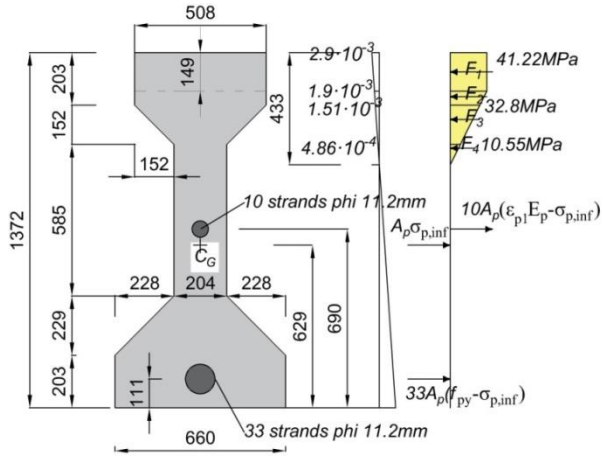

Figure 5-15: Case PB3: Forces acting on a section, ULS

Horizontal force equilibrium to determine a compression zone height; assumptions: bilinear stress block and yielding of the bottom strands.

$$F_C = 43\sigma_{pe}A_p + 33A_p(f_{pyd} - \sigma_{pe}) + 10A_p(\varepsilon_{p1}E_p - \sigma_{pe}) \rightarrow x_{CompZone} = 433mm$$

where:

$$F_1 = 149mm \times b_{flange} f_{cd} = 3127kN$$

$$F_2 = \left(h_{flange} - 149mm\right)\frac{f_{cd} + \sigma_{fl}}{2} b_{flange} = \left(203mm - 149mm\right)\frac{41.22MPa + 32.8MPa}{2} = 1102kN$$

$$F_3 = \frac{b_{flange} + b_{web}}{2}\frac{\sigma_h + \sigma_{flange}}{2} h_{inclined} = \frac{508mm + 204mm}{2}\frac{10.55MPa + 32.8MPa}{2} 229mm = 1172kN$$

$$F_4 = 10.55MPa\left(h_{comp.zone} - h_{flange} - h_{inclined}\right)0.5b_{web} = 77.809kN$$

$\varepsilon_{p1} = \frac{2.9\times10^{-3}(h-690mm-x_{comp.zone})}{x_{comp.zone}} + \frac{\sigma_{pe}}{E_p} = 6.061\times10^{-3}$ which is lower than the yielding strain of prestressing steel $\varepsilon_{py} = \frac{f_{yd}}{E_p} = 6.712\times10^{-3}$ therefore the increase of force in prestressing steel at this location is as given in the equation for the horizontal force equilibrium. At the level of straight strands, the strain in prestressing steel reached the yielding strain therefore assuming no hardening of the steel, the increase of force in prestressing steel is: $33A_p(f_{pyd}-\sigma_{pe})$.

$M_{Rd} = F_c(z_{ct}-y) + 33A_p(f_{pyd}-\sigma_{pe})(C_g - 111mm) + 10A_p(\varepsilon_{p1}E_p - \sigma_{pe})(690mm - C_G) =$
$5478kN\times(0.734m-0.142m) + 768.04kNm + 19.86kNm = 4082kNm$

With superposition of bending moments from Load cases 1 and 2 at the location of load P on the left hand side of the equation and the calculated design bending moment resistance on the other, it is possible to determine the maximum load that can be applied. It is:

$4.42m\times P - 1286kNm + 257.5kNm = 4082kNm \rightarrow P = 1156kN$

Shear resistance

Shear resistance calculated according to **EC2**.

Resistance of stirrups:

$V_{Rd,s} = \frac{A_{sw}}{s} z\, f_{ywd}\cot\theta = \frac{265.4mm^2}{531mm} 934mm\times365.4MPa\times2.5 = 426.87kN$

$V_{Rd,\max} = \frac{f_{cd}b_{web}z\alpha_{cw}\nu_1}{\tan\theta+\cot\theta} = \frac{41.23MPa\times203mm\times1.18\times0.59}{0.4+2.5} = 187.7kN$

Where: $\sigma_{cp} = \frac{A_p\sigma_{p,\inf}}{A_{beam}} = 7.21MPa \rightarrow \alpha_{cw} = 1+\frac{\sigma_{cp}}{f_{cd}} = 1.18$

and $\nu_1 = 0.9 - \frac{f_{ck}}{200} = 0.591$

The value of load *P* after accounting for the contribution of prestressing and the effect of self-weight is:

$74.4kN + 426.87kN = 0.62P + 86.45kN \rightarrow P = 668.42kN$

The design value of shear resistance of PB3 beam is also calculated according to the **Model Code 2010** (fib, 2013) applying three levels of approximations proposed for analytical calculations.

Table 5-2: Case PB3. Parameters used in the calculation of V_{Rd}

	Level I	**Level II**	**Level III**
θ_{min} (°)	25	20	20
θ_{max} (°)	45	45	45
k_ε	0.55	0.65	0.65

Level I Approximation

$V_{Rd,s}(\theta_{\min}) = \frac{A_s}{s} z f_{ywd}\cot(\theta_{\min}) = \frac{265.4mm^2}{531mm} 934mm\times365.4MPa\times\cot(25°) = 365.8kN$

$V_{Rd,\max}(\theta_{\min}) = k_c\frac{f_{ck}}{\gamma_c} b_w z\sin\theta_{\min}\cos\theta_{\min} = 0.432\times\frac{61.84MPa}{1.5} 203mm\times934mm\sin(25°)\cos(25°)$
$= 1294kN$

Level II Approximation

Because of ε_x is negative for a whole range of V_{Ed}, the minimum angle of compressive struts in taken in the calculations. It follows that:

$\theta_{\min} = (20\text{deg} + 10000\varepsilon_x) = 20\text{deg}$

$k_\varepsilon = \frac{1}{1.2 + 55\varepsilon_1} = 0.493$

$\eta_{fc} = \left(\frac{30MPa}{f_{ck}}\right)^{\frac{1}{3}} = 0.786 < 1$

$k_c = k_\varepsilon \eta_{fc} = 0.387$

$V_{Rd,s}(\theta_{\min}) = \frac{A_s}{s} z f_{ywd} \cot(\theta_{\min}) = \frac{265.4mm^2}{531mm} 934mm \times 365.8MPa \times \cot(20°) = 468.7kN$

$V_{Rd,\max}(\theta_{\min}) = k_c \frac{f_{ck}}{\gamma_c} b_w z \sin\theta_{\min} \cos\theta_{\min} =$

$= 0.387 \times \frac{61.84MPa}{1.5} \times 203mm \times 934mm \sin(20°)\cos(20°) = 973.04kN$

Level III Approximation

$\varepsilon_x = \frac{\frac{M_{Ed}}{z} + V_{Ed,trial} - N_{Ed}\left(\frac{1}{2} - \frac{\Delta e}{z}\right)}{2\left(\frac{z_s}{z} E_s A_s + \frac{z_p}{z} E_p A_p\right)} < 0$ calculated at the critical section at the distance d from the edge of the support for $V_{Ed,trial} = 615kN$. Because $\varepsilon_x < 0$, the minimum value of an angle of compressive struts is investigated.

$\theta_{\min} = (20\,\text{deg} + 10000\varepsilon_x) = 20\,\text{deg}$

$\varepsilon_1 = \varepsilon_x + (\varepsilon_x + 0.002)\cot\theta_{\min}^{\,2} = 0.015$

$k_\varepsilon = \frac{1}{1.2 + 55\varepsilon_1} = 0.493$

$\eta_{fc} = \left(\frac{30MPa}{f_{ck}}\right)^{\frac{1}{3}} = 0.786 < 1$

$k_c = k_\varepsilon \eta_{fc} = 0.387$

$V_{Rd,\max}(\theta_{\min}) = k_c \frac{f_{ck}}{\gamma_c} b_w z \sin\theta_{\min} \cos\theta_{\min} = 0.387 \times \frac{61.84MPa}{1.5} \times 203mm \times 934mm \sin(20°)\cos(20°)$

$= 973kN$

$V_{Rd,s}(\theta_{\min}) = \frac{A_s}{s} z f_{ywd} \cot(\theta_{\min}) = \frac{265.4mm^2}{531mm} 934mm \times 365.8MPa \times \cot(20°) = 468.7\,kN$

$k_v = \frac{0.4}{1 + 1500\varepsilon_x}\left(1 - \frac{V_{Ed,trial}}{V_{Rd,\max}}\right) = 0.147$

$V_{Rd,c} = k_v \frac{\sqrt{f_{ck}}}{\gamma_c} b_w z = 0.182 \times \frac{\sqrt{61.84MPa}}{1.5} \times 203mm \times 934mm = 192.6kN$

$V_{Rd} = (V_{Rd,s} + V_{Rd,c}) < V_{Rd,\max}(\theta_{\min})$

$V_{Rd} = V_{Rd,s}(\theta_{\min}) + V_{Rd,c} = 615.4kN$

The assumed trial shear resistance is equal to the calculated design shear resistance hence no further iterations are required. The load *P* calculated including advantageous contribution of prestressing and self-weight e.g. for LoA III:

$V_{Rd,s} = 0.62P_{Rd} + V_{SW} - V_p \rightarrow 615.4kN = 0.62P_{Rd} + 70.5kN - 74kN$ gives $P_{Rd} = 998.23kN$

Similar calculations were performed for the remaining levels of approximation.
The design value of beam resistance expressed in terms of applied load P_{Rd} are summarized in Table 5-3.

Table 5-3: Case PB3. Design value of beam resistance expressed in terms of applied load P_{Rd} (Model Code 2010)

	EC2	**Level I**	**Level II**	**Level III**
P_{Rd}(kN)	668.42	595.64	761.6	998.23

5.3 Finite element model

Units
Units are N, mm.

Material models and parameters
The concrete model is based on a total strain rotating crack model with:

- exponential softening in tension and parabolic behavior in compression,
- variable Poisson's ratio of concrete,
- reduction of compressive strength of concrete due to lateral cracking with a lower limit of 0.6.
- increase in compressive strength due to lateral confinement according to the model proposed by Selby and Vecchio (Selby and Vecchio 1993).

The mechanical properties are summarized in Table 5-4. On input, the G_F value has been decreased with a factor $\sqrt{2}$ in order to compensate for an underestimation of the crack band width for cracks with an inclination angle of 45 degrees. The uniaxial stress-strain curve is shown in Figure 5-16.

Table 5-4: Case PB3. Constitutive model parameters for concrete

	f_{cm} (N/mm^2)	f_{ctm} (N/mm^2)	E_c (N/mm^2)	ν	G_F (Nmm/mm^2)
Mean measured value	69.84	4.40*	34819	var	0.157*

*Not specified in reference; calculated according to Model Code 2010 (fib, 2013)
$f_{ct} = 2.12\ln(1 + 0.1 \cdot f_{cm})$

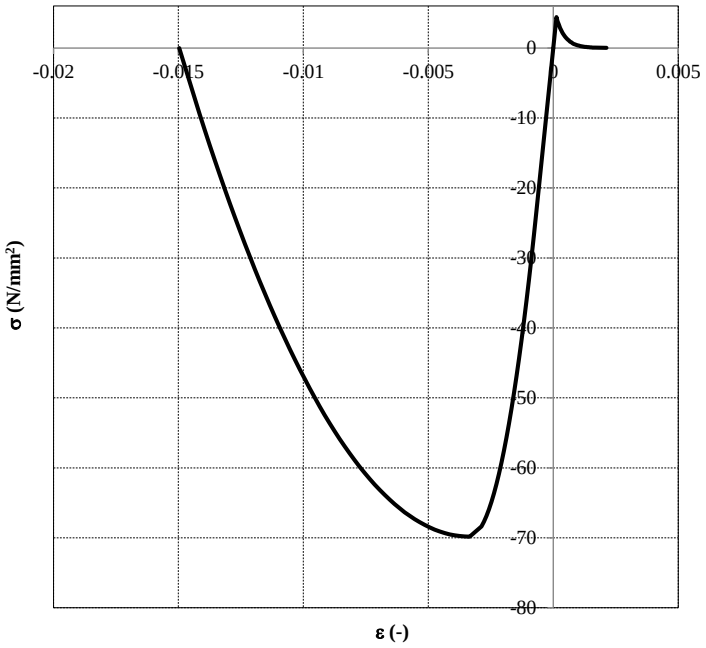

Figure 5-16: Case PB3. Stress-strain curve for concrete

The model for the reinforcement bars and stirrups is based on hardening plasticity. Geometrical and mechanical properties of reinforcement are summarized in Table 5-1. The stress-strain curve of stirrups is plotted in Figure 5-17.

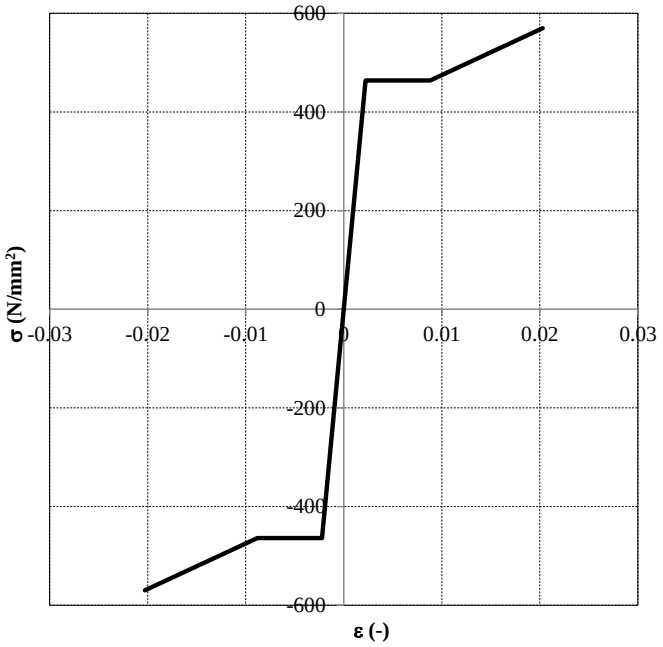

Figure 5-17: Case PB3. Stress-strain curve adopted for stirrups

For the steel plates a linear elastic behavior is assumed, see Table 5-5.

Table 5-5: Case PB3. Steel plates properties

E (N/mm^2)	ν
210000	0.3

Interface elements were used between the steel support plates and the concrete beam at the supports and loading positions. The interface stiffness was derived based on the concrete properties. The total thickness of interface elements equals 1 mm.
A bilinear behavior in the normal direction (see Figure 5-18) and a linear elastic relation in the shear direction were assumed. The normal stiffness in tension and the stiffness in the shear direction were taken as almost equal to zero.
The mechanical properties of the interface elements are summarized in Table 5-6.

Table 5-6: Case PB3. Interface properties

$K_{nn\ in\ tension}$ (N/mm^3)	$K_{nn\ in\ compression}$ (N/mm^3)	K_t (N/mm^3)
3.48E-02	3.48E+04	3.48E-02

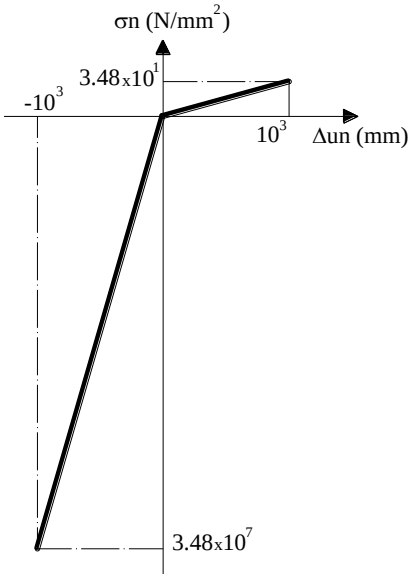

Figure 5-18: Case PB3. Traction-displacement diagram in normal direction for interfaces

Element types and finite element mesh

To mesh concrete beam 8-node membrane elements (CQ16M) with a full integration scheme (3×3) were used. The average element size is 72×72 mm^2. The dimensions of the elements were established on the basis of an assumed constant thickness per element, Figure 5-21 (c).
The reinforcement bars and stirrups were modelled with embedded truss elements with two Gauss integration points along the axis of the element. Perfect bond is assumed. Strands placed at the bottom were grouped and placed in the centerline. For the steel plates 8-node membrane elements (CQ16M) were used. The 6-node interfaces elements have three Lobatto integration points.
The adopted dimensions for the beam and for the transversal cross section of the beam are given in Figure 5-19. The mesh of the beam is presented in Figure 5-20(a). The different materials are indicated with different colors in Figure 5-20(b).

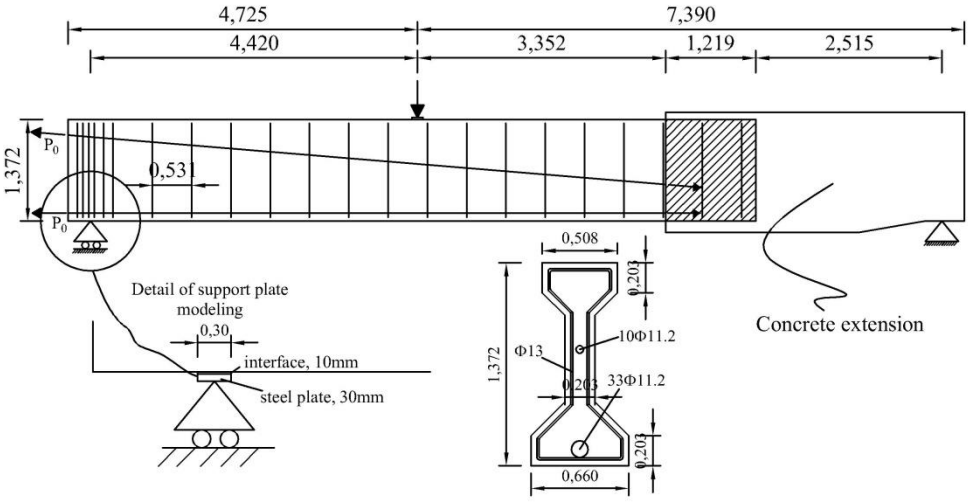

Figure 5-19: Case PB3. Dimensions of the beam and loading scheme; reinforcement, cross section and support plate details (in m)

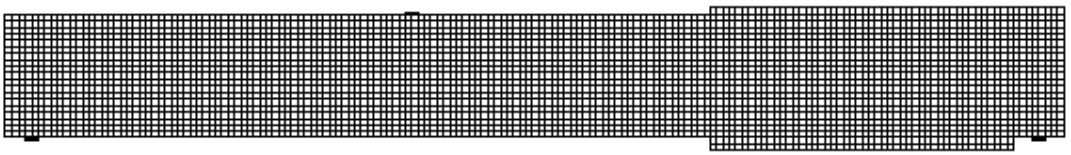

(a)

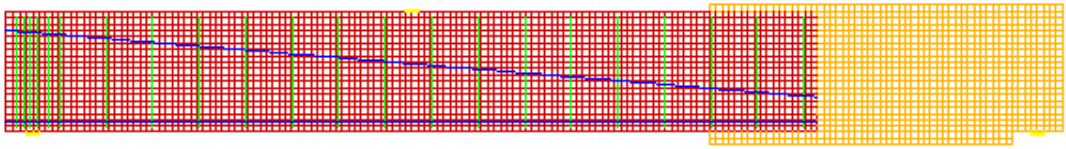

(b)

Figure 5-20: Case PB3. (a) Mesh and (b) material sets

Different groups of elements were defined to distinguish the concrete elements and the steel elements. These groups will be used in section 5.4 to monitor the failure mode during the analysis. For monitoring yielding of applied steel, groups STIRRUPS and STRANDS refer to stirrups and strands of the beam respectively, see Figure 5-21 (b). Figure 5-21 shows the groups of elements named SHEAR, used for tracking inelastic behavior of concrete. Figure 5-21(c) shows the groups of element named FL_INF_C, FL_INF_P, FL_INF_S, FL_INF_T, WEB, FL_SUP_P, FL_SUP_S, FL_SUP_C used to model the cross section dimensions.

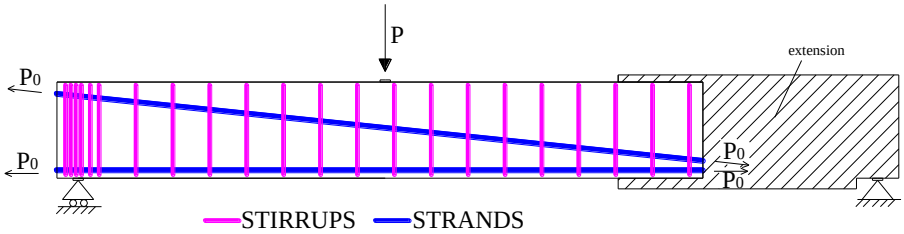

(a)

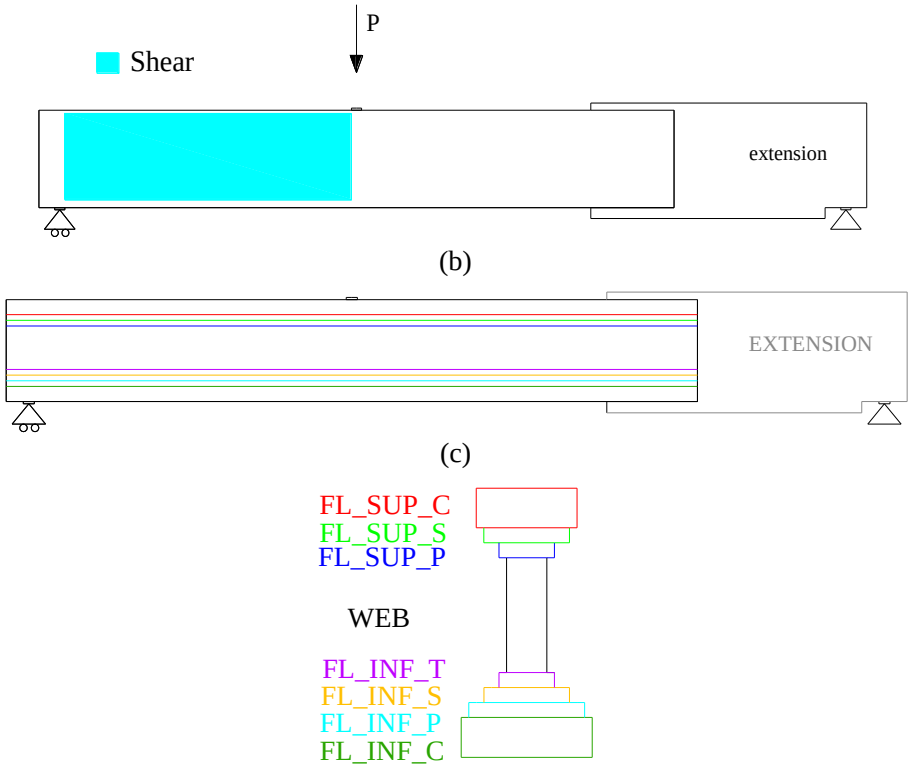

Figure 5-21: Case PB3. Groups of steel elements monitoring (a) yielding of reinforcement, (b) inelastic behavior of concrete, (c) groups of elements used to model the beam cross sectional dimensions

Boundary conditions and loading

Boundary conditions were applied to nodes of steel plate. Translation along *x* and *y* axes at a single node of the left steel plate (support 1) and translation along *y* axis at a single node of the right steel plate (support 2) were constrained, Figure 5-22.

In load case 1 the prestressing force $P_0(1)$ was applied. In load case 2, the dead load $q(2)$ was applied and in Load case 3 a concentrated load $P(3)$ was added to load case 2 at the middle node of the loading plate as a unit load of 1×10^5 N, Figure 5-22(a). The effective stress in prestressing steel σ_{pcs} ($P_0 = \sigma_{pcs} \times A_p$), measured during experiments after all losses as 864 N/mm^2, was introduced gradually through a transmission length, Figure 5-22(b), calculated according to the Eurocode 2 (CEN, 2005), with:

$$l_{pt} = \frac{\alpha_1 \alpha_2 \phi \sigma_{pm0}}{f_{bpt}}$$

$$f_{bpt} = \eta_{p1} \eta_1 f_{ct}$$

where:

$\alpha_1 = 1$ for gradual release, $\alpha_2 = 0.19$ for strands, $\varphi = 13\,mm$ = nominal diameter, $\sigma_{pm0} = 1186\,N/mm^2$ = prestressing stress after elastic losses (assumed equal to 9% of the initial prestressing stress of 1303 N/mm^2), $\eta_{p1} = 3.2$, $\eta_1 = 1$ for good bond.

For calculation at ultimate state, the transmission length L_{pt} can be taken equal to $1.2 l_{pt}$ so that for $L_{pt} = 250mm$.

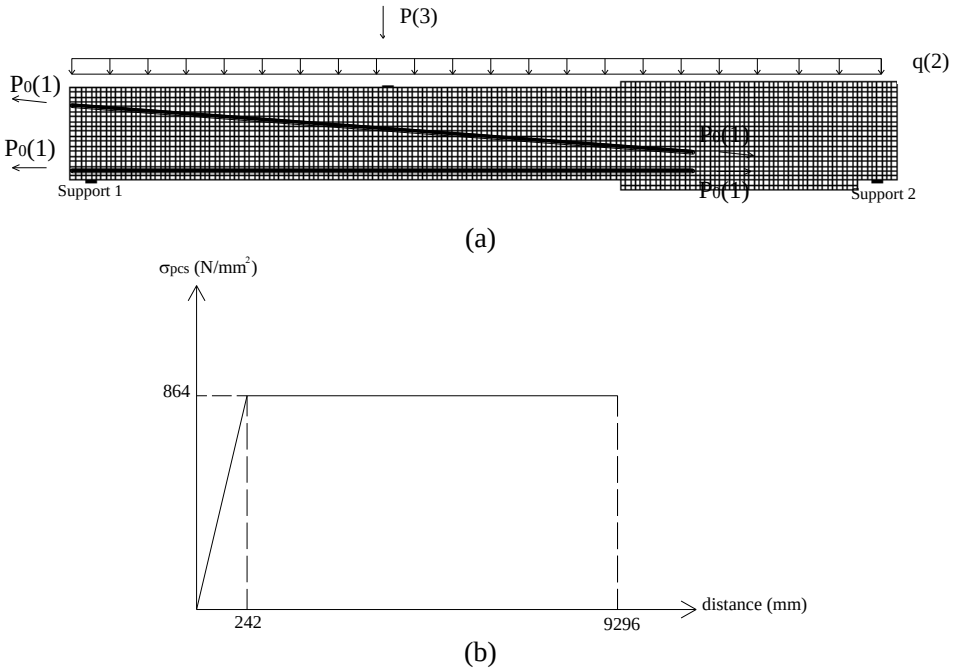

Figure 5-22: Case PB3. (a) Boundary conditions and load cases 1 and 2, (b) initial stress in prestressing steel distribution

Load increments and convergence criteria

Load case 1 was applied in 2 steps. The regular Newton-Raphson method with a maximum of 25 iterations was used. As convergence criteria, the force and energy norms were selected. The analysis was set to continue even if the convergence criteria were not satisfied. The convergence tolerances were equal to 1×10^{-2} for the force norm and 1×10^{3} for the energy norm. A Line Search algorithm was used to improve the convergence performance.

Load case 2 was applied in 1 step. The regular Newton-Raphson method with a maximum of 25 iterations was used. As convergence criteria, the norms of the force and energy were selected. The analysis continued even if the convergence criteria were not satisfied. The convergence tolerances were equal to 1×10^{-2} for the force norm and equal to 1×10^{-3} for the energy norm. A Line Search algorithm was used to improve the convergence performance.

Load case 3 was applied with automatic adaptive load increments, based on energy has been selected. The initial load factor was 5, the upper limit of the incremental load factor equaled 10 and the lower limit of the incremental load factor equaled 3. The maximum number of steps was 100. Arc-length control was applied based on translation along y axis of node 2394 (“indirect displacement control”), Figure 5-23. The analysis continued even if the convergence criteria were not satisfied. The convergence tolerance was equal to 1×10^{-3} and 1×10^{-2} for the energy and force norms respectively. A maximum of 50 iterations was used. A line search algorithm was used to improve the convergence performance.

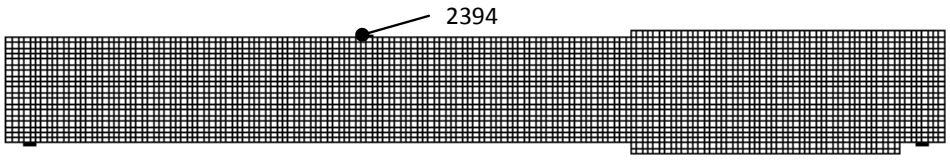

Figure 5-23: Case PB3. `Indirect Displacement control' technique applied referring to node 2394

5.4 Nonlinear finite element analysis

Load deflection

The load-deflection curve with marked values of the applied load corresponding to the beginning of yielding of stirrups and crushing of concrete are presented in Figure 5-24. The depicted load-deflection curve does not include the response of the beam from application of prestressing and dead load.

The onset point of crushing of concrete was registered when the first integration point reaches the minimum principal strain value of -3.5‰.

For the load case 3, the peak load was defined as the highest load step where the energy norm ratio satisfied the fixed tolerance of 1×10^{-3}.

The convergence behavior was quite poor after reaching the peak load. After step 75, the analysis continued even if the energy convergence criteria were not satisfied within the maximum number of iterations equal to 50. The post peak branch of the load – deflection curve is for this reason plotted with a dot line.

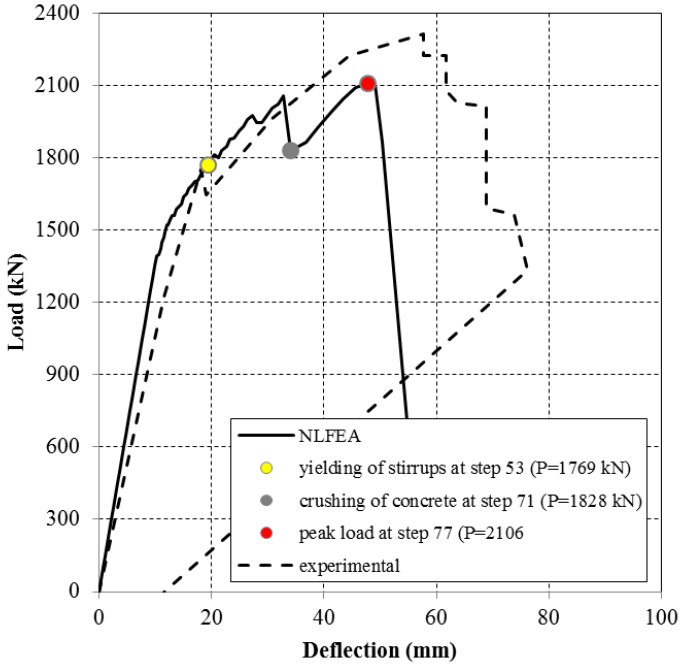

Figure 5-24: Case PB3. Load-deflection curve

Convergence behavior

For most steps convergence was achieved on the basis of the energy criterion, Figure 5-25-Figure 5-26. For load case 3, the energy norm ratio satisfied the fixed tolerance of 1×10^{-3} for almost all the steps of the analysis until to the peak load, while force norm ratio was higher than the fixed tolerance for most of steps.

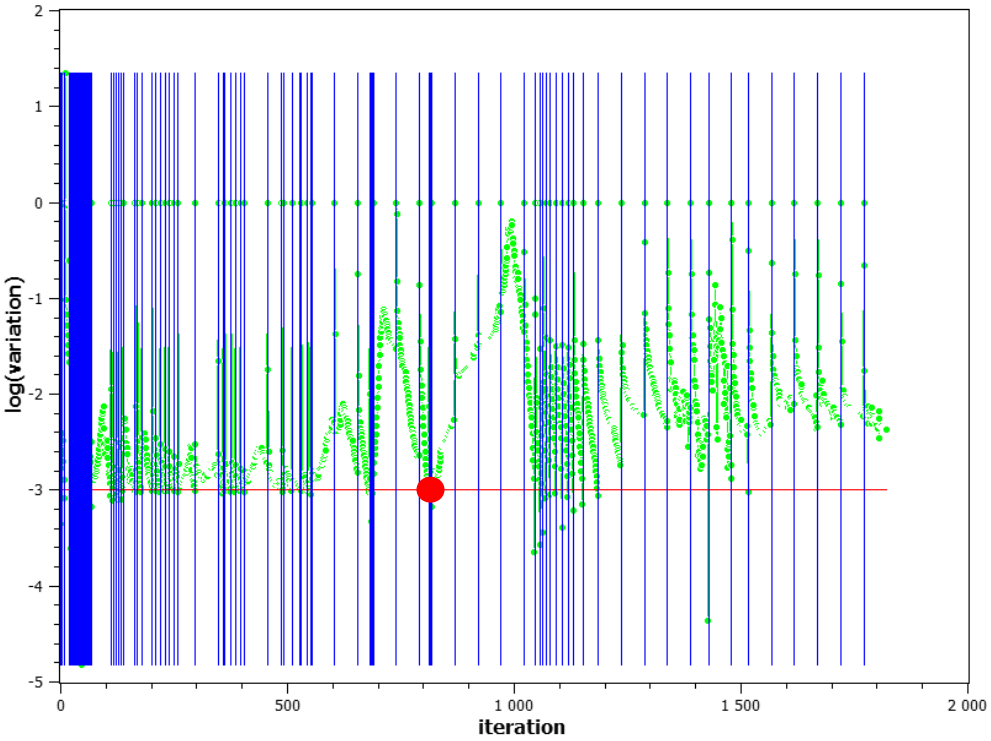

Figure 5-25: Case PB3. Evolution of the energy norm (blue lines indicate steps, red line indicates tolerance, green points indicate iterative results)

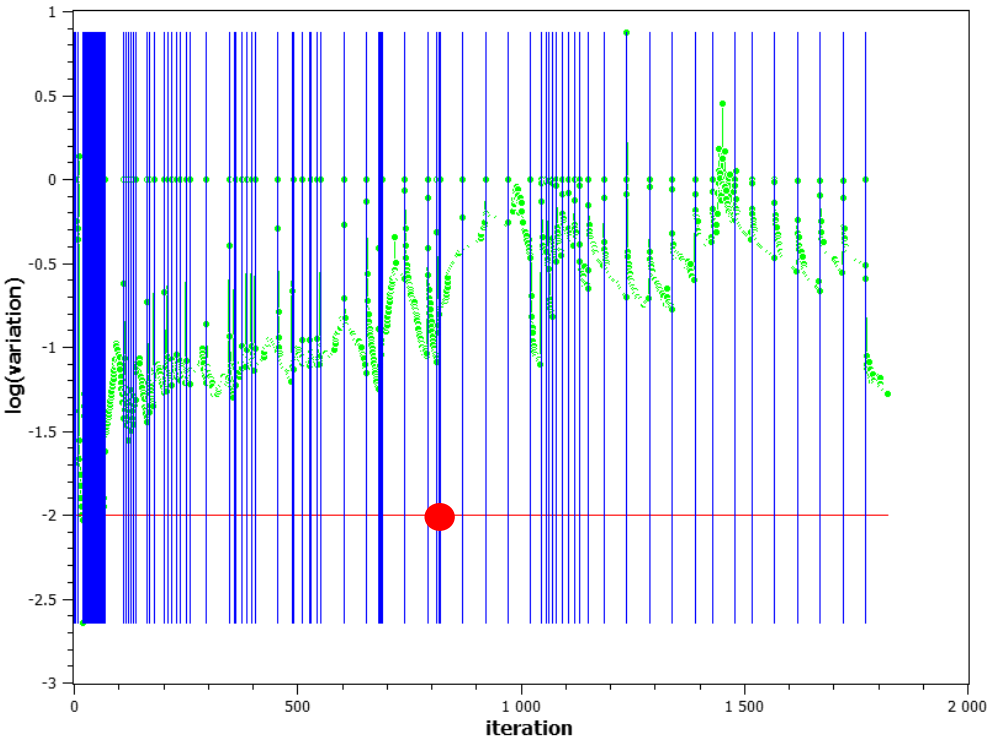

Figure 5-26: Case PB3. Evolution of the force norm (blue lines indicate steps, red line indicates tolerance, green points indicate iterative results)

Strains

Figure 5-27 shows the crack strain values at the peak load –step 75. Figure 5-28 shows the minimum principal strain values at crushing of concrete – step 71. From the values of crack strain and the contours which can be regarded as the representation of crack pattern, it can be concluded that the beam failed due to diagonal-tension. The crack pattern from the NLFEA can be compared with the experimental crack pattern in Figure 5-29

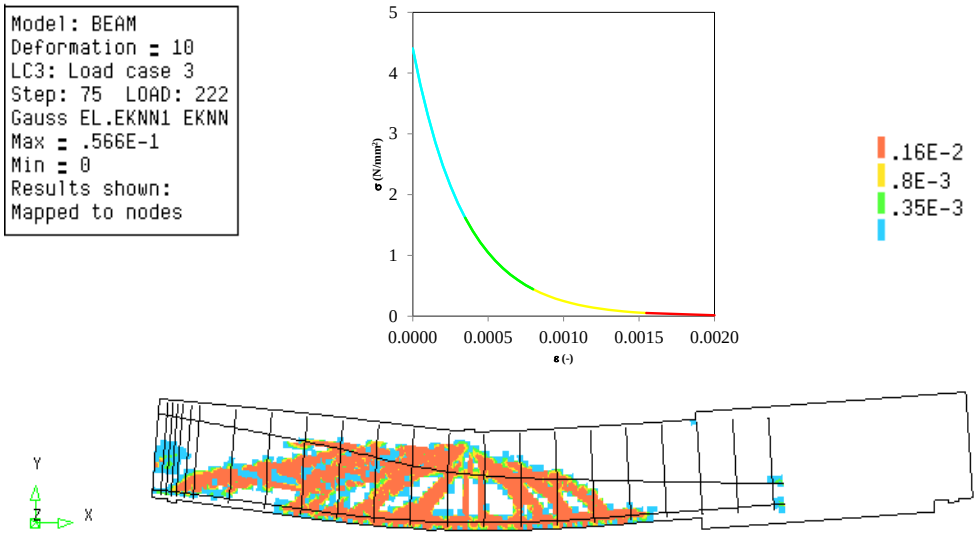

Figure 5-27: Case PB3. Crack strain values at step 75 (peak load)

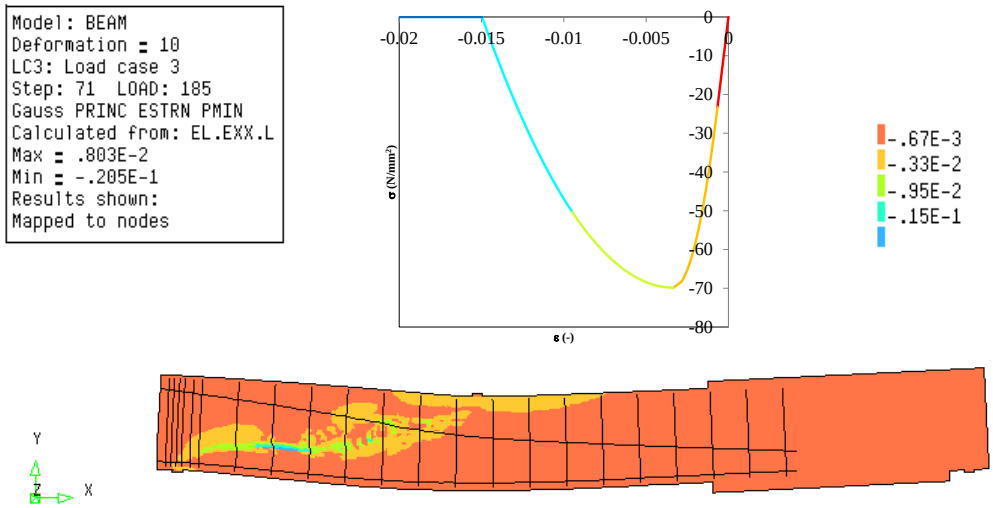

Figure 5-28: Case PB3. Minimum principal strain values at step 71

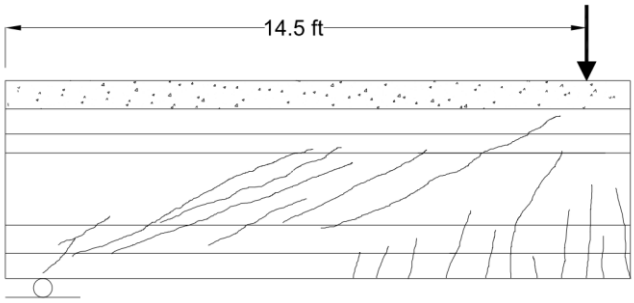

Figure 5-29: Case PB3. Experimental crack pattern at failure (load $P = 2313kN$)

The yielding strain for stirrups is equal to $464MPa/210GPa = 2.22\times10^{-3}$. The stirrups start to yield at a load equal to 1770 kN (step 53). Figure 5-30 shows yielding of stirrups a few steps after the yielding point – step 65.

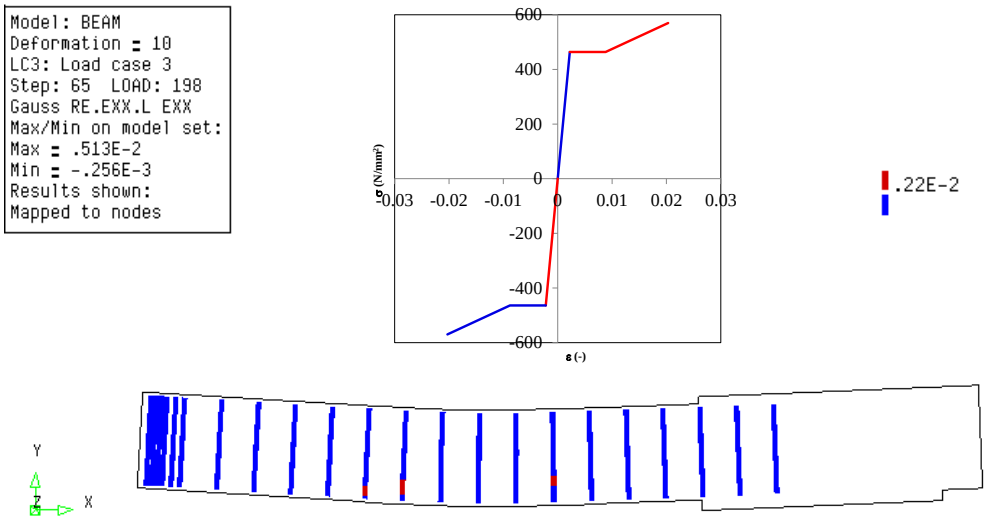

Figure 5-30: Case PB3. Yielding of stirrups at step 65

Gauss point statistics

In Table 5-6 the number of cracking points, crushing points and yield points are reported at step 53 (yielding of stirrups), at step 71 (crushing of concrete) and at step 77 (peak load).

Table 5-7: Case PB3. Number of cracking points, crushing points and yield points

STEP	**53**	**ITERATIONS**		8		
GROUP NAME	**PLAST**	**PRV. PL**	**CRITIC**	**PLAST NEW**	**PRV.PL NEW**	**CRITIC NEW**
STIRRUPS	1	0	0	1	0	0
TOTAL MODEL	1	0	0	1	0	0
CRACKING LOGGING SUMMARY						
GROUP NAME	**CRACK**	**OPEN**	**CLOSED**	**ACTIVE**	**INACTI**	**ARISES**
WEB	488	483	5	360	128	41
fl_sup_c	2	2	0	0	2	0
fl_inf_p	98	89	9	76	22	12

fl_inf_s	60	54	6	49	11	0
fl_inf_t	101	95	6	75	26	1
fl_inf_c	990	971	19	615	375	33
shear	447	447	0	375	72	29
TOTAL MODEL	1739	1694	45	1175	564	87
STEP	**71**	**ITERATIONS**		50		
GROUP NAME	**PLAST**	**PRV. PL**	**CRITIC**	**PLAST NEW**	**PRV.PL NEW**	**CRITIC NEW**
WEB	18	0	0	18	0	0
fl_sup_c	20	29	0	7	29	0
STIRRUPS	52	25	0	52	13	0
shear	18	0	0	18	0	0
TOTAL MODEL	90	54	0	77	42	0
CRACKING LOGGING SUMMARY						
GROUP NAME	**CRACK**	**OPEN**	**CLOSED**	**ACTIVE**	**INACTI**	**ARISES**
WEB	3727	3597	130	2312	1415	1918
fl_sup_c	8	8	0	6	2	6
fl_inf_p	349	326	23	78	271	70
fl_inf_s	315	291	24	122	193	113
fl_inf_t	495	472	23	285	210	276
fl_sup_p	156	150	6	112	44	98
fl_sup_s	49	48	1	43	6	38
fl_inf_c	1976	1927	49	242	1734	141
shear	4084	3952	132	2708	1376	2392
TOTAL MODEL	7075	6819	256	3200	3875	2660
STEP	**75**	**ITERATIONS**		1		
GROUP NAME	**PLAST**	**PRV. PL**	**CRITIC**	**PLAST NEW**	**PRV.PL NEW**	**CRITIC NEW**
WEB	3	67	0	3	0	0
fl_sup_c	106	0	0	15	0	0
STIRRUPS	69	48	0	25	0	0
fl_inf_t	0	1	0	0	0	0
shear	12	68	0	4	0	0
TOTAL MODEL	178	116	0	43	0	0
CRACKING LOGGING SUMMARY						
GROUP NAME	**CRACK**	**OPEN**	**CLOSED**	**ACTIVE**	**INACTI**	**ARISES**
WEB	4553	3640	913	1854	2699	47
fl_sup_c	18	18	0	16	2	2
fl_inf_p	473	431	42	315	158	8
fl_inf_s	452	399	53	318	134	9
fl_inf_t	621	503	118	221	400	7
fl_sup_p	203	186	17	138	65	4
fl_sup_s	69	66	3	57	12	2
fl_inf_c	2364	2269	95	1641	723	43
shear	5455	4379	1076	2298	3157	49
TOTAL MODEL	8753	7512	1241	4560	4193	122

5.5 Application of safety format

As proposed by the Model Code 2010 (fib, 2013), the safety formats for non-linear analyses include three numerical methods denoted as GRF (Global Resistance Factor method), PF (Partial Factor method) and ECOV (Method of Estimation of a Coefficient of Variation of resistance). In Table 5-8 to Table 5-10, the mechanical properties of concrete and steel applied in the non-linear analyses are summarized.

Table 5-8: Case PB3. Constitutive model parameters for concrete

	f_c (N/mm^2)	f_{ct} (N/mm^2)	E_c (N/mm^2)	ν	G_F (Nmm/mm^2)	G_C (Nmm/mm^2)
Mean measured	69.84	4.40	34819	var	0.157	39.1924
Characteristic	61.84	3.08	37138	var	0.153	38.3435
Mean GRF	52.56	4.21	35371	var	0.149	37.2380
Design	41.22	2.05	32885	var	0.143	35.6447

Table 5-9: Case PB3. Constitutive model parameters for reinforcing bars (stirrups)

	Φ (mm)	A_s (mm^2)	f_y (N/mm^2)	f_t (N/mm^2)	E_s (N/mm^2)	ε_{sy} (-)
Mean measured	13	132.7	464	570	210000	0.0022
Characteristic	13	132.7	420.26	516.27	210000	0.0020
Mean GRF	13	132.7	462.29	567.90	210000	0.0022
Design	13	132.7	365.45	448.93	210000	0.0017

Table 5-10: Case PB3. Constitutive model parameters for reinforcing bars (strands)

	Φ (mm)	A_s (mm^2)	f_y (N/mm^2)	f_t (N/mm^2)	E_s (N/mm^2)	ε_{sy} (-)
Mean measured	43×11.2	4247	1675	1862	196500	0.0085
Characteristic	43×11.2	4247	1517.11	1686.49	196500	0.0077
Mean GRF	43×11.2	4247	1668.83	1855.14	196500	0.0084
Design	43×11.2	4247	1319.23	1466.51	196500	0.0067

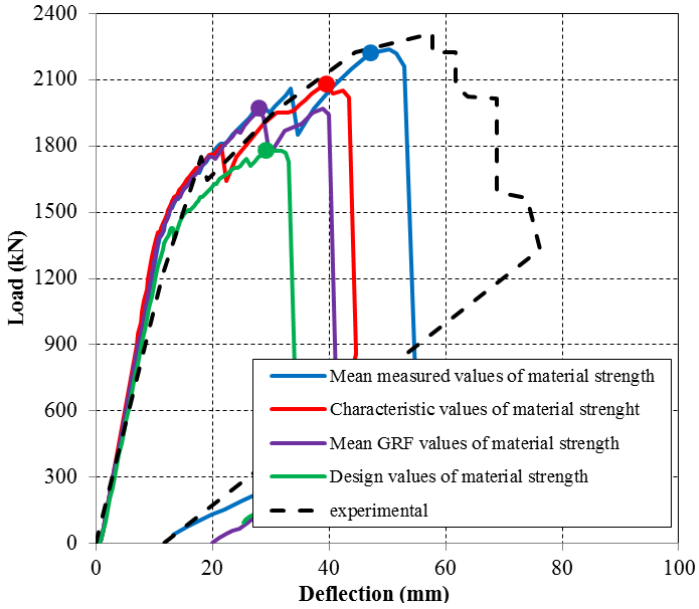

Figure 5-31: Case PB3. Load-deflection curves obtained with mean measured, characteristic, mean GRF and design mechanical properties

PB3 beam was analyzed with the analytical and numerical methods. Figure 5-32 shows the comparison between analytical and numerical design values of beam resistance P_{Rd} expressed in terms of a percentage of the experimental ultimate value of applied load. The analysis named "no safety format" refer to a NLFE analysis carried out using mean measured values of material strengths without applying any safety coefficient.

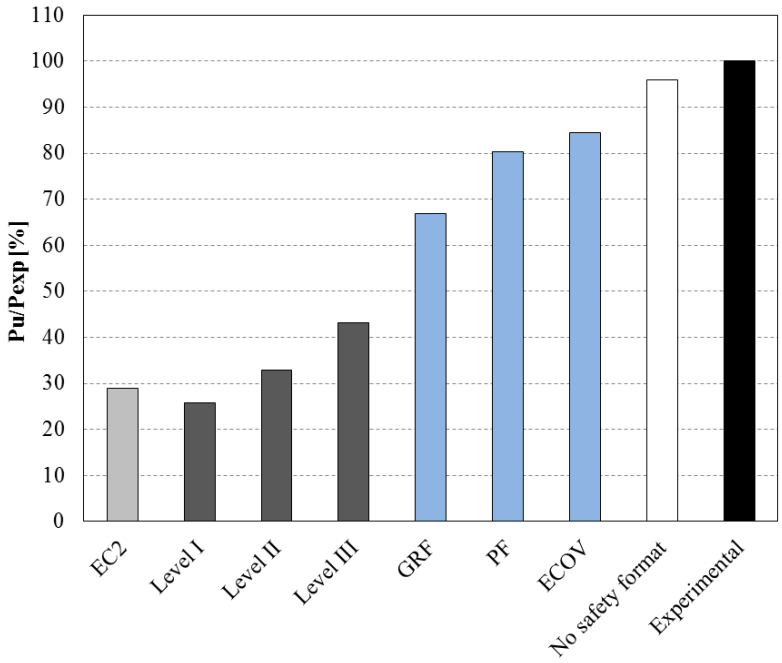

Figure 5-32: Case PB3. Analytical and numerical design values of beam resistance expressed in terms of a percentage of the experimental ultimate value of applied load, $P_{Exp} = 2313kN$

In Table 5-11 the design values of beam resistance, expressed in terms of applied load P_{Rd}, obtained from numerical and analytical procedures are summarized.

Table 5-11: Case PB3. Values of beam resistance, expressed in terms of applied load P_{Rd}, [in kN]

P_{Exp}	EC2	Level I MC2010	Level II MC2010	Level III MC2010	GRF	PF	ECOV	No safety formats
2313	668.42	595.64	761.61	998.23	1548.74	1857.49	1951.98	2220

5.6 Parametric study on crack models

A parametric study was performed by varying some sensitive parameters of the concrete constitutive model, such as the crack model and the fracture energy of concrete in tension.

In Table 5-12 the material parameters applied in NLFE analyses carried out for the parametric study are reported. Analyses 1 to 3 refer to the three analyses carried out with mean measured values of material strength and varying material parameters (crack model and tensile fracture energy) of a concrete constitutive model. A parabolic law in compression and an exponential law in tension were used for concrete, while the steel was modelled with an elasto-plastic law with hardening. A variable Poisson's ratio was adopted for all analyses. The analyses were performed in load-control with arc-length control.

For all analyses the limit value of reduction of the concrete compressive strength due to lateral cracking was determined as follows:

$$\beta_{\sigma,\min} = \frac{f_{c,red}}{f_{cm}} = 0.6$$

The effects of the applied value of the fracture energy of concrete in tension on the beam response was investigated by means of comparison of the formulation of Model Code 1990 (CEB-FIB, 1993) and Model Code 2010 (fib, 2013). The fracture energy of concrete in compression was considered for all analyses equal to $250G_F$ (Nakamura et al. 2001).

In the fixed crack model, a variable shear retention factor dependent on a mean aggregate size d_{aggr}, a crack normal strain ε_n and a crack bandwidth value h was calculated as follows from:

$$\beta = 1 - \left(\frac{2}{d_{aggr}} \right) \varepsilon_n h$$

In Figure 5-33 the load-deflection curves obtained from the parametric study are plotted with the peak load of each analysis being marked with a circular indicator. The peak load was defined as the highest load step for which the energy norm ratio satisfied the fixed tolerance of 1×10^{-3}. The peak load values are reported in Table 5-12.

Table 5-12: Case PB3. Parametric study on crack models

Analysis	Total strain crack model	G_F	G_C	Peak load value (kN)
Analysis 1	rotating	MC2010	250 G_F	2220
Analysis 2	rotating	MC1990	250 G_F	2110
Analysis 3	fixed	MC2010	250 G_F	2550

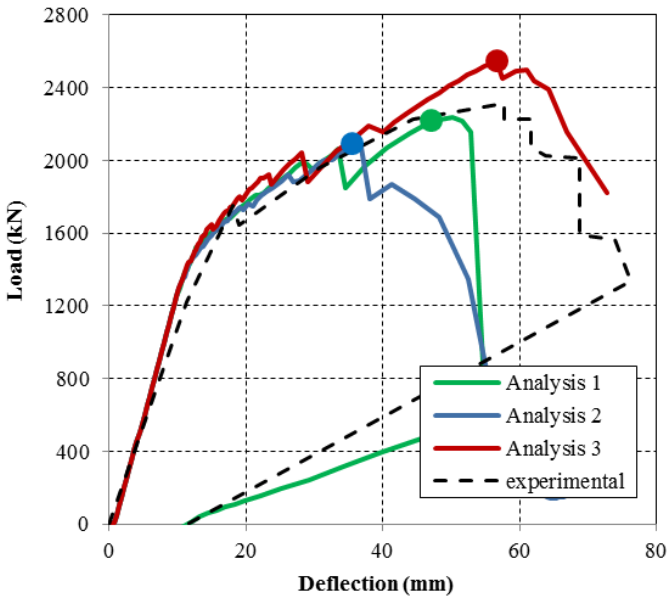

Figure 5-33: Case PB3. Load-deflection curves of parametric study

Comparing analysis 1 to analysis 2, a relatively small influence of the adopted values of the fracture energy of concrete in tension ($G_{F,MC1990} = 0.117 N/mm$; $G_{F,MC2010} = 0.157 N/mm$) and the corresponding values of the fracture energy of concrete in compression ($G_{C,MC1990} = 29.24 N/mm$; $G_{C,MC2010} = 39.19 N/mm$) can be noted, despite the beam having failed in shear compression. It is due to the fact that by increasing the compressive strength, the difference between the fracture energy of concrete in tension calculated according to the Model Code 2010 and Model Code 1990 decreases; with the fracture energy of concrete in tension being exponentially dependent on the compressive strength. Since the compressive strength of PB3 beam is equal to 69.84 MPa, the difference between the fracture energy of concrete in tension calculated according to the Model Code 2010 and the Model Code 1990 is relatively small.

From the comparison of analyses 1 and 3, it can be noted that for beam PB3 the adopted crack model (total strain rotating or fixed crack model) has a big influence on the beam response, especially in terms of peak deformation. The peak load and peak deformation are significantly overestimated if a fixed crack model with the aggregate size based shear retention factor is applied. Furthermore, the crack pattern and failure mode from experiments can be better reproduced with the analysis containing the rotating crack model.

5.7 Concluding remarks

Prestressed beam PB3 subjected to a concentrated loading exhibited a shear-compressive failure mechanism at a load equal to $P = 2313 kN$.
The beam was modeled with 8-node membrane elements for the concrete and embedded truss elements for the reinforcement. Perfect bond is assumed. The concrete model is based on a total strain rotating crack model with exponential tension softening in tension and parabolic behavior in compression, variable Poisson's ratio of concrete and reduction of compressive strength of concrete due to lateral cracking with a lower limit of 0.6. The model for the stirrups is based on hardening plasticity.
A shear-compressive failure mechanism was achieved from NLFEA carried out with mean measured values of material strengths. The peak value of applied load obtained

from NLFEA is equal to 2020 kN and the failure mode is characterized by sudden opening of shear cracks in the web, yielding of stirrups and crushing of concrete in the web.
Safety formats for non-linear finite element analyses as proposed by the Model Code 2010 (fib, 2013) were applied to compute the design values of beam resistance expressed in terms of applied load. From the results, it was concluded that the design resistance obtained with the safety formats was higher than the design resistance calculated with the analytical methods for sectional analysis.

Next, a sensitivity study on models which contained different values of fracture energy of concrete in tension i.e. according to the Model Code 2010 and 1990, the corresponding fracture energy of concrete in compression and different crack models were examined.Since the beam failed in shear due to crushing of concrete, the failure mode was influenced by both the adopted crack model and the values of fracture energy of concrete in tension and in compression.

Based on the results, it can be concluded that consistent and reliable results can be obtained by adopting variable Poisson's ratio, reduction of the compressive strength due to lateral cracking with a low limit of 0.6, total strain rotating crack model and fracture energy of concrete in tension according to Model Code 2010. An energy norm with a tolerance of 10^{-3} is recommended.

6 Case PB4: Leonhardt, Koch et Rostásy (1973)

This prestressed beam case is beam TP2 from the experiments of Leonhardt, Koch, and Rostásy (Leonhardt et al. 1973). The beam was loaded in 3-points until to the shear compressive failure was reached. Beam PB4 (TP2 in experiments) was selected as case study due to its shear-compression failure mechanism.

6.1 Experimental setup and results

Geometry

The geometry, cross-sectional details and the reinforcement details are shown in Figure 6-1, Figure 6-2 and Figure 6-3. The span is 6.5 m with a total length equal to 7.0 m. The depth of the beam is 0.97 m with a variable thickness of the web. The beam has longitudinal reinforcement, non-symmetric layout of stirrups characterized by stirrups ϕ12 on the left hand-side and stirrups ϕ10 on the right hand-side and two post-tensioned prestressing strands which are slightly curved upwards near the ends of the beam. Each strand contains 12 wires with a diameter of 12.2 mm. The initial stress in each tendon, measured after the losses is equal to 681 MPa.

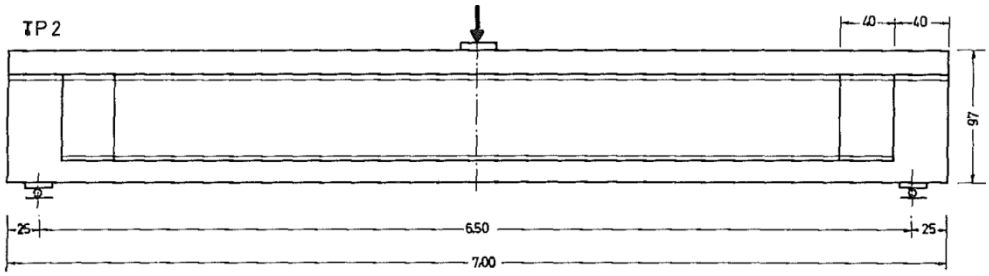

Figure 6-1: Case PB4. Overall dimensions (in cm) (Leonhardt et al. 1973)

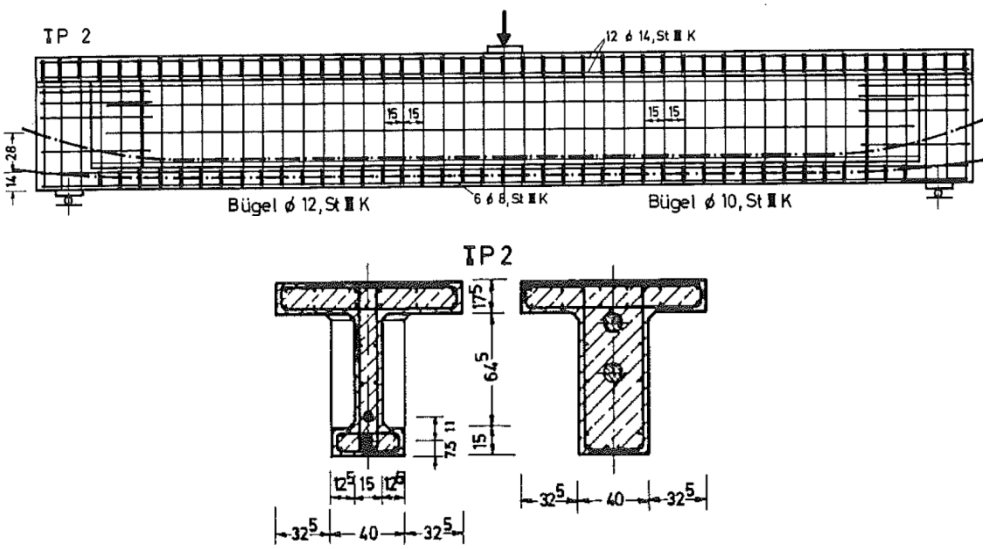

Figure 6-2: Case PB4. Reinforcement details and cross-sectional dimensions (in cm) (Leonhardt et al. 1973)

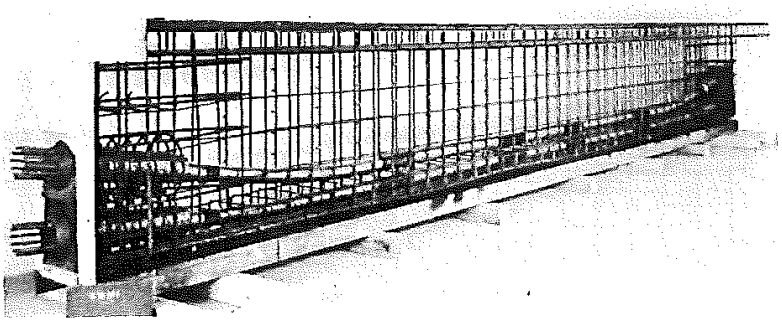

Figure 6-3: Case PB4. Reinforcement cage and prestressing cables (Leonhardt et al. 1973)

Material Properties

Concrete and reinforcement properties given in references are presented in Table 6-1.

Table 6-1: Case PB4. Reinforcement properties

Concrete properties					
f_{cm} (N/mm^2)	$f_{ctm,sp}$ (N/mm^2)	E_c (N/mm^2)	d_{max} (mm)		
24.02	2.35	25977	22		
Reinforcement properties					
Bar	Φ (mm)	A_s (mm^2)	E_s (N/mm^2)	f_{ym} (N/mm^2)	f_{tm} (N/mm^2)
Φ8	8.0	49	197000	460	567
Φ10	10.0	79	202000	431	556
Φ12	12.0	109	201000	489	637
Φ14	14.0	152	207000	397	517
Φ12.2	12x12.2	12x117	207000	1225	1363

Loading and Boundary Conditions

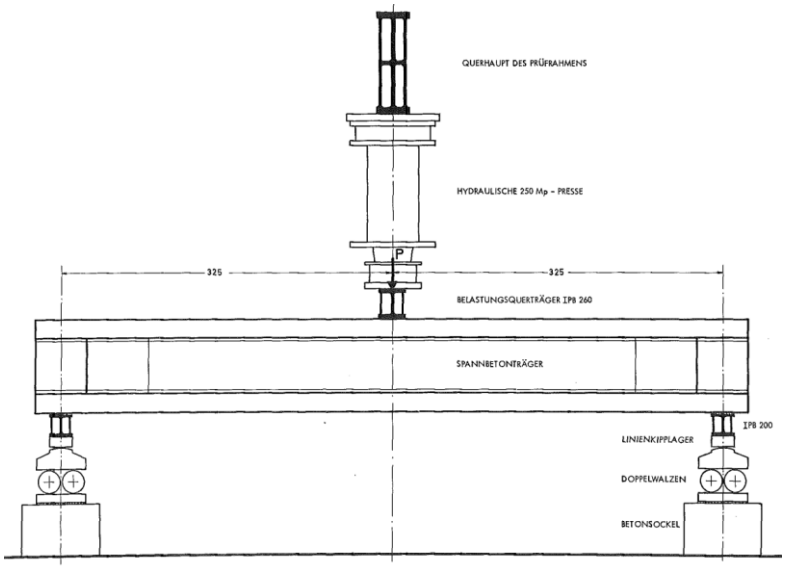

Figure 6-4: Case PB4. Loading and boundary conditions (Leonhardt et al. 1973)

The loading and boundary conditions in the experimental setup are shown in Figure 6-4. The unit for the forces used in the reference is Mp which is approximately 10 kN. The prestressing was applied 20 days after casting in four step of stressing to the stress level of 995kN in each cable. The measured prestressing after losses was equal to 956kN in each cable. During the prestressing process, a vertical load equal to 588 kN, was applied as the counteraction force to minimize the tensile stress in the upper flange of the beam.

Experimental Results

The beam exhibited a shear-compressive failure mode at the maximum load equal to 1491.12 kN (152 Mp) at which the concrete in the top part of the web at right hand side clearly crushed. In Figure 6-5 the experimental crack pattern at failure is shown. The development of the crack pattern is shown Figure 6-6. The measured deflections at various points across the span are shown in Table 6-2 and the load-deflection curve of the center of the beam (point D0) is shown in Figure 6-7.

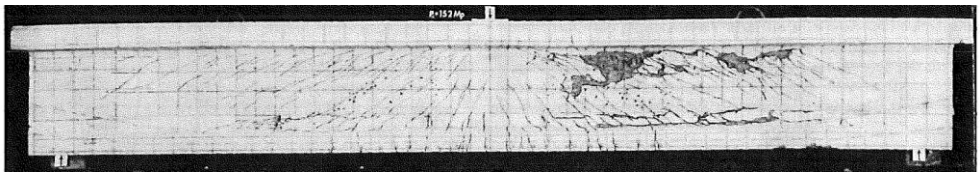

Figure 6-5: Case PB4. Crack pattern at ULS load level, equal to 1491.12 kN (Leonhardt et al. 1973)

Table 6-2: Case PB4. Measured deflection at various points across the span (Leonhardt et al. 1973)

LAST P Mp	D3ℓ $\bar{x}$ = 2,437	D2ℓ $\bar{x}$ = 1,625	D1ℓ $\bar{x}$ = 0,812	D0 $\bar{x}$ = 0	D1r $\bar{x}$ = 0,812	D2r $\bar{x}$ = 1,625	D3r $\bar{x}$ = 2,437
60	- 1,79	- 2,43	- 2,47	- 2,37	- 2,38	- 2,41	- 1,70
60	- 2,08	- 2,63	- 2,43	- 2,16	- 2,20	- 2,36	- 1,72
80	- 1,79	- 1,96	- 1,46	- 1,09	- 1,26	- 1,77	- 1,50
90	- 1,52	- 1,34	- 0,53	- 0,07	- 0,36	- 1,23	- 1,30
100	- 1,15	- 0,53	0,72	1,38	0,91	- 0,38	- 0,88
120	0,17	2,48	5,56	7,00	5,79	2,51	0,27
140	1,79	6,28	11,72	14,17	12,15	6,16	1,71

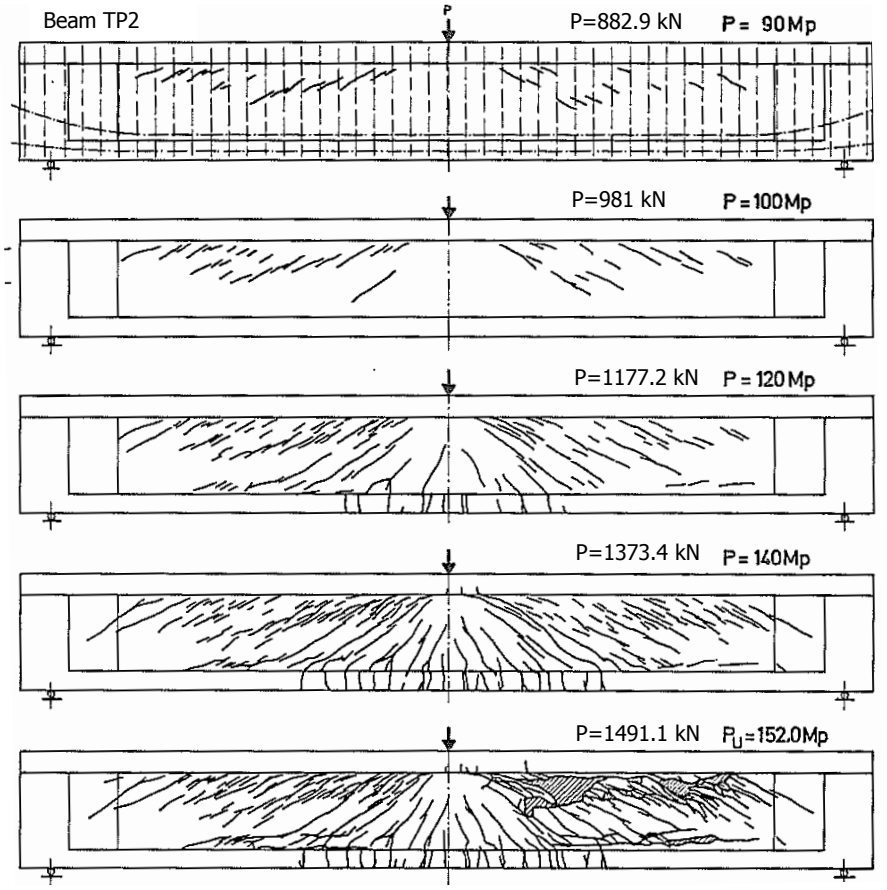

Figure 6-6: Case PB4. Development of the crack pattern during the experiment (Leonhardt et al. 1973)

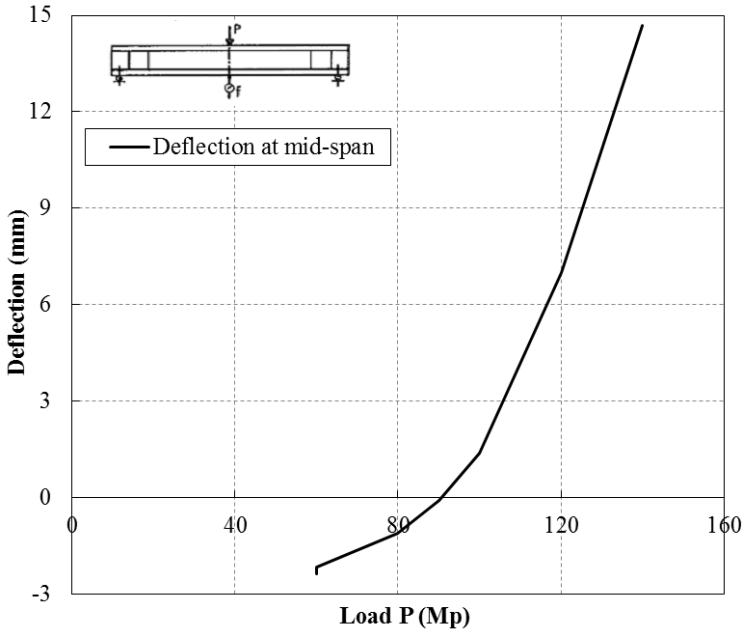

Figure 6-7: Case PB4. Load-deflection of point D0 – mid-span

6.2 Analytical analysis

In Figure 6-8 the load configuration at failure is reported.

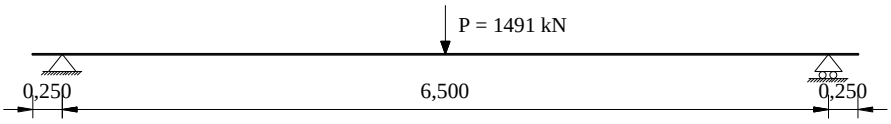

Figure 6-8: Case PB4. Load configuration at failure (dimensions in m)

Load case 1: Self-weight

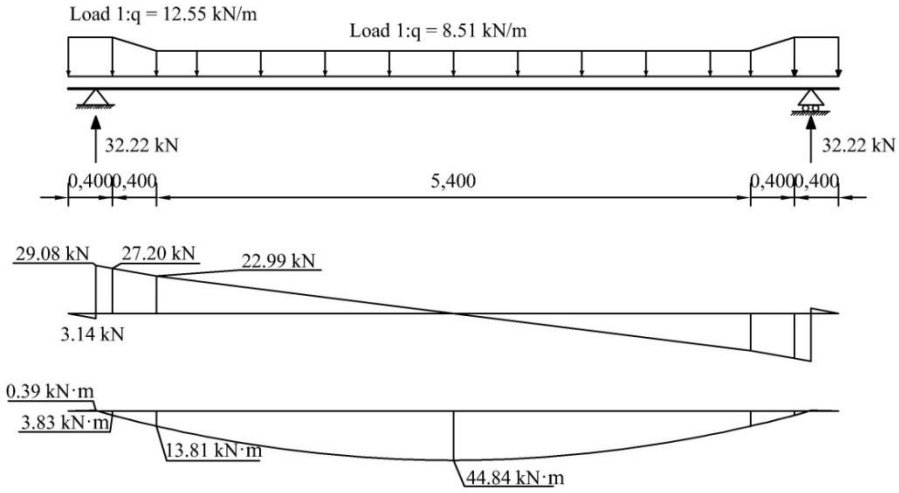

Figure 6-9: Case PB4. Internal forces from self-weight (dimensions in m)

Counteracting point load:

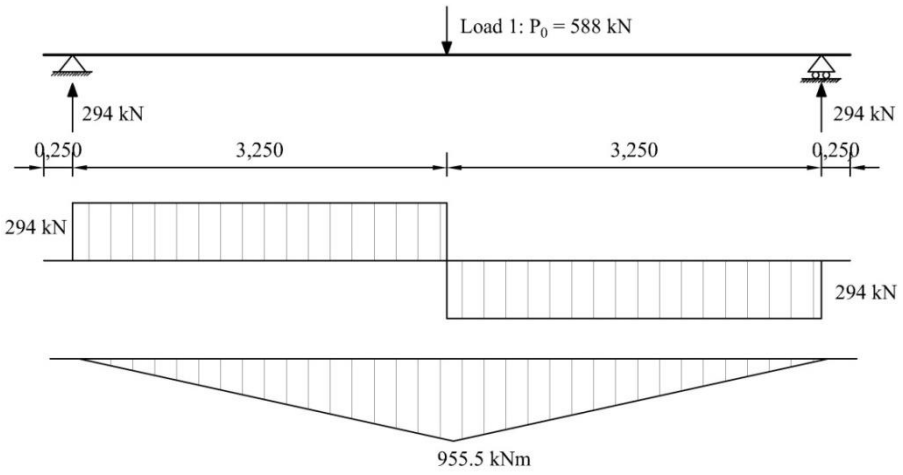

Figure 6-10: Case PB4. Load 1: Internal forces from counteracting point load (dimensions in m)

Prestressing force:
Prestressing applied on to the beam on an eccentricity gives rise to bending moment of the value:

$$M_P = 2A_P\sigma_{p\inf}e_p = 1912kN \times 0.494m = 944kNm$$

where e_p is the difference between the centroidal axis and the centre of gravity of prestressing steel: $e_p = C_G - \frac{A_p \times 185mm + A_p \times 75mm}{2A_p} = 0.624m - 0.13m = 0.494m$

It is assumed that the bottom strand is straight whereas the upper inclined 14 degrees to horizontal at the ends.

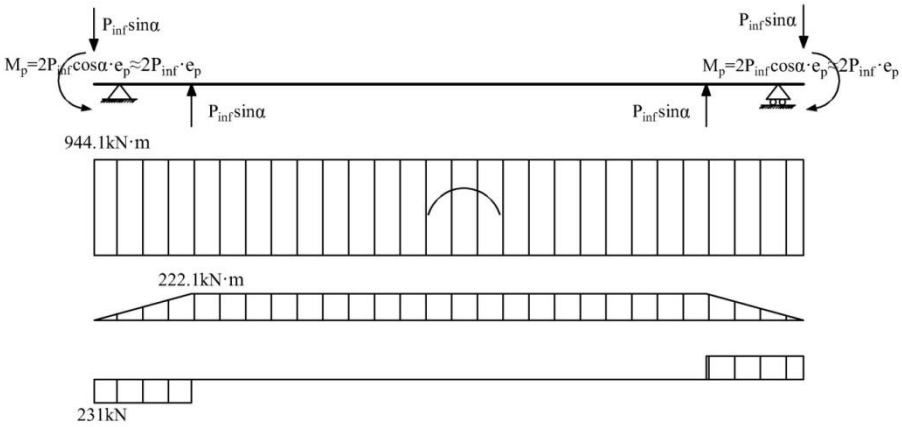

Figure 6-11: Case PB4: Internal forces from prestressing

Load case 2:
Figure 6-12 shows the maximum moment at mid-span

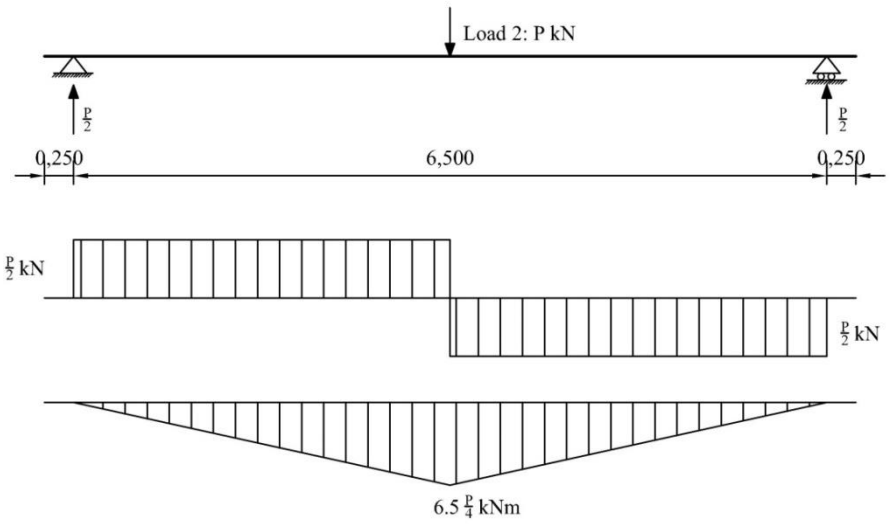

Figure 6-12: Case PB4. Load 2: Internal forces from point load (dimensions in m)

Bending moment resistance:

The design value of bending moment resistance was calculated assuming a bi-linear concrete stress block, an elastic-plastic stress-strain relation without hardening (horizontal plastic branch) and safety factors as given in Eurocode 2.
The bending moment capacity of the section presented in Figure 6-13 was calculated assuming yielding of the reinforcement located in the top and bottom flange. The reinforcement in the web remained in the elastic range.
The height of the compression zone was determined from the horizontal force equilibrium.

$$A_{sb} f_{yd1} + A_{s,web}\varepsilon_{s,web1}E_s + A_{s,web}\varepsilon_{s,web2}E_s + 2A_p\sigma_{p,\inf} + 2A_p(f_{py} - \sigma_{p,\inf}) = f_{cd} b_{flange} h_{flange} + f_{cd} b_{web}\left(x/2 - h_{flange}\right) + 0.5 f_{cd}\, x/2\; b_{web} + A_{stop} f_{yd2}$$

Solving the quadratic equation, the height of compressive zone is: 474mm

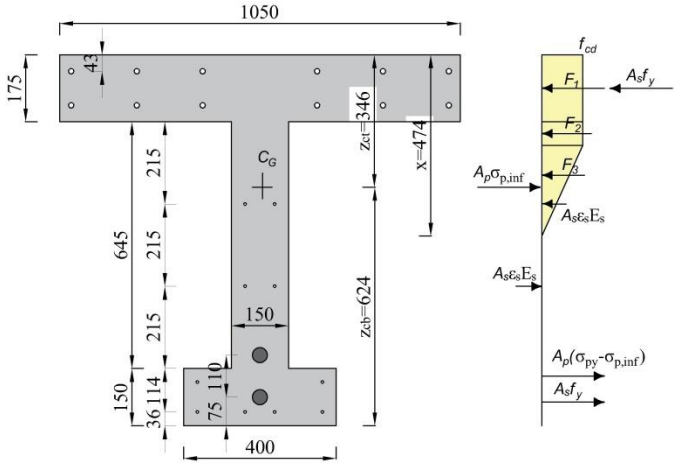

Figure 6-13: Case PB4: Forces acting on a section

The design bending moment resistance calculated around the centre of gravity of the section C_G

$M_{Rd} = 1150 kN \cdot m$

In order to determine the maximum value of the load that the member is able to withstand, the design bending moment has to be equated with the loads acting on the beam, $M_{Ed} = M_{Rd}$

$$448.4 kN \cdot m + 955.5 kN \cdot m - 944 kN \cdot m - 222.1 kN \cdot m + 6.5/4\, P = 1150 kN \cdot m \rightarrow P = 790 kN$$

is the additional load that can be applied apart from the counteracting point load.

Shear resistance

EC2 calculations

$$V_{Rd,s} = \frac{A_{sw}}{s} z f_{ywd} \cot\theta_{\max} = \frac{157 mm^2}{150 mm} 744.26 mm \times 339.5 MPa \times \cot(38.4°) = 333.7 kN$$

$$V_{Rd,\max} = \frac{\alpha_{cw} b_w z v_1 f_{cd}}{\cot(\theta) + \tan(\theta)} = \frac{1.25 \times 115 mm \times 744 mm \times 0.6 \times 10.68 MPa}{\cot(38.4^\circ) + \tan(38.4^\circ)} = 333.7 kN$$

taking into account that:

$\varphi = 70 mm$ is external grouted sleeve dimeter $\geq b/8 = 150/8 = 18.75 \Rightarrow b_w = b - 0.5\varphi$

Model Code 2010, Levels of Approximation II and III

Table 6-3: Case PB4. Parameters used in the calculation of V_{Rd}

	Level I	**Level II**	**Level III**
θ_{min} (°)	25	20	20
θ_{max} (°)	45	45	45
k_g	0.55	0.65	0.65

Level of approximation I

$$V_{Rd,s} = \frac{A_{sw}}{s} z f_{ywd} \cot\theta_{\max} = \frac{157mm^2}{150mm} 744mm \times 339.5MPa \times \cot(45°) = 264.5kN$$

$$V_{Rd,\max} = k_c \frac{f_{ck}}{\gamma_c} b_w z \sin\theta_{\max} \cos\theta_{\max} = 0.55 \times \frac{16MPa}{1.5} 115mm \times 744mm \sin(45°)\cos(45°) = 251.4kN$$

Thus solution acc. to LoA I is not possible.

Level of approximation II

The shear resistance was considered at the critical section located *d* from the edge of the support. For the whole range of the assumed values of $V_{Ed,trial}$, the resulting value of strain parameter ε_x was very low or negative (then according to the code $\varepsilon_x = 0$). This translates into a low angle of inclination of compressive struts i.e. the value close to the prescribed minimum of 20 degrees. It is well known that, although it increases the resistance attributed to stirrups, low angles may imply crushing of concrete at a lower load. Because of a brittle nature of shear failure due to crushing of concrete, shear resistance of stirrups must be lower than shear force that would lead to crushing of concrete.

In the considered case study the shear resistance is governed by crushing of concrete and consequently it was necessary to find such an angle $\theta_{\min}$ that fulfilled the balance condition. It constitutes the highest possible shear resistance, yet the code's provisions are still met. The balance condition was obtained for the angle of 41.9 degrees. The angle fits within the allowable range of angles given in the code. The shear resistance is:

$$V_{Rd,s} = \frac{A_{sw}}{s} z f_{ywd} \cot\theta = \frac{157mm^2}{150mm} 744.26mm \times 339.5MPa \times \cot(41.9°) = 295kN$$

$$V_{Rd,\max} = k_c \frac{f_{ck}}{\gamma_c} b_w z \sin\theta \cos\theta = 0.65 \times \frac{16MPa}{1.5} 115mm \times 744.26mm \times \sin(41.9°) \times \cos(41.9°) = 295kN$$

Level of approximation III

Because from the calculations it appears that the governing failure mechanism is due to crushing of concrete, the concrete contribution to the total shear resistance cannot be accounted for. Hence, the shear resistance is calculated as in the level II approximation.

In Table 6-4 the results of the shear resistance calculations according to the EC2 and Model Code 2010 are listed. These results were obtained taking into account the self-weight but excluding the positive effect of prestressing (active only in the regions were inclined strands are present i.e. closer than the location of the critical section *d* from the support). An example of such calculations is given for the case of EC2 and shear force from the self-weight at the section *d* from the support:

$333.7kN = 0.5P + 20.71kN \rightarrow P = 626kN$ is the total load which can be applied to a member.

Table 6-4: Case PB4. Design value of beam resistance expressed in terms of applied load P_{Rd} (Model Code 2010)

	EC2	**Level I**	**Level II**	**Level III**
$\boldsymbol{P_{Rd}}$ **(kN)**	626.0	-	548.58	548.58

From the above calculations, it is concluded that the beam fails in shear.

6.3 Finite element model

Units
Units are N, mm.

Material models and parameters
The concrete model is based on a total strain rotating crack model with:

- exponential softening in tension and parabolic behavior in compression,
- variable Poisson's ratio of concrete and
- reduction of compressive strength of concrete due to lateral cracking with a lower limit of 0.6
- increase in compressive strength due to lateral confinement according to the model proposed by Selby and Vecchio (Selby and Vecchio 1993).

The mechanical properties are summarized in Table 6-5. On input, the G_F value has been decreased with a factor $\sqrt{2}$ in order to compensate for an underestimation of the crack band width for cracks with an inclination angle of 45 degrees. The uniaxial stress -strain curve is shown in Figure 6-14.
The model for the reinforcement bars and stirrups is based on hardening plasticity. Geometrical and mechanical properties of reinforcement are summarized in Table 6-1. The stress – strain curve of the stirrups Φ10 is plotted in Figure 6-15.

Table 6-5: Case PB4. Constitutive model parameters for concrete

	f_{cm} (N/mm^2)	f_{ctm} (N/mm^2)	E_c (N/mm^2)	ν	G_F (Nmm/mm^2)
Mean measured value	24.02	2.12[#]	25977	var	0.129[*]

*Not specified in reference; estimated according to Model Code 2010 (fib, 2013)
[#]Estimated from the mean splitting tensile strength of concrete as $f_{ctm} = 0.9 f_{ctm,sp}$ according to Eurocode 2 formulation (CEN, 2005)

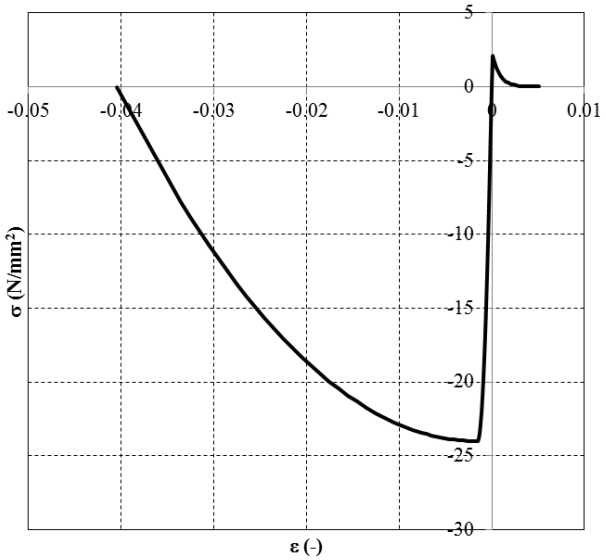

Figure 6-14: Case PB4. Stress-strain curve for concrete

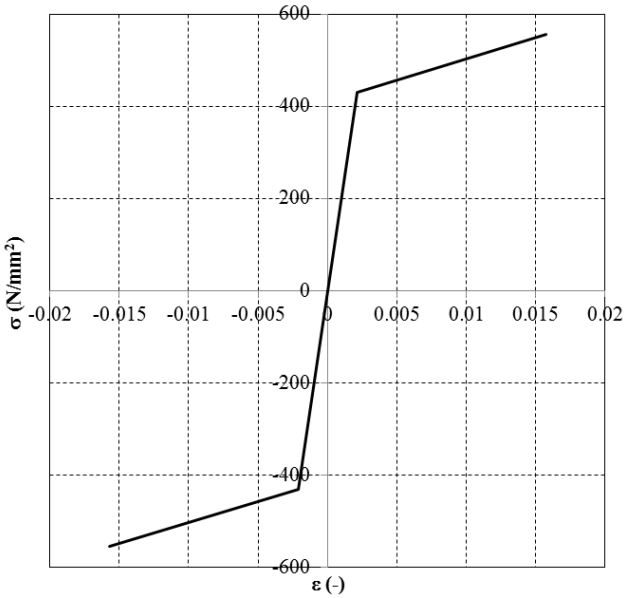

Figure 6-15: Case PB4. Stress-strain curve adopted for stirrups Φ10

For the steel plates a linear elastic behavior is assumed, see Table 6-6.

Table 6-6: Case PB4. Steel plates properties

E **(N/mm²)**	***ν***
210000	0.3

Interface elements were used between the steel support plates and the concrete beam at the supports and loading positions. The interface stiffness was derived on the basis of concrete properties. The total thickness of interface elements equals 1 mm. A bilinear behavior is assumed in the normal direction (see Figure 6-16) and a linear elastic relation is assumed in the shear direction. The normal stiffness in tension and the stiffness in shear direction were assumed almost equal to zero. The mechanical properties of the interface elements are summarized in Table 6-7.

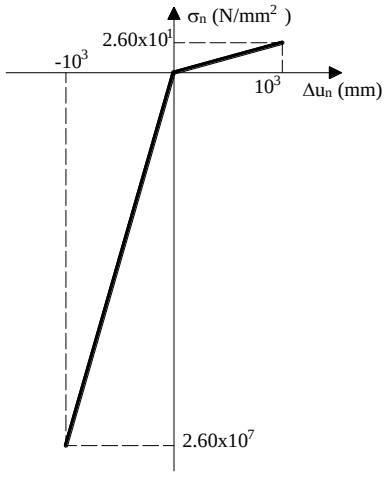

Figure 6-16: Case PB4. Traction-displacement diagram in normal direction for interfaces

Table 6-7: Case PB4. Interface properties

$K_{nn\ in\ tension}$ (N/mm^3)	$K_{nn\ in\ compression}$ (N/mm^3)	K_t (N/mm^3)
2.60E-02	2.60E+04	2.60E-02

Element types and finite element mesh

To mesh concrete beam 8-node membrane elements (CQ16M) with a full integration scheme (3×3) were used. The average element size is 50×54 mm^2.
The reinforcement bars and stirrups are modelled with embedded truss elements with two Gauss integration points along the axis of the element. Perfect bond is assumed. To model post-tensioning of tendons no-bond has been assumed during the prestressing phase. For the steel plates 8-node membrane elements (CQ16M) are used. The 6-node interfaces elements have three Lobatto integration points.
The adopted dimensions for the beam and for the transversal cross section of the beam are given in Figure 6-17and Figure 6-18 respectively.
The mesh of the beam is presented in Figure 6-19(a). The different materials are indicated with different colors in Figure 6-19(b).

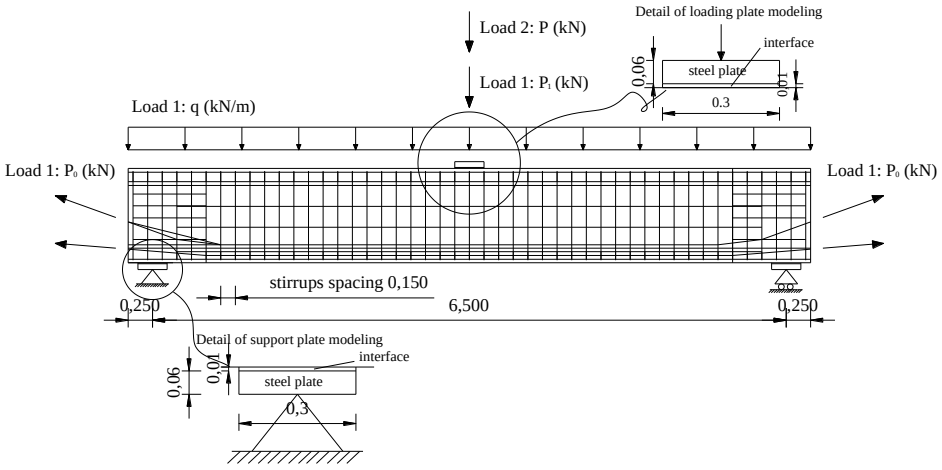

Figure 6-17: Case PB4. Dimensions adopted for the beam (in m)

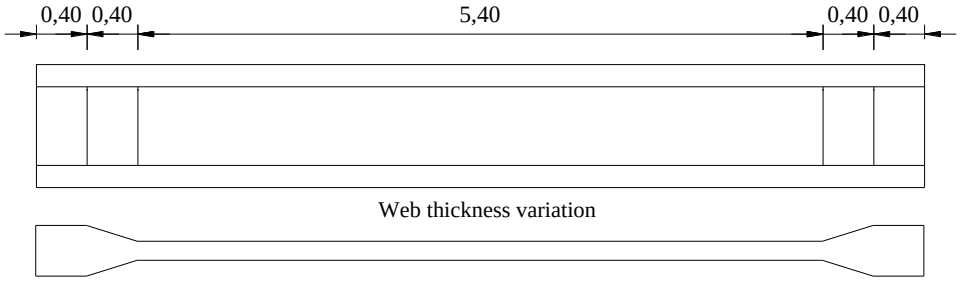

(a)

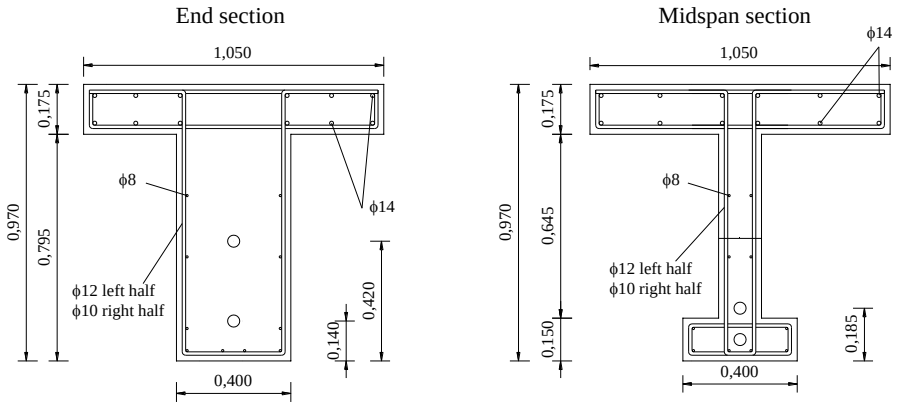

(b)

Figure 6-18: Case PB4. (a) Web thickness variation along length of the beam (in m) (b) Dimensions adopted for the transversal cross section of the beam (in m)

The web thickness variation along the length of the beam was modeled as shown in Figure 6-19(a). The groups name used to model the web thickness variation, starting from the end to the middle of the beam are: WEB_RING, WEB_VA, WEB_VB, WEB_VC, WEB_VD, WEB_VE, WEB_VF, WEB_VG, WEB_VH, WEB_VI, WEB_VL, WEB_VM, WEB_VN. The different materials are indicated with different colors in Figure 6-19(b).

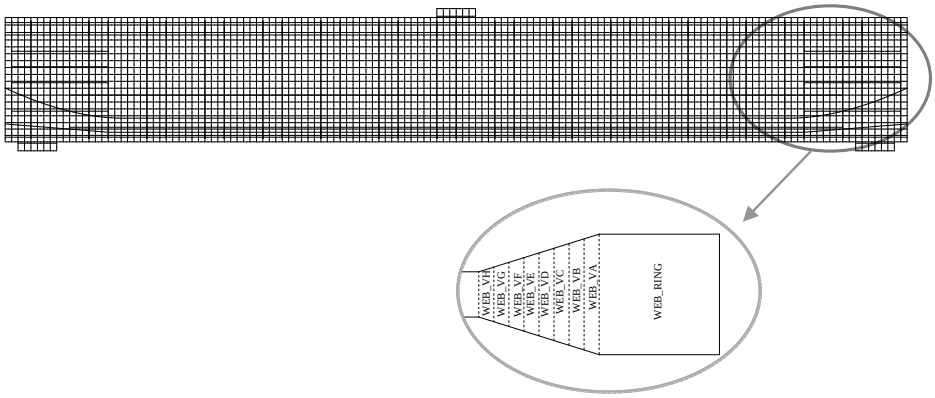

(a)

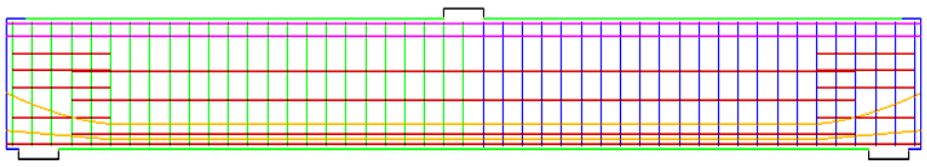

(b)

Figure 6-19: Case PB4. (a) Mesh and modeling of web thickness variation, (b) material sets

Different groups of elements were generated to distinguish these concrete and steel elements that can undergo crushing and yielding.In this manner, these groups of elements can be monitored during the analysis in order to recognize the failure mode. For the ease of monitoring yielding of reinforcing steel, groups “REBTOPF14”, “REBWEBF8”, “REBBOTTF8”, “STIRRLEFTF12”, “STIRRRIGHTF10”, “STRANDS” were created. The groups are indicated in Figure 6-20(a).

Figure 6-20(b) shows the groups of elements named SHEAR, used for tracking the inelastic behavior of concrete in compression. The group of element named SHEAR has the length equal to the space between the end of the loading plate and the end of the support plate and a depth equal to the space between upper and lower reinforcement.

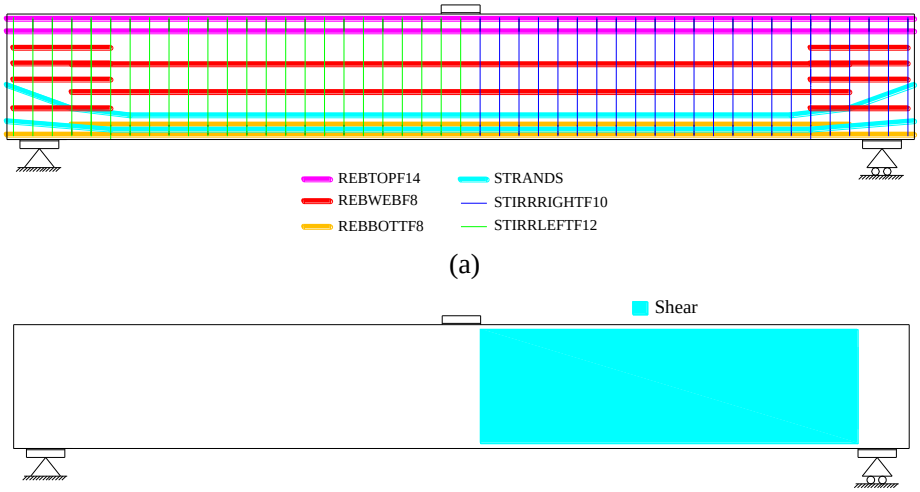

Figure 6-20: Case PB4. Groups of steel elements monitoring (a) yielding of reinforcement, (b) inelastic behavior of concrete

Boundary conditions and loading

Boundary conditions were applied to nodes of steel plate. Translation along x and y axes at a single node of the left steel plate (support 1) and translation along y axis at a single node of the right steel plate (support 2) were constrained, Figure 6-21.

In Load case 1, the beam was subjected to the dead load q(1), pre-stress [$P_0(1)$] and a concentrated load P [$P_1(1)$=588kN] counteracting the effect of the post-tensioning applied to the middle node of the loading plate.

In Load case 2, a concentrated load P [P(2)] applied at the middle node of the loading plate as a unit load of 3×10^3 N was added to load case 1, Figure 6-21.

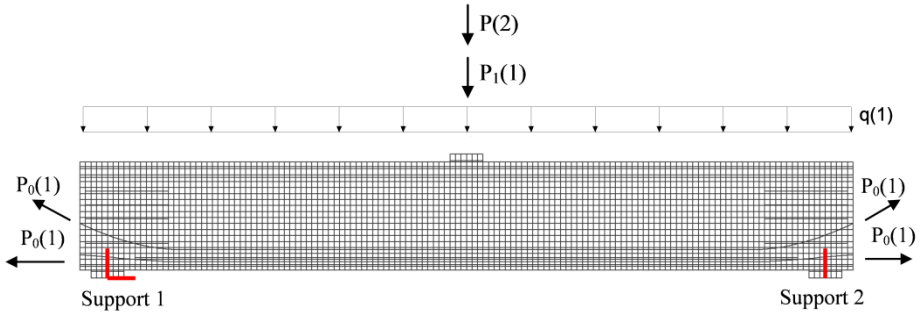

Figure 6-21: Case PB4. Boundary conditions and load cases

Load increments and convergence criteria

Load case 1 was applied in 1 step. The regular Newton-Raphson method was used.

Load case 2 was applied with automatic adaptive load increments based on energy. The initial load factor was 5, the upper limit of the incremental load factor equaled 10 and the lower limit of the incremental load factor was 2. The maximum number of steps was 180. Arc-length control was applied based on translation along y axis of node 4529 (“indirect displacement control”), Figure 6-22. The analysis was set continue even if the convergence criteria were not satisfied. The convergence tolerance was equal to

1×10^{-3} and 1×10^{-2} for energy and force respectively. A maximum of 70 iterations was used. To improve the convergence performance, a line search algorithm was applied.

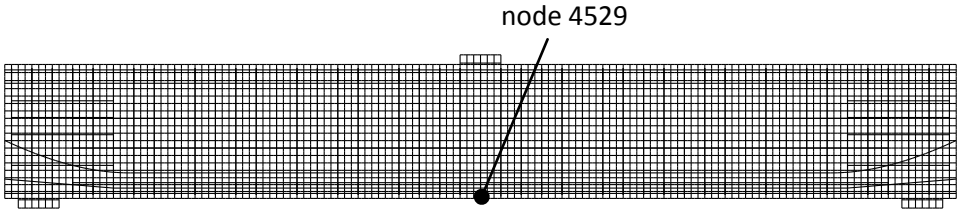

Figure 6-22: Case PB4. `Indirect Displacement control' technique applied referring to node 4529

6.4 Nonlinear finite element analysis

Load deflection

The load-deflection curve is presented in Figure 6-23. The applied load values corresponding to the beginning of yielding of stirrups placed at the right side, yielding of bars and crushing of concrete are highlighted with markers. The onset of crushing of concrete occurred when the first integration point reaches the minimum principal strain value equal to -3.5‰.

For load case 2 the peak load was defined in correspondence of the highest load step where the energy norm ratio satisfied the fixed tolerance of 1×10^{-3}. The convergence behavior was quite poor after reaching the peak load. After step 137, the analysis continued even if the energy convergence criteria were not satisfied within the maximum number of iterations equal to 50. The post peak branch of the load-deflection curve was for this reason plotted with a dot line.

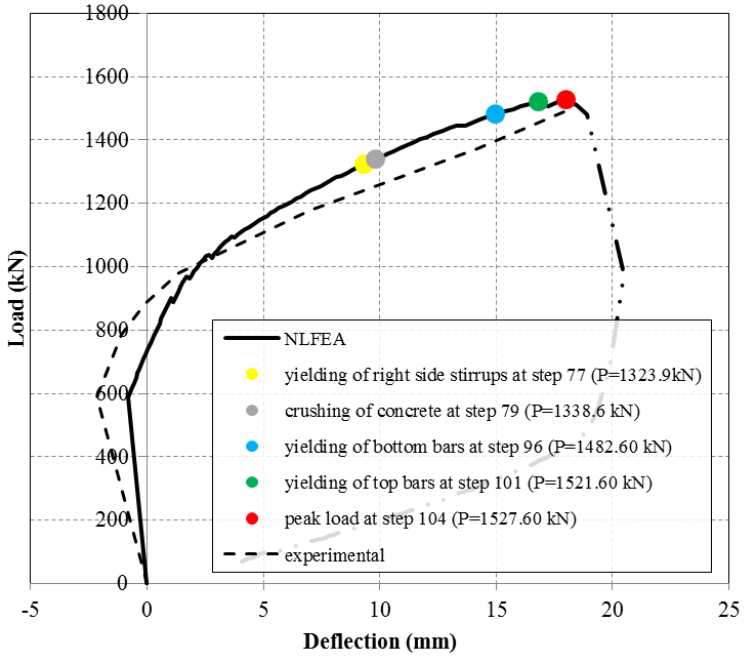

Figure 6-23: Case PB4. Load-deflection curve

Convergence behavior

For the majority of steps the convergence was achieved on the basis of both energy and force criteria, Figure 6-24- Figure 6-25. For load case 2, the energy norm ratio satisfied the fixed tolerance of 1×10^{-3} for most of the steps of the analysis prior to the peak load,

while force norm ratio was higher than the fixed tolerance for some steps. In the figures, the peak load positions are indicated in the graph with the red marker.

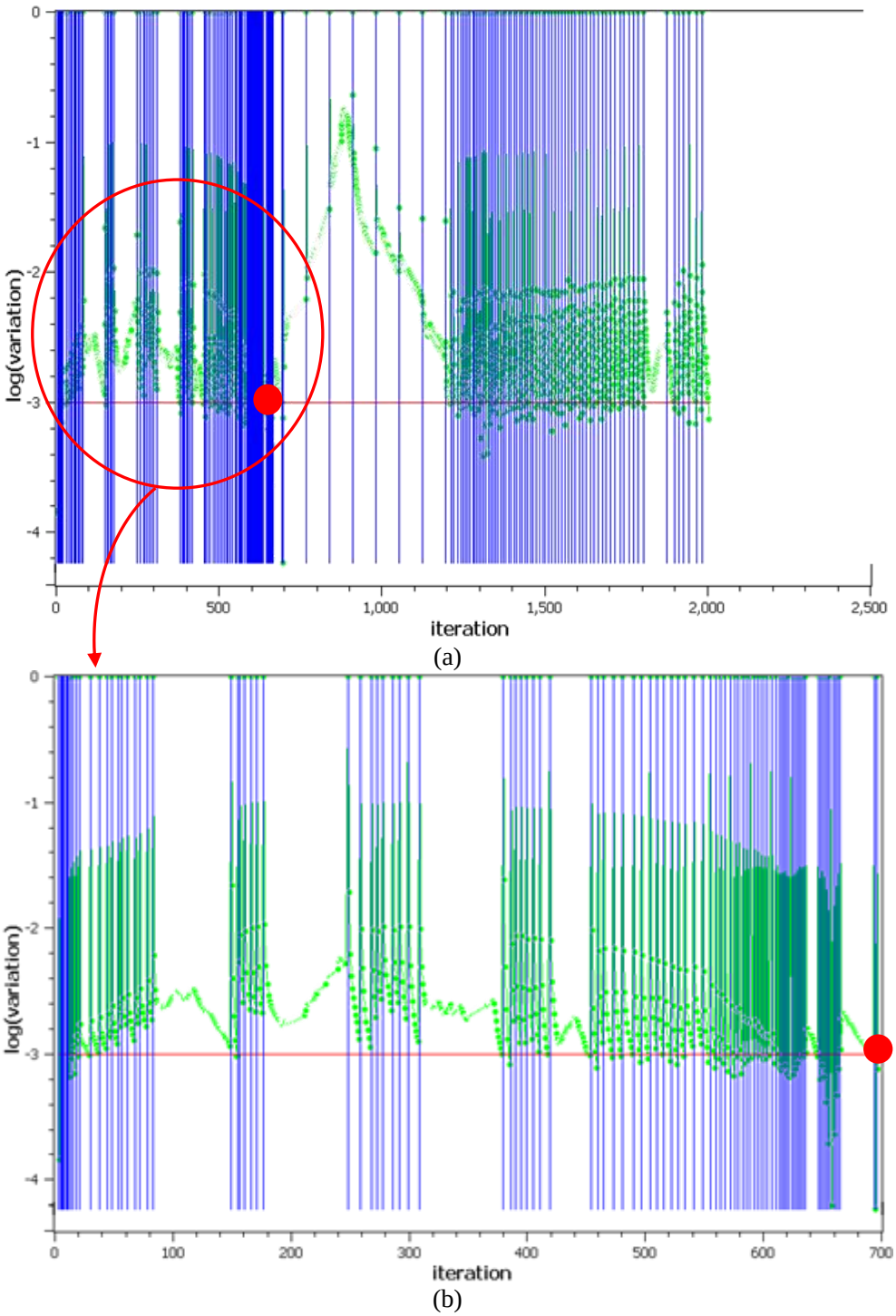

Figure 6-24: Case PB4. (a) Evolution of the energy norm (blue lines indicate steps, red line indicates tolerance, green points indicate iterative results), (b) enlargement of the iterations prior to the peak load

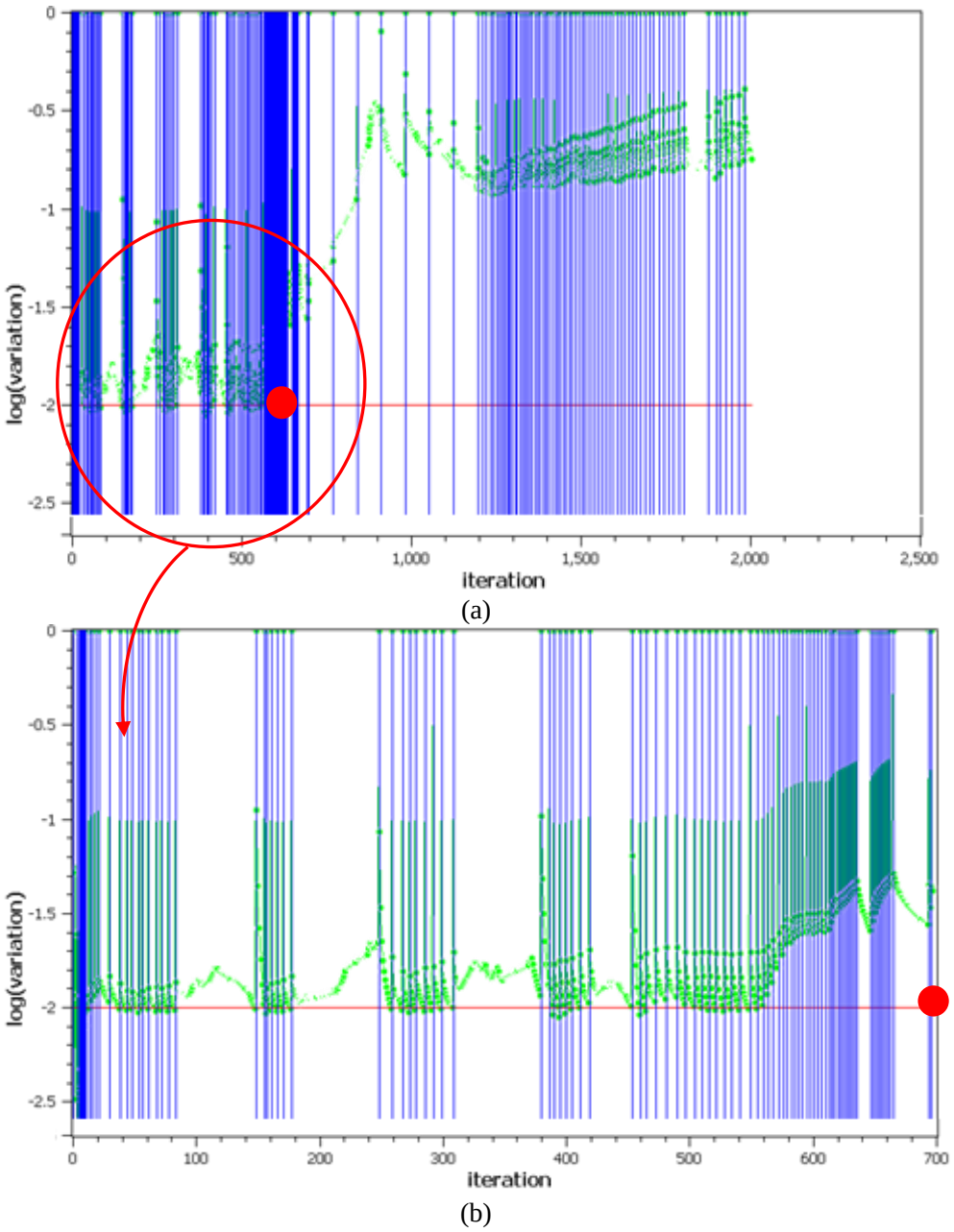

Figure 6-25: Case PB4. (a) Evolution of the force norm (blue lines indicate steps, red line indicates tolerance, green points indicate iterative results), (b) enlargement of the iterations prior to the peak load

Strains

Figure 6-26 shows the crack strain values at the peak load at step 104.

The first crack strain plotted value, equal to 0.00083, corresponds to the ultimate crack strain value calculated as $\varepsilon_{t,u} = \frac{G_f}{h_{eq} \cdot f_{ctm}}$ (in this case $h_{eq} = \sqrt{2}h$). The third crack strain value, equal to 0.0038, is the crack strain value corresponding to 1% of f_{ctm}. The intermediate crack strain value was added in the contour plot.

Figure 6-27 and Figure 6-28 show the minimum principal strain values at step 79 – at point of crushing of concrete and at step 104, where crushing of concrete is more advanced hence more visible.

The first minimum principal strain value plotted in Figure 6-27, equal to -0.0003, corresponds to the elastic principal strain value $\varepsilon_{c,el} = \frac{f_{cm}}{3 \cdot E_c}$. The second minimum principal strain value depicted in Figure 6-27, equal to -0.0015, is the peak strain value $\varepsilon_{c,p}$. The lowest negative value of the principal strain -0.040 is the crushing strain calculated with $\varepsilon_{c,u} = \varepsilon_{c,p} - \frac{3G_c}{2hf_{cm}}$. The two intermediate values were added between $\varepsilon_{c,p}$ and $\varepsilon_{c,u}$.

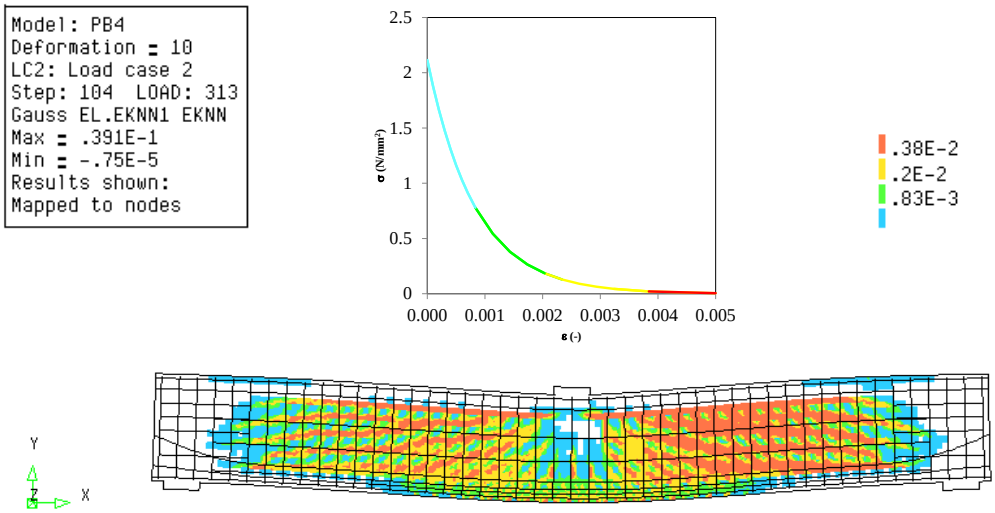

Figure 6-26: Case PB4. Crack strain values at step 104 (peak load)

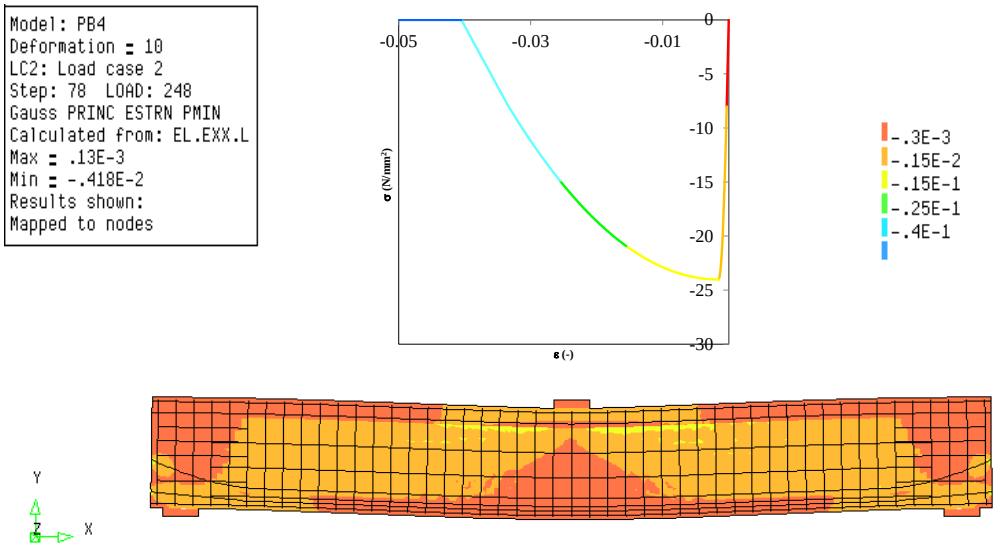

Figure 6-27: Case PB4. Minimum principal strain values at step 79 (crushing of concrete)

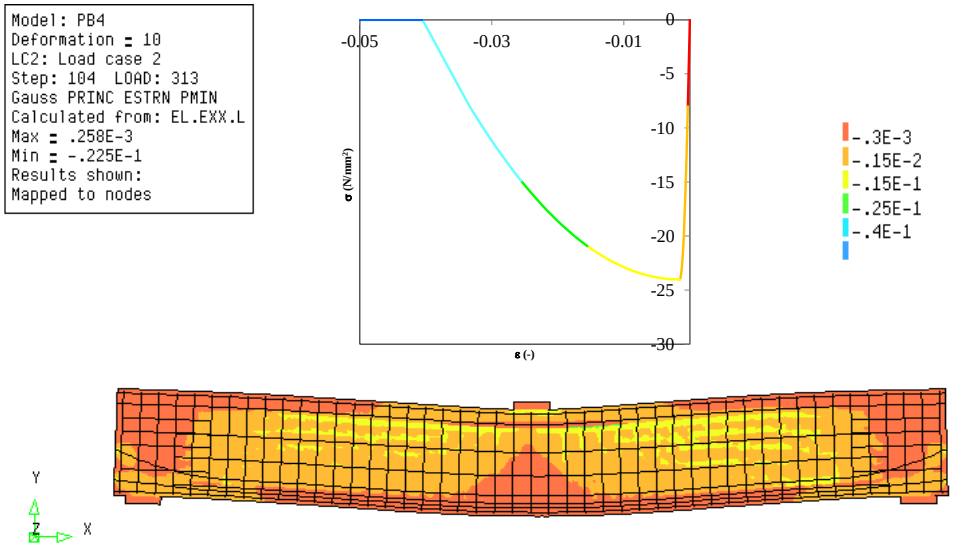

Figure 6-28: Case PB4. Minimum principal strain values at step 104 (peak load)

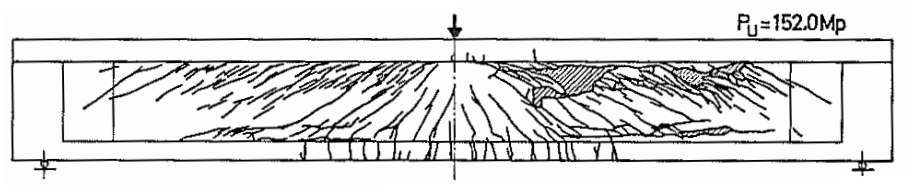

Figure 6-29: Case PB4. Experimental crack pattern at failure (load $P = 1491.12kN$)

Yielding strain for stirrups Φ10 is equal to $431MPa/202GPa = 2.1\times10^{-3}$. Stirrups start to yield at a load equal to 1323.60 kN (step 77). Figure 6-30 shows yielding of stirrups a few steps after the yielding point (at step 80).

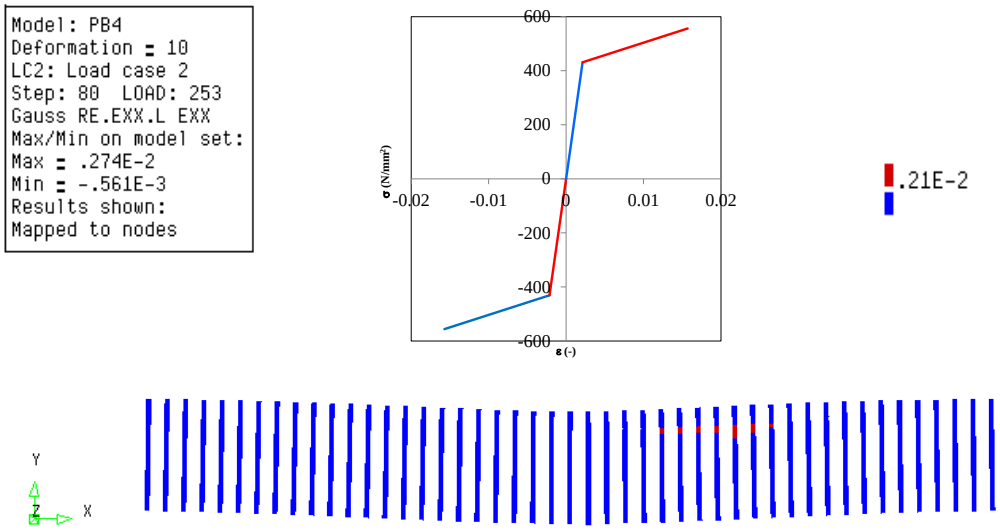

Figure 6-30: Case PB4. Yielding of stirrups Φ10 at step 80

Yielding strain for the bottom longitudinal reinforcement Φ8 is equal to $460MPa/197GPa = 2.33\times10^{-3}$. The bars start to yield at the load equal to 1482.60 kN (step 96).

Figure 6-31 shows yielding of the bars several steps after the yielding point (at step 104).

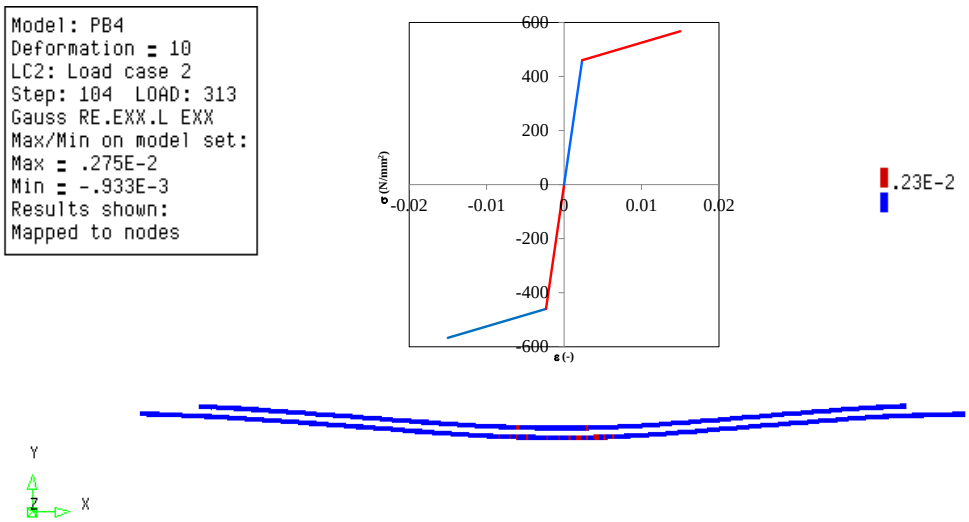

Figure 6-31: Case PB4. Yielding of bottom bars Φ8 at step 104

Yielding strain for top longitudinal reinforcement Φ14 is equal to $397MPa/207GPa = 1.9\times10^{-3}$. The bars start to yield at the load equal to 1521.60 kN (step 101). Figure 6-32 shows the progression of yielding of the Φ14 bars a number of steps after the yielding point (at step 104).

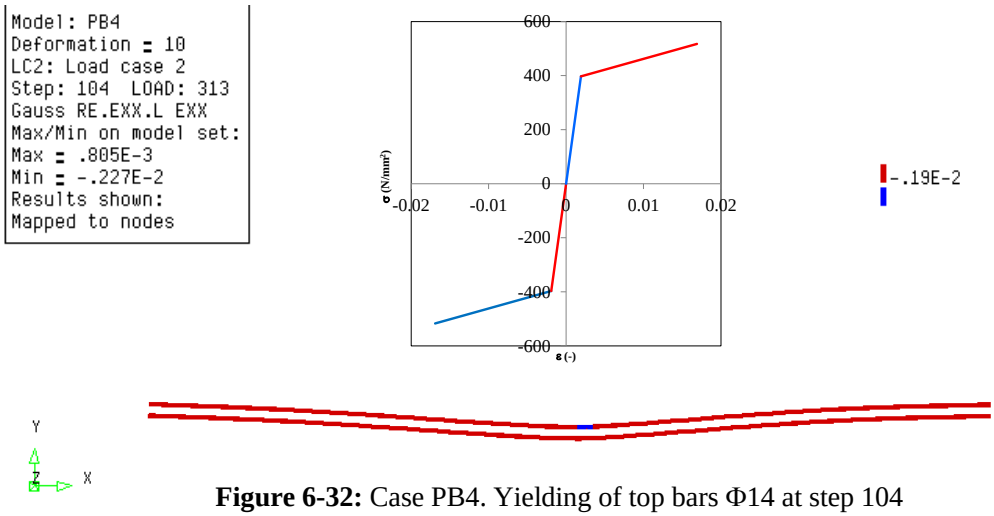

Figure 6-32: Case PB4. Yielding of top bars Φ14 at step 104

The contour plot of the crack strain values can be interpreted as a crack pattern. Based on this it can be said that the crack pattern is extensive with most of the crack being inclined –thus shear, stress free (open) cracks. At the same time, from the contour plot of the negative principal strains it can be observed that compressive struts undergo crushing. On the other hand, yielding of stirrups as well as bending reinforcement occurred only locally and its effect is significantly less far-reaching. From the above consideration, it is concluded that the beam failed in shear due to crushing of concrete compressive struts.

Gauss point statistics

In Table 6-8 the number of cracking points, crushing points and yield points are reported at step 77 (yielding of right side stirrups), at step 79 (crushing of concrete), at

step 96 (yielding of bottom bars Φ8), at step 101 (yielding of top bars Φ14) and at step 104 (peak load).

Table 6-8: Case PB4. Number of cracking points, crushing points and yield points

STEP	**77**	**ITERATIONS**		2		
GROUP NAME	**PLAST**	**PRV. PL**	**CRITIC**	**PLAST NEW**	**PRV.PL NEW**	**CRITIC NEW**
FL_SUP	65	0	0	2	0	0
FL_INF	3	0	0	0	0	0
WEB	935	16	0	56	4	0
SHEAR	1362	31	0	74	7	0
STIRRRIGHTF10	3	0	0	3	0	0
TOTAL MODEL	2368	47	0	135	11	0
CRACKING LOGGING SUMMARY						
GROUP NAME	**CRACK**	**OPEN**	**CLOSED**	**ACTIVE**	**INACTI**	**ARISES**
WEB_VB	1	1	0	1	0	0
WEB_VC	12	12	0	11	1	0
WEB_VD	23	23	0	21	2	1
WEB_VE	44	44	0	37	7	2
WEB_VF	70	70	0	47	23	2
WEB_VG	81	81	0	46	35	0
WEB_VH	129	129	0	90	39	0
FL_SUP	109	109	0	74	35	3
FL_INF	1365	1365	0	1157	208	19
WEB	5051	5049	2	4239	812	20
SHEAR	4956	4952	4	4073	883	14
TOTAL MODEL	11841	11835	6	9796	2045	61
STEP	**79**	**ITERATIONS**		3		
GROUP NAME	**PLAST**	**PRV. PL**	**CRITIC**	**PLAST NEW**	**PRV.PL NEW**	**CRITIC NEW**
FL_SUP	71	0	0	5	0	0
FL_INF	3	0	0	0	0	0
WEB	1003	39	0	55	22	0
SHEAR	1442	74	0	73	36	0
STIRRRIGHTF10	8	0	0	4	0	0
TOTAL MODEL	2527	113	0	137	58	0
CRACKING LOGGING SUMMARY						
GROUP NAME	**CRACK**	**OPEN**	**CLOSED**	**ACTIVE**	**INACTI**	**ARISES**
WEB_VB	3	3	0	3	0	2
WEB_VC	13	13	0	12	1	1
WEB_VD	23	23	0	19	4	0
WEB_VE	48	48	0	42	6	2
WEB_VF	72	72	0	47	25	0
WEB_VG	81	81	0	44	37	0
WEB_VH	136	136	0	92	44	1
FL_SUP	126	126	0	92	34	6
FL_INF	1407	1407	0	1172	235	24
WEB	5093	5091	2	4155	938	22
SHEAR	4987	4983	4	4002	985	18
TOTAL MODEL	11989	11983	6	9680	2309	76
STEP	**96**	**ITERATIONS**		1		
GROUP NAME	**PLAST**	**PRV. PL**	**CRITIC**	**PLAST NEW**	**PRV.PL NEW**	**CRITIC NEW**

WEB_VH	1	0	0	0	0	0
FL_SUP	139	0	0	3	0	0
FL_INF	16	0	0	2	0	0
WEB	1941	80	0	88	0	0
SHEAR	2572	126	0	105	7	0
STIRRRIGHTF10	141	0	0	9	0	0
REBBOTTF8	1	0	0	1	0	0
TOTAL MODEL	4811	206	0	208	7	0
CRACKING LOGGING SUMMARY						
GROUP NAME	**CRACK**	**OPEN**	**CLOSED**	**ACTIVE**	**INACTI**	**ARISES**
WEB_VA	5	5	0	5	0	1
WEB_VB	13	13	0	13	0	0
WEB_VC	33	33	0	27	6	1
WEB_VD	45	45	0	37	8	0
WEB_VE	84	84	0	75	9	1
WEB_VF	96	96	0	74	22	0
WEB_VG	91	91	0	68	23	0
WEB_VH	164	164	0	148	16	2
FL_SUP	219	219	0	184	35	11
FL_INF	1718	1718	0	1554	164	18
WEB	5309	5307	2	4174	1135	5
SHEAR	5195	5191	4	4123	1072	7
TOTAL MODEL	12972	12966	6	10482	2490	46
STEP	**101**	**ITERATIONS**		1		
GROUP NAME	**PLAST**	**PRV. PL**	**CRITIC**	**PLAST NEW**	**PRV.PL NEW**	**CRITIC NEW**
WEB_VH	4	0	0	3	0	0
FL_SUP	160	0	0	5	0	0
FL_INF	24	0	0	2	0	0
WEB	2256	51	0	64	5	0
SHEAR	2974	100	0	77	10	0
STIRRRIGHTF10	205	0	0	12	0	0
REBTOPF14	1	0	0	1	0	0
REBBOTTF8	5	0	0	2	0	0
TOTAL MODEL	5629	151	0	166	15	0
CRACKING LOGGING SUMMARY						
GROUP NAME	**CRACK**	**OPEN**	**CLOSED**	**ACTIVE**	**INACTI**	**ARISES**
WEB_VA	8	8	0	8	0	1
WEB_VB	18	18	0	17	1	2
WEB_VC	44	44	0	35	9	1
WEB_VD	55	55	0	44	11	1
WEB_VE	91	91	0	79	12	3
WEB_VF	98	98	0	76	22	1
WEB_VG	96	96	0	74	22	1
WEB_VH	168	168	0	155	13	0
FL_SUP	255	255	0	210	45	9
FL_INF	1799	1799	0	1676	123	14
WEB	5348	5346	2	4323	1025	7
SHEAR	5231	5228	3	4373	858	9
TOTAL MODEL	13211	13206	5	11070	2141	49
STEP	**104**	**ITERATIONS**		1		
GROUP NAME	**PLAST**	**PRV. PL**	**CRITIC**	**PLAST NEW**	**PRV.PL NEW**	**CRITIC NEW**
WEB_VH	9	0	0	2	0	0

FL_SUP	143	19	0	63	0	0
FL_INF	33	0	0	2	0	0
WEB	2127	319	0	268	0	0
SHEAR	2651	641	0	365	0	0
STIRRRIGHTF10	220	10	0	15	0	0
REBTOPF14	4	0	0	0	0	0
REBBOTTF8	10	1	0	4	0	0
TOTAL MODEL	5197	990	0	719	0	0
CRACKING LOGGING SUMMARY						
GROUP NAME	**CRACK**	**OPEN**	**CLOSED**	**ACTIVE**	**INACTI**	**ARISES**
WEB_VA	10	10	0	8	2	0
WEB_VB	21	21	0	19	2	0
WEB_VC	53	53	0	39	14	1
WEB_VD	56	56	0	44	12	0
WEB_VE	100	100	0	89	11	3
WEB_VF	107	107	0	86	21	2
WEB_VG	99	99	0	78	21	1
WEB_VH	170	170	0	154	16	0
WEB_RINGR	1	1	0	1	0	1
FL_SUP	293	293	0	214	79	7
FL_INF	1836	1836	0	1479	357	17
WEB	5369	5367	2	3353	2016	2
SHEAR	5275	5272	3	3888	1387	3
TOTAL MODEL	13390	13385	5	9452	3938	37

6.5 Application of safety format

As proposed by the Model Code 2010 (fib, 2013) safety formats for nonlinear analyses include three numerical methods denoted as GRF (Global Resistance Factor method), PF (Partial Factor method) and ECOV (Method of Estimation of a Coefficient of Variation of resistance). In Table 6-9 to Table 6-14 the mechanical properties of concrete and steel applied in the nonlinear analyses are summarized.

Table 6-9: Case PB4. Constitutive model parameters for concrete

	f_c (N/mm^2)	f_{ct} (N/mm^2)	E_c (N/mm^2)	ν	G_F (Nmm/mm^2)	G_C (Nmm/mm^2)
Mean measured	24.02	2.12	25977	var	0.129	22.839
Characteristic	16.02	1.48	24765	var	0.120	21.233
Mean GRF	13.62	1.71	23586	var	0.117	20.621
Design	10.68	0.99	21928	var	0.111	19.739

Table 6-10: Case PB4. Constitutive model parameters for reinforcing bars (Φ8)

	Φ (mm)	A_s (mm^2)	f_y (N/mm^2)	f_t (N/mm^2)	E_s (N/mm^2)	ε_{sy} (-)
Mean measured	8	49	460.00	567.00	197000	0.0023
Characteristic	8	49	416.64	513.56	197000	0.0021
Mean GRF	8	49	458.31	564.91	197000	0.0023
Design	8	49	362.30	446.57	197000	0.0018

Table 6-11: Case PB4. Constitutive model parameters for reinforcing bars (Φ10)

	Φ (mm)	A_s (mm^2)	f_y (N/mm^2)	f_t (N/mm^2)	E_s (N/mm^2)	ε_{sy} (-)
Mean measured	10	79	431.00	556.00	201000	0.0021
Characteristic	10	79	390.38	503.59	201000	0.0019
Mean GRF	10	79	429.41	553.95	201000	0.0021
Design	10	79	339.46	437.91	201000	0.0017

Table 6-12: Case PB4. Constitutive model parameters for reinforcing bars (Φ12)

	Φ (mm)	A_s (mm^2)	f_y (N/mm^2)	f_t (N/mm^2)	E_s (N/mm^2)	ε_{sy} (-)
Mean measured	12	109	489.00	637.00	202000	0.0024
Characteristic	12	109	442.91	576.96	202000	0.0022
Mean GRF	12	109	487.20	634.65	202000	0.0024
Design	12	109	385.14	501.70	202000	0.0019

Table 6-13: Case PB4. Constitutive model parameters for reinforcing bars (Φ14)

	Φ (mm)	A_s (mm^2)	f_y (N/mm^2)	f_t (N/mm^2)	E_s (N/mm^2)	ε_{sy} (-)
Mean measured	14	152	397.00	517.00	207000	0.0019
Characteristic	14	152	359.58	468.27	207000	0.0017
Mean GRF	14	152	395.54	515.10	207000	0.0019
Design	14	152	312.68	407.19	207000	0.0015

Table 6-14: Case PB4. Constitutive model parameters for reinforcing bars (strands)

	Φ (mm)	A_s (mm^2)	f_y (N/mm^2)	f_t (N/mm^2)	E_s (N/mm^2)	ε_{sy} (-)
Mean measured	12.2	12x117	1225.00	1363.00	207000	0.0059
Characteristic	12.2	12x117	1109.53	1234.53	207000	0.0054
Mean GRF	12.2	12x117	1220.49	1357.98	207000	0.0059
Design	12.2	12x117	964.81	1073.50	207000	0.0047

In Figure 6-33 the load-deflection curves obtained with mean measured, characteristic, mean GRF and design values of material strengths are shown. The analysis carried out with the design values of material strength interrupted after the application of the first load step which is the dead load, the prestressing force and the vertical force equal to 588 kN. The maximum load reached using the design values of material strength was then considered equal to 588 kN.

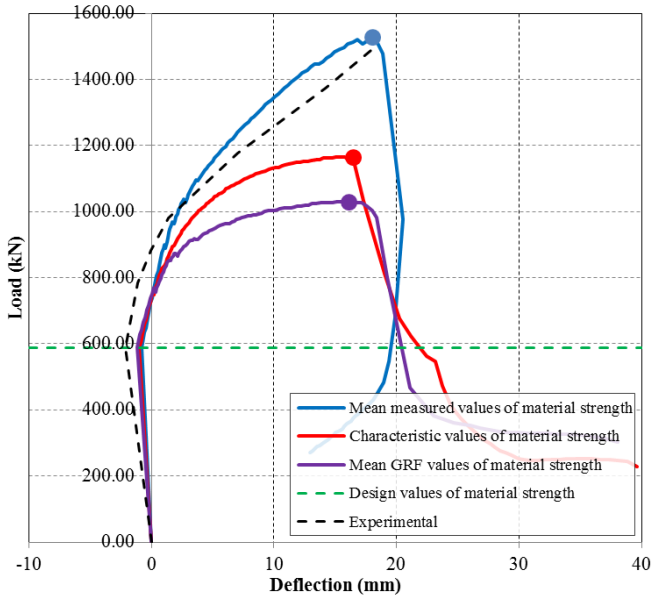

Figure 6-33: Case PB4. Load-deflection curves obtained with mean measured, characteristic, mean GRF and design mechanical properties

PB4 beam is analyzed with analytical and numerical approaches. Figure 6-34 shows the comparison of the analytical and numerical design values of beam resistance P_{Rd} expressed in terms of a percentage of the experimental ultimate value of applied load. The analysis named "no safety format" refers to the NLFE analysis carried out using mean measured values of material strengths without applying any safety coefficient.

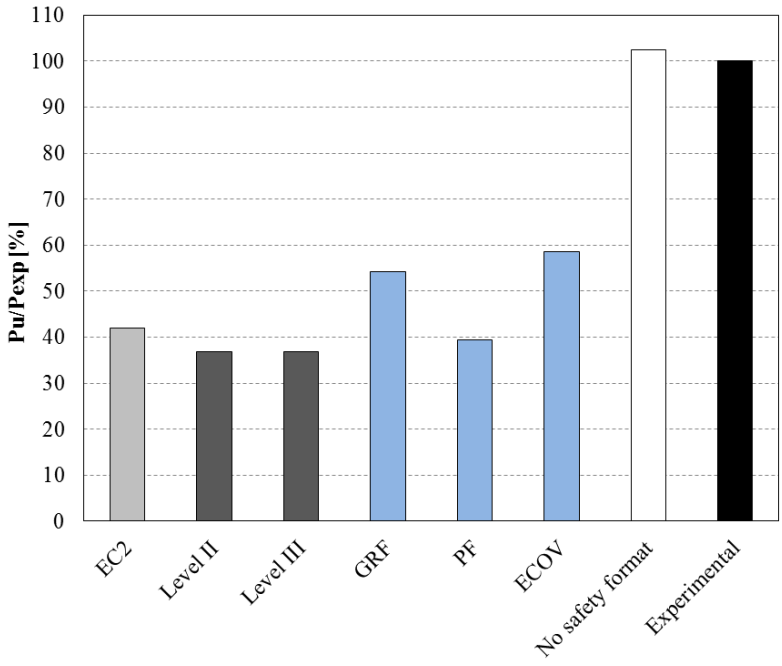

Figure 6-34: Case PB4. Analytical and numerical design values of beam resistance expressed in terms of a percentage of the experimental ultimate value of applied load, $P_{Exp} = 1491.12kN$

From Figure 6-34 it can be noted that due to the low value of concrete compressive strength the design values of beam resistance is significantly influenced by the safety coefficients.
In Table 6-15 the design values of beam resistance obtained from numerical and analytical procedures expressed in terms of applied load P_{Rd}, are listed.

Table 6-15: Case PB4. Beam resistance P_{Rd} in kN

P_{Exp}	EC2	Level I MC2010	Level II MC2010	Level III MC2010	GRF	PF	ECOV	No safety formats
1491.12	625.98	-	548.58	548.58	809.43	588.60	874.19	1527.60

6.6 Parametric study on crack models

A parametric study was carried out by varying some sensitive parameters of the concrete constitutive model, such as the crack model, and the fracture energy of concrete in tension.
In Table 6-16 the material parameters applied in NLFE analyses performed for the parametric study are reported. Analyses 1 to 3 refer to the three analyses carried out by varying the aforementioned material parameters. In all analyses mean measured values of material strength were considered. Parabolic law in compression and exponential law in tension were used for concrete, while an elasto-plastic with hardening law was adopted for steel. A variable Poisson's ratio was adopted for all analyses. The analyses were carried out in load-control with arc-length control.
For all analyses the limit value of the reduction of the compressive strength of concrete due to lateral cracking was determined according to (Vecchio et al., 1986) as follows:

$$\beta_{\sigma,\min} = \frac{f_{c,red}}{f_{cm}} = 0.6$$

The effects of the applied value of the fracture energy of concrete in tension on the beam response was investigated by means of comparison of the formulation of Model Code 1990 (CEB-FIB, 1993) and Model Code 2010 (fib, 2013). The two values used are respectively equal to $G_{F,MC1990} = 0.062\,N/mm$ and $G_{F,MC2010} = 0.129\,N/mm$. The fracture energy of concrete in compression was considered for all analyses equal to $250G_F$ (Nakamura et al. 2001).
In the fixed crack model, a variable shear retention factor dependent on the mean aggregate size d_{aggr}, the crack normal strain ε_n and the crack bandwidth value h follows from:

$$\beta = 1 - \left(\frac{2}{d_{aggr}} \right) \varepsilon_n h$$

In Figure 6-35 the load-deflection curves obtained from the parametric study are plotted. The peak load of each analysis, which is defined as the highest load step for which the energy norm ratio satisfied the fixed tolerance of 1×10^{-3} , is marked with a circular indicator. The peak load values are given explicitly in Table 6-16.

Table 6-16: Case PB4. Parametric study on crack models

Analysis	Total strain crack model	G_F	G_C	Peak load value (kN)
Analysis 1	rotating	MC2010	250 G_F	1527.60
Analysis 2	rotating	MC1990	250 G_F	1464.60
Analysis 3	fixed (β=variable)	MC2010	250 G_F	1662.60

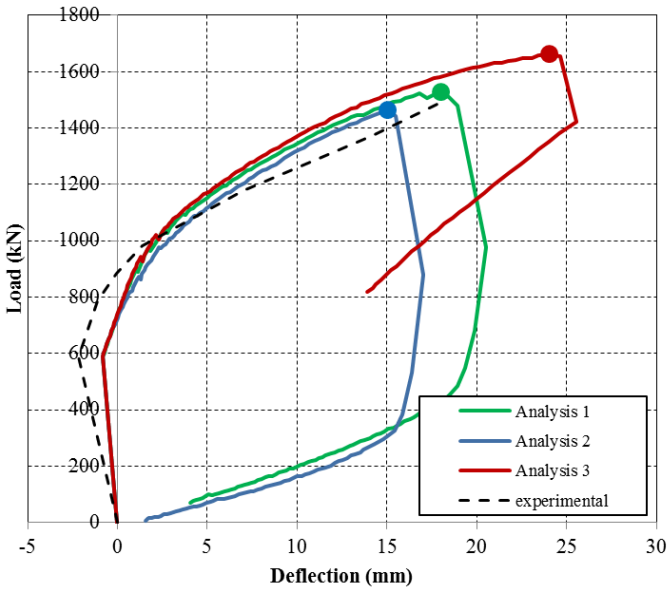

Figure 6-35: Case PB4. Parametric study

Comparing analysis 1 with analysis 2, the influence of the adopted values of the fracture energy of concrete in tension ($G_{F,MC1990}$=0.062*N/mm*; $G_{FM,C2010}$=0.129*N/mm*) and the corresponding values of the fracture energy of concrete in compression ($G_{C,MC1990}$=15.58*N/mm*; $G_{C,MC2010}$=32.34*N/mm*) is visible. Since the beam fails in shear with crushing of concrete, both the fracture energy of concrete in tension and in compression play an important role on the load-deflection response.
From the comparison of analyses 1 and 3, it can be recognized that for PB4 the adopted crack model (total strain rotating and fixed crack model) has a big influence on the beam response, both in terms of the peak load and peak deformation. The peak load and peak deformation are significantly overestimated if a fixed crack model with the aggregate size based shear retention factor is applied. Furthermore, the crack pattern and the failure mode obtained from NLFEA bears a better resemblance to the experimental crack pattern when the rotating crack model is adopted.

6.7 Concluding remarks

The simply support prestressed beam PB4 subjected to three point bending exhibited a shear-compressive failure mechanism at a load equal to P=1491.12*kN*.
The beam was modeled with 8-node membrane elements for the concrete and embedded truss elements for the reinforcement. Perfect bond is assumed. The concrete model is based on a total strain rotating crack model with exponential tension softening in tension and parabolic behavior in compression, variable Poisson's ratio of concrete and reduction of compressive strength of concrete due to lateral cracking with a lower limit value equal to 0.6. The model for the reinforcement bars and stirrups is based on hardening plasticity.
A shear-compressive failure mechanism was achieved from NLFEA carried out with mean measured values of material strengths. The peak value of applied load obtained from NLFEA is equal to 1527.60 kN and the failure mode is characterized by crushing of concrete at the junction of web and upper flange, yielding of right side stirrups and yielding of bottom bars.
Safety formats for nonlinear finite element analyses as proposed by the Model Code 2010 (fib, 2013) were applied to obtain the design value of beam resistance expressed in terms of applied load. The design values of beam resistance obtained with the

application of safety formats were higher than the design resistance calculated with the analytical methods for sectional analysis.

To investigate an influence of different input parameters such as fracture energy of concrete in tension, the corresponding fracture energy of concrete in compression and shear behaviour through implementation of fixed crack model, a sensitivity study was performed. From the registered results, it was recognized that because the failure was caused by crushing of compressive struts, the response of the beam is highly influenced by these parameters. Another very influential parameter is the concrete compressive strength. It could be well observed from the results of the analyses with safety formats. The design values of the beam resistance are significantly lower than from the model with mean measured material properties. Moreover, the design beam resistance obtained with the Partial Factor method is comparable to the design value of beam resistance obtained with analytical calculations.

Based on the results, it can be concluded that consistent and reliable results can be obtained by adopting variable Poisson's ratio, reduction of the compressive strength due to lateral cracking with a low limit of 0.6, total strain rotating crack model and fracture energy of concrete in tension according to Model Code 2010. An energy norm with a tolerance of 10^{-3} is recommended.

References

CEB-FIP Model Code 1990. (1993), *Bullettin d'Information n° 213/214*. Thomas Telford.

CEN (2005), Eurocode 2 - Design of concrete structures - Part 1-1: General rules and rules for buildings, EN 1992-1-1, Brussels: CEN.

fib (2013), fib Model Code for Concrete Structures 2010, Ernst & Sohn.

Leonhardt, F., Koch R. & Rostacy, F.S. (1973), "Schubversuche an Spannbetonträgern", Heft 227, Berlin: Deutscher Ausschuss für Stahlbeton.

Nakamura, H. & Higai T. (2001), "Compressive Fracture Energy and Fracture Zone Length of Concrete" in "Modeling of Inelastic Behavior of RC Structures under Seismic Loads", Benson P. Shing (editor), *ASCE J. Str. Eng.*, 471-487, Benson P. Shing.

Oliver, J. (1989), "A consistent characteristic length for smeared cracking models", *International Journal for numerical Methods in Engineering*, 28, 461- 474

Runzell B., Shield C., French C., (2007). "Shear capacity of prestressed beams", Minnesota Department of transportation Research Services Section.

Selby R.G., Vecchio F.J. (1993). "Three-dimensional Constitutive Relations for Reinforced Concrete", Tech. Rep. 93-02, Univ. Toronto, dept. Civil Eng., Toronto, Canada.

Sun S., Kuchma D. A. (2007), "Shear behavior and capacity of large- scale prestressed high- strength concrete bulb- tee girders", Department of Civil and Environment Engineering University of Illinois at Urbana- Champaign, Report No. NSEL-002, November.

Vecchio F. J. & Collins M. P. (1986), "The modified compression-field theory for reinforced concrete elements subjected to shear", *ACI Journal* 83, 219-231

Vervuurt, A.H.J.M. & Leegwater, G.A. (2008), "Workshop on the assessment of the shear strength of concrete structures", TNO report 2008-D-R0010.